

- 1 TOOL FOR THE SYNTHESIS OF MECHANISMS OF NEW ENGINES BASED ON DASY
David Richtr
- 9 OPTIMIZATION OF 2-STAGE TURBOCHARGED GAS SI ENGINE
UNDER STEADY STATE OPERATION
Oldřich Víttek, Jan Macek, Jiří Klíma, Martin Vacek
- 37 EVALUATION OF THE PREDICTIVE CAPABILITIES OF A PHENOMENOLOGICAL COMBUSTION
MODEL FOR NATURAL GAS SI ENGINE
Rastislav Toman, Jan Macek
- 49 STUDY OF THE EFFECTS OF ETHANOL AS AN ADDITIVE WITH A BLEND OF POULTRY
LITTER BIODIESEL AND ALUMINA NANOPARTICLES ON A DIESEL ENGINE
Ramesha D K, Nishad Rajmalwar, T Sreeharsha Varma, Mrithyunajaya Swamy K M



THIS ISSUE IS FOCUSED ON RESEARCH IN: INTERNAL COMBUSTION ENGINES

AIM

Published in the heart of Europe on Czech Technical University in Prague the journal reports about research in the field of internal combustion engines and all other components and aspects of vehicle engineering and vehicle design. The articles from the whole world are welcome.

THE FOLLOWING TOPICS ARE RELEVANT FOR THE JOURNAL MECCA:

- Engines and fuels
- Powertrains (hybrid vehicles, transmissions,...)
- Chassis
- Vehicle body
- Experimental testing
- Mechatronics
- Vehicle dynamics
- Safety
- Transport Systems
- Electronics in vehicles

PERIODICITY

Three times a year

REVIEW PROCESS

All articles are peer and blind reviewed. At least two reviewers per article.

LANGUAGE

English, bilingual abstract and legends (English/Czech or English/Slovak). Articles coming from non-English speaking countries are submitted to English correction.

ABSTRACTING AND INDEXING

The journal is part of database of open access publications (DOAJ): <https://doaj.org/toc/1804-9338>

Publisher of the open access articles: De Gruyter.

MEMBERS OF EDITORIAL BOARD

EDITOR IN CHIEF

Prof. Ing. Jan Macek, DrSc.

Czech Technical University, Prague, CZ
Technická 4, Praha 6, 16607, Czech republic

SENIOR EDITOR

Dr. Ing. Gabriela Achtenová Czech Technical University, Prague, CZ

EDITORIAL BOARD

Prof. Dr. Ing. Milan APETAUR Technical University Ústí nad Labem, CZ

Dr. Ing. Eduardo Jose BARRIENTOS Czech Technical University in Prague, CZ

Prof. Dr. Ing. Stanislav BEROUN Technical University Liberec, CZ

Dr. Ing. Yann MARCO Ensieta, France

Prof. Dr. Vladimir MEDICA University of Rijeka, Croatia

Dr. Ing. Tamás MERÉTEI Institute for Transport Sciences Ltd., Hungary

Ing. Antonín MIKULEC Czech Technical University, Prague, CZ

Prof. Dr. Vladimír MORAVEC Technical University Ostrava, CZ

Dr. Ing. Thomas MOREL Gamma Technologies, USA

Prof. Dr. Ir. Joop PAUWELUSSEN HAN University, The Netherlands

Prof. Dr. Ing. Václav PÍŠTĚK Brno University of Technology, CZ

Doc. Dr. Ing. Miloš POLÁŠEK Porsche Engineering Services, CTU Prague, CZ

Doc. Dr. Marián POLÓNI Slovak University of Technology, Slovakia

Dr. Ing. Vladimír ŠATOCHIN Motor Vehicle Research Institute Ltd., CZ

Dr. Ing. Václav TAJZICH Motor Vehicle Research Institute Ltd., CZ

Prof. Dr. Ing. Michal TAKÁTS Czech Technical University, Prague, CZ

Prof. Dr. Ing. Michael VALÁŠEK Czech Technical University, Prague, CZ

Dr. Ing. Jiří VÁVRA University of Michigan, Michigan, USA

Dr. Ing. Oldřich VÍTEK Czech Technical University, Prague, CZ

Ing. Jan WANGLER formerly Praga, a.s., CZ

This journal is published using financial support from the budget of the Centre of Vehicles for Sustainable Mobility, Faculty of Mechanical Engineering, Czech Technical University in Prague. A part of support comes from the project Josef Božek Competence Centre for Automotive Industry TE 0102 0020, funded by the Technological Agency of Czech Republic. These sources are gratefully acknowledged.



IMPRINT MECCA – VOLUME XV, NUMBER 02, YEAR 2017, <http://bozek.cvut.cz/mecca>, gabriela.achtenova@fs.cvut.cz

Editor: České vysoké učení technické v Praze MECCA, Technická 4, 16607, Praha 6, Czech republic, **ISSN 1214-0821, ISSN 1804-9338 (Online), MK ČR E 13720**

Proofreading: Channel Crossings, Prague, Czech Republic **Advertising:** gabriela.achtenova@fs.cvut.cz or jan.macek@fs.cvut.cz **Production/Layout:** studio pixl-e (studio@pixl-e.cz)

TOOL FOR THE SYNTHESIS OF MECHANISMS OF NEW ENGINES BASED ON DASY

DAVID RICHTR

CTU in Prague, Faculty of Mechanical Engineering, Technická 4, 166 07, Praha 6. Tel.: +420728462851, E-mail: richtrd@gmail.com

SHRNUTÍ

Článek se zabývá prezentací nástroje pro syntézu mechanismů motoru založený na DASY a jeho využití při návrhu parametrů experimentálního jednoválcového motoru. Nástroj obsahuje parametrický model motoru založený na DASY. Model umožní simulovat termodynamiku motoru a jeho mechanismy. Skládá ze submodelů, které řeší termodynamiku, kinematiku a dynamiku rozvodového mechanismu, jeho řemenový pohon a hydraulický okruh natáčení vačkových hřídelí. Metodik syntézy mechanismů bylo využito pro nalezení hodnot kalibračních parametrů. Následně byly parametry submodelů validovány experimentálními daty a jejich hodnoty jsou obsaženy v DASY. Ze submodelů byl sestaven model experimentálního jednoválce, který ověřuje jeho konstrukci, umožňuje optimalizovat jeho parametry a předpovídat jeho chování v různých simulovaných stavech.

KLÍČOVÁ SLOVA: VARIABILNÍ VENTILOVÝ ROZVOD, VAČKA, VENTIL, VAČKOVÁ HŘÍDEL, HYDRAULICKÝ PŘESUVNÍK VAČKOVÉ HŘÍDELE, SIMULACE, EXPERIMENTÁLNÍ ZÁŽEHOVÝ MOTOR, DYNAMIKA, VÝPOČET, GT-SUITE

ABSTRACT

The article presents a tool for the synthesis of engine mechanisms based on DASY and the use thereof for designing the parameters of an experimental single-cylinder engine. The tool includes a parametric engine model based on DASY. The model will make it possible to simulate the engine thermodynamics and its mechanisms. It consists of sub-models which deal with the thermodynamics, kinematics and dynamics of the valve timing mechanism, its belt drive, and hydraulic circuit for camshaft adjustment. The methodologies of synthesis of mechanisms were used to determine the values of the calibration parameters. The parameters of the sub-models were subsequently validated by experimental data, and the values thereof are included in DASY. The sub-models were used to assemble the model of an experimental single-cylinder engine which validates the design thereof, makes it possible to optimize its parameters and predict its behavior in different simulated conditions.

KEYWORDS: VARIABLE VALVE TRAIN, CAM, VALVE, CAMSHAFT, HYDRAULIC CAM PHASER, EXPERIMENTAL SI ENGINE, SIMULATION, DYNAMICS, CALCULATION, GT-SUITE

1. INTRODUCTION AND RESEARCH

The creation of the model of the single-cylinder parametric model was based on a four-cylinder engine. Parameters of the different parts were available for this engine from CAD models. Data such as valve acceleration curves, actual speed and the forces acting on the rocker arm were available from experiments. The entire parametric model was divided into sub-models which were subjected to calibration according to this available data.

A conventional approach to the simulation of the dynamics of the mechanism consists of modeling individual subsystems separately and subsequently using the results of its marginal conditions for another sub-model. It is advisable to approach the analysis of the individual interactions between individual subsystems holistically. It is possible to use commercial or

university software. The commercial software includes, for example, GT-SUITE, a Ricardo software suite (Valvedyn, Wave, Engdyn...), or SIMPACK. University software includes, for example, MBSim of the Munich Technical University. Individual solutions are offered by modeling of a system of 1D/2D/3D bodies using an approach where the bodies can be solid or flexible. The finite element method is used to address the deformations of each body.

Depending on the complexity of the model and the required results, it is important to pick a suitable approach with respect to the time-intensity of the calculations. The advantage of modeling of individual subsystems separately is a greater number of parameters which describe the real model in greater



detail and contribute to greater capability of calibration of the model with a relatively low time-intensity of the calculation. Synthesis of the individual mechanisms therefore increases the number of parameters which are used for sufficient description of the entire mechanism, and thus the calculation demands. It is necessary to optimize the number of parameters, such as to achieve a reasonable calculation time and describe all important dynamic phenomena. Out of the freely available sources, we can mention – as an example of holistic approach to the synthesis of mechanisms in [1].

The software used for calibration of the parameters of the individual sub-models was DASY as a multi-parametric solver that uses a genetic algorithm.

2. DESCRIPTION OF THE SUB-MODELS

The creation of the parametric engine model involved division of the entire model into sub-models. The parameters of these sub-models were calibrated according to the available measurement data; see Chapter 3.

2.1 THERMODYNAMIC SUB-MODEL

The thermodynamic sub-model makes it possible to simulate the thermodynamics of the engine such as, for example, a model of the SI combustion, heat transfer to the cylinder walls, fluid dynamics in the pipes. The sub-model can be used for determination of the performance characteristics of the engine, specific fuel consumption, and other parameters. An important capability of the thermodynamic model is determination of the optimal

timing of the intake and exhaust valves to maximize the torque and minimize consumption, which should ensure reduction of the emissions in the exhaust gases. The determination of the optimal timing must be considered with regard to the design limits of the engine, respecting for example the collision of the piston and the valves.

2.2 MODEL OF THE INTAKE AND EXHAUST VALVE DYNAMICS

One of the more sophisticated sub-models for calibration is the model of the intake and exhaust valve dynamics. Their models are identical and only differ by the cam profiles used and input parameters of the individual elements. The specific type of the valve-operating mechanism used in the model is DOHC. For the single-cylinder engine model it includes two intake valves and two exhaust valves. For calibration and acceleration of the calculation time, the sub-model was simplified to include one separate valve in order to find the values of the calibration parameters. The model is described by a total of 37 parameters with which it was calibrated. The calibration parameters are divided into two parts. The first part is physical, input parameters of the elements such as stiffness of the individual parts (valve, rocker arm...) which were determined using the FEM. These parameters remain constant with the changing rotation speed. The second group is parameters of the contact points (Figure 3) which are generally used for mathematic transmission of information between the individual elements and the value of which is difficult to determine. It is assumed that they can change with the change of the actual rotation speed. The reason is that some of these elements ensure convergence of the numerical solution. For example, the ramp function of stiffness simulates the flexibility upon contact of two bodies and deals with the step change of stiffness of the contact which would cause the complications in the numerical solution. The model includes an active predictive tribological model dealing with the elastohydrodynamic contact between the individual elements.

2.3 MODEL OF A TIMING BELT WITH HYDRAULIC CAM PHASER

The model includes a toothed belt pulley with hydraulic cam phaser on the intake and exhaust side, a toothed belt pulley on the crankshaft, idler and tensioner, and a toothed belt. The GT-ISE environment models a toothed belt as a system of flexible beam elements and rigid bodies in the form of teeth. The beams are considered loaded with axial and shear stress and bending moment. The entire system is discretized using the principle of the finite element method. The number of teeth represents the number of the finite elements which are connected in nodes. In physical terms, the belt consists of a rubber body and steel cord. It is the steel cord that increases the overall stiffness of the belt and reduces the amplitude of inherent oscillation. Based on the density of the composition of the rubber and the steel cord, the

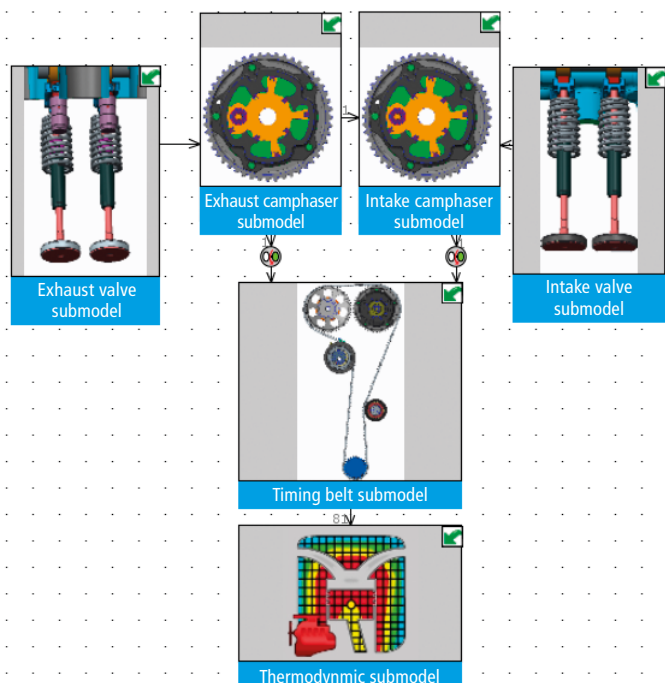


FIGURE 1: Schematic single-engine model in GT-ISE.

OBRÁZEK 1: Schematický model parametrického jednoválcového motoru.



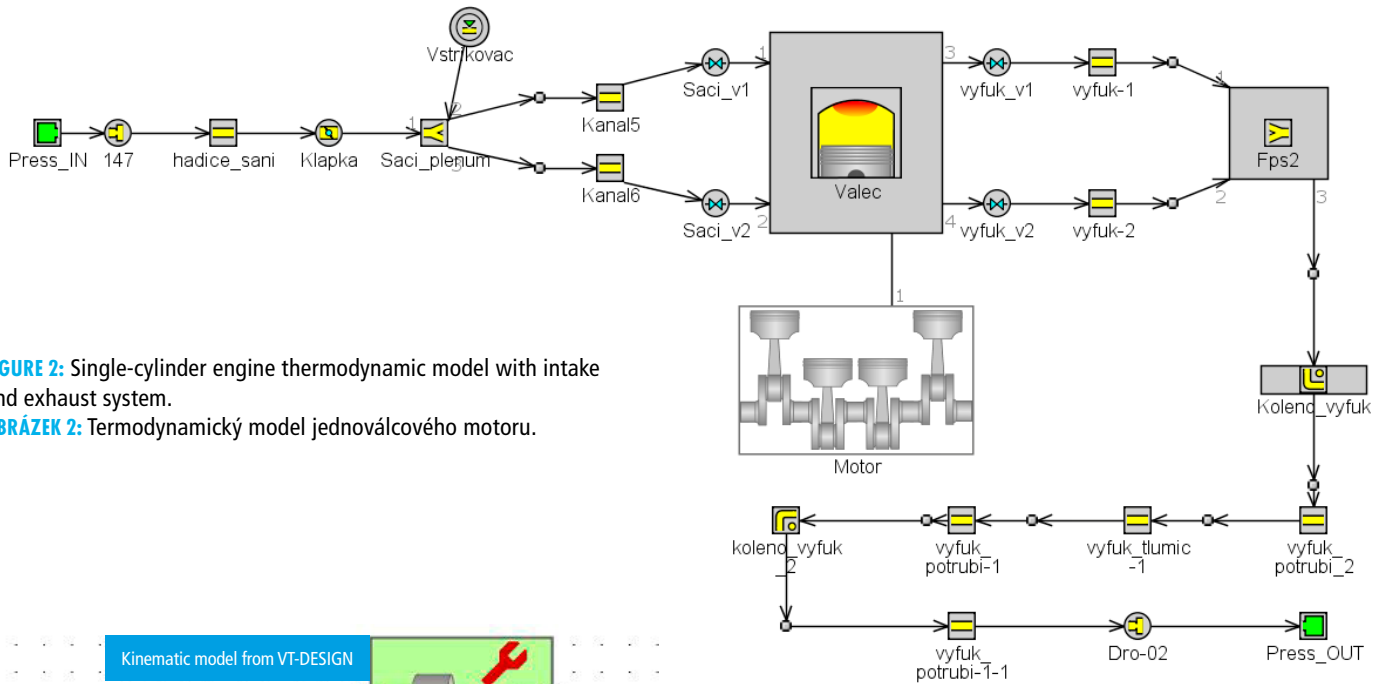


FIGURE 2: Single-cylinder engine thermodynamic model with intake and exhaust system.

OBRÁZEK 2: Termodynamický model jednoválcového motoru.

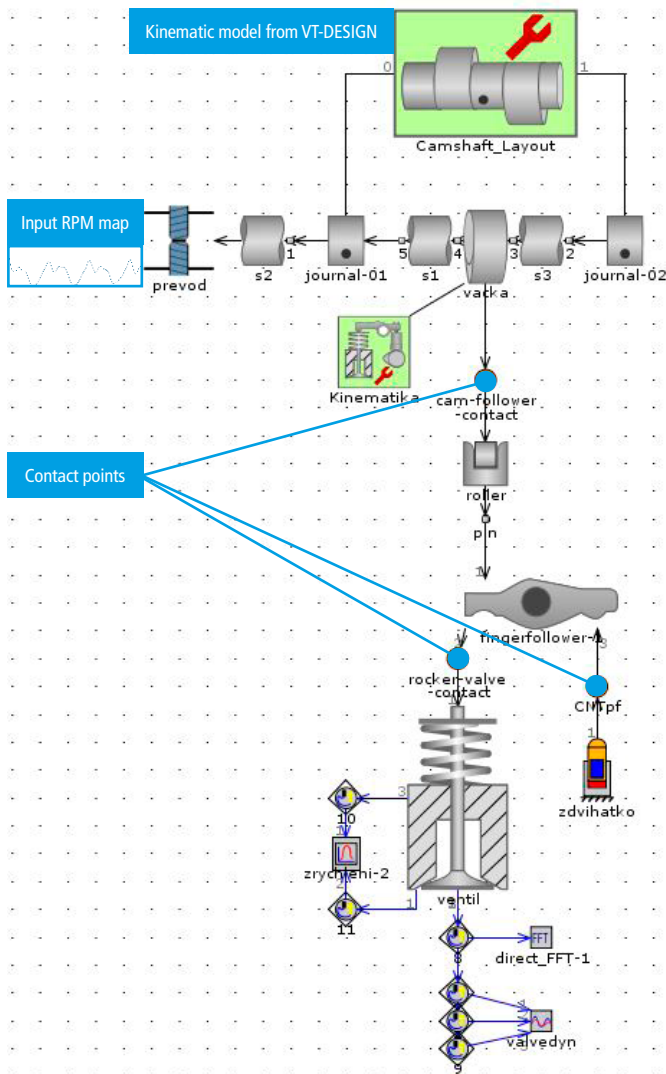


FIGURE 3: Model of single-valve mechanism.

OBRÁZEK 3: Model sacího ventilu.

weight and the moment of inertia of one element are estimated for the model. More accurate values of these parameters were determined based on calibration the results of which are provided in chapter 3.2.

The parameters of the hydraulic cam phaser and the other inlet pipes and volumes were measured out from the available CAD data. For the cam phaser were important moments of inertia of the stator and rotor, number and volume of the advance and retard chambers and the maximum angle of the phase change and the size of the effective area of the rotor blades. Measurement data was not available for the hydraulic part, and therefore the results of the hydraulic model only server as prediction. The model of a drive of timing mechanism with cam phasers is shown on Figure 4.

3. CALIBRATION AND VALIDATION OF THE SUB-MODELS

The calibration of individual sub-models was performed according to the available measurement data, at multiple rotation speed points. This approach ensures that a broader interval of dynamic phenomena is covered.

The calibration and validation of the sub-models was performed using the DASY software in the case of the intake and exhaust valve dynamics and the thermodynamic sub-model. This software uses a genetic algorithm which is based on the principle of evolution biology and uses processes such as crossbreeding,



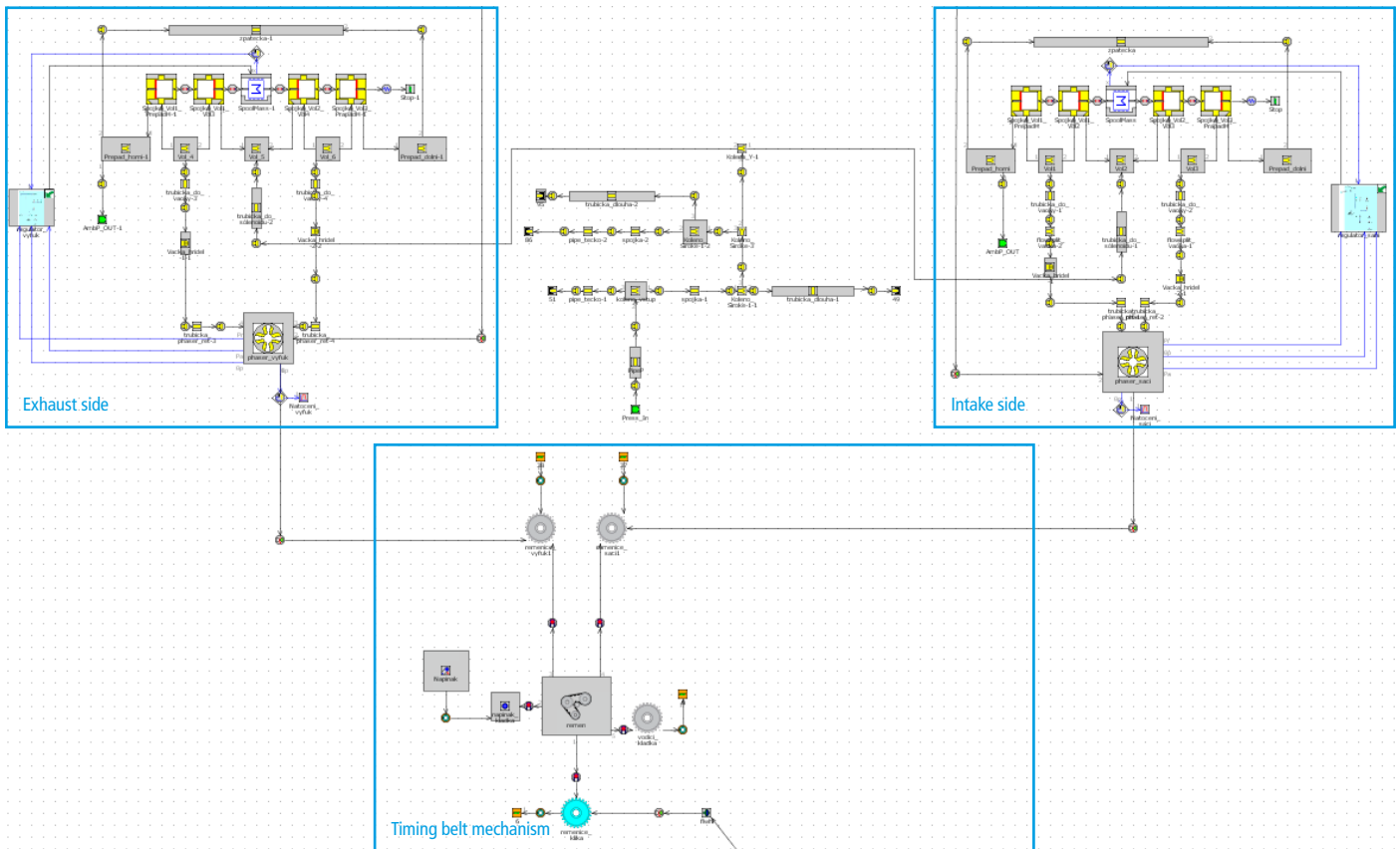


FIGURE 4: Model of timing belt with pulleys and hydraulic cam phaser
OBRÁZEK 4: Model řemenového rozvodu a hydraulického camphaseru

mutation, natural selection or heritability. The advantage of this software is that it solves optimization tasks with many variable parameters and looks for the optimal solution according to the predefined criteria. GT-SUITE includes a program called GT-POST which is used for displaying the simulation results. The results are divided into two types. The first type is display of the calculated values of magnitudes such as continuous function depending on time or angle in one or more operation cycles. The other type is display of the value of the magnitude as a single integral value in the form of average, maximum, minimum, or cumulative value integrated over a cycle. An example is effective mean pressure, average torque, average consumption, etc. This form of result is called RLT.

3.1 OPTIMIZATION OF THE THERMODYNAMIC MODEL

Optimization of the valve timing is based on the RLT-type results. The optimization was performed in order to determine the maximum torque along with the minimum specific consumption. The results file of the GT-POST program exports output RLT magnitudes of the specific consumption and torque into a text file. This file, together with the model from GT-ISE, is uploaded to the DASY environment where independent and dependent parameters are chosen. The independent parameters are defined

as input values, i.e., starts of valve lift. In addition, an interval is defined in which the input variables should change in order to prevent collision of the piston and valves. The dependent parameters are output magnitudes, i.e., values of the specific consumption and torque. A sample of the parameter settings together with a simple flowchart is shown on Figure 5. The output is a set of results from which the compromise between the maximum torque and minimum consumption must be selected manually. In addition, it is necessary to respect

```

    < E0 bsfc >
    < IO tq >
    casovani_opt
  
```

Parameter	Value	Units	Limits	Block
Known				
<input checked="" type="checkbox"/> E0	250	Input parametrs	[220; 2...	casovani_opt
<input checked="" type="checkbox"/> IO	10		[-20; 20]	casovani_opt
Unknown				
<input type="checkbox"/> bsfc	309.81	Output parametrs	No Limits	casovani_opt
<input type="checkbox"/> tq	27.642		No Limits	casovani_opt

FIGURE 5: Setting the known and unknown parameters in DASY
OBRÁZEK 5: Nastavení známých a neznámých parametrů v DASY



TABLE 1: Results of valve timing optimization
TABULKA 1: Výsledky hodnot optimálního časování ventilů

RPM	IO before TDC [CA]	EO before BDC [CA]
1000	17	29
2000	16	37.5
3000	14	42
4000	13	28
5000	10	25
6500	2	24

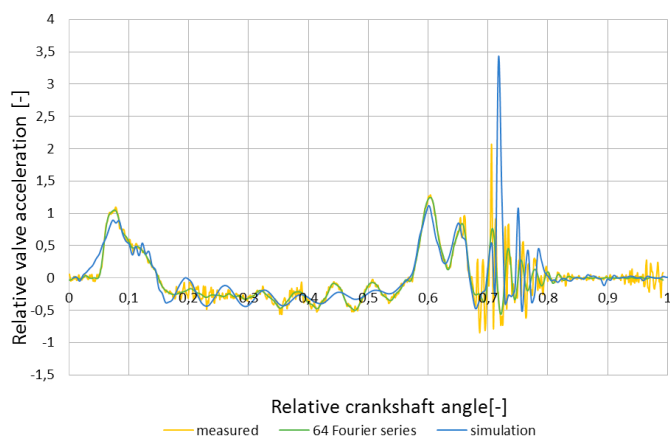


FIGURE 6: Comparison of simulation and measured data for intake valve acceleration

OBRÁZEK 6: Srovnání simulace a měření zrychlení sacího ventilu

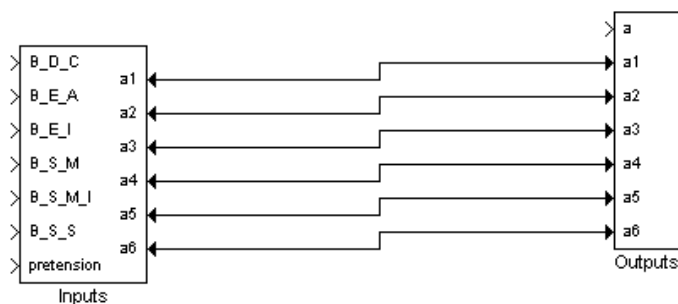


FIGURE 7: Flowchart for calibration of the rotation speeds of camshafts in DASY

FIGURE 7: DASY set for camshaft RPMs

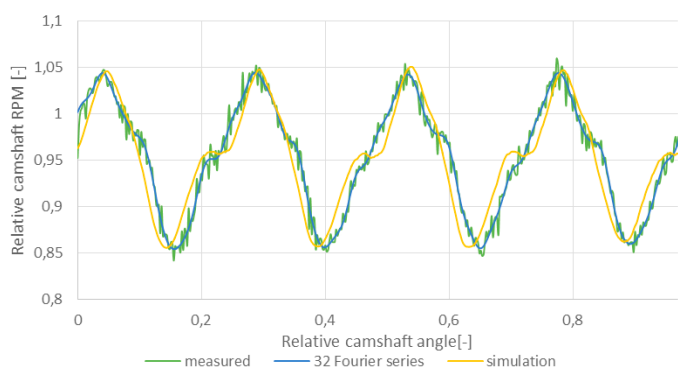


FIGURE 8: Comparison of the intake camshaft RPM from simulation and from measurement

OBRÁZEK 8: Porovnání průběhu okamžitých otáček na sací vačkové hřídeli ze simulace a měření

the rotation speed of the engine for which the optimization was performed. The optimal timing determined for the version used in this model, i.e., single-cylinder, unsupercharged engine with external formation of the mixture, is shown in Table 1. The optimization was performed for maximum engine load.

3.2 CALIBRATION OF THE DYNAMICS OF THE INTAKE AND EXHAUST VALVE

Calibration of the dynamic characteristics of the valve train mechanism was also performed using the DASY software. The process and evaluation of the calibration is identical as in the case of [3]. For the evaluation of the objective function, the genetic algorithm searched for the minimum value of the sum of the squares of the deviations between the objective function and the current curve from the simulation at the reference points. The deviations were observed on the valve acceleration curve in the time and frequency domain.

The measured curve was decomposed by Fourier transform into 64 harmonics where 15 reference points were determined (see [3]).

3.3 CALIBRATION OF THE TIMING BELT TRANSMISSION

Curves of actual rotation speed from the measurement and from the simulation results were compared in the toothed belt mechanism. As stated above, the material properties of the belt were used as parameters for calibration.

The available data from the measurement, however, was for a four-cylinder engine, not for the single-cylinder engine under review. Therefore, an auxiliary, purely mechanical model of four-cylinder engine was built. This model was composed of the timing mechanism and intake and exhaust camshaft where the data from chapter 2.2 was used as the values of the valve mechanism parameters. This model was used only for more accurate determination of the toothed belt parameters. The basic material properties and the nominal pretensioning of the belt were determined by an estimate, and the more accurate value thereof was determined by calibration. The identical process was used as in the calibration of valve acceleration. In this case, however, there was sufficient decomposition into 32 harmonics using Fourier transform of the actual rotation speed of the camshafts and only 6 reference points because the curve is periodical. The diagrammatic model from the DASY environment is shown below. The model includes the input parameters in the form of the material properties of the belt and the pretensioning thereof. The output is the reference points on the decomposed curve of the actual rotation speed.

The best match was achieved at 2000 rpm. The parameters corresponding to this curve were used in the other rpm points. The value of the nominal pretensioning of the toothed belt was based on simulation of 253 N. According to the available



information, this value ranges between 305–380 N in a real four-cylinder engine. This can be considered sufficiently accurate approximation to reality, to which also the below-pictured curve of the actual rotation speed corresponds.

4. REFERENCE RESULTS OF THE PREDICTIVE MODEL

Connection of the sub-models resulted in a predictive model of a single-cylinder engine which was used for calculations supporting the design of the parameters and design of a real engine. The parameters obtained from the auxiliary calibration sub-models were put in this predictive model for each rotation speed point. They are parameters of the toothed belt, the intake and exhaust valves. The predictive model of a virtual single-cylinder engine can be used also for prediction of the behavior of a real engine in different conditions which cannot yet be performed on a real engine as it is still under development. This can prevent conditions in which the timing elements would be damaged.

A synthesis of the thermodynamic and mechanical model can be used to predict the load upon the timing system parts. The mechanical model provides the thermodynamic model with information on the lift curves and, on the other hand, receives information on the curve of the pressure in the channels, in the cylinder, and temperature gradients, which includes these influences on the calculation of the dynamics of mechanisms.

The following three sub-chapters include the reference results of the single-cylinder engine. This data has not yet been validated experimentally.

4.1 DETERMINATION OF THE MAXIMUM ROTATION SPEED

The determination of the maximum rotation speed (rpm) of the timing mechanism is based on the monitoring of the valve lift curve and dynamic influences. The limit condition is one where the masses of the timing mechanism are accelerated and the valve spring is excited with a frequency approximating its natural frequency. At this moment the spring loses its pre-tensioning and ability to close the valve in accordance with the defined cam profile. The valve seating velocity is also higher than the pre-scribed velocity, and valve separation occurs. This condition is undesirable because it increases the load and wear and tear of the entire mechanism. One of the possible methods to determine the limit rotation speed is monitoring and comparing the kinematic and dynamic lift curve of the valve. In the optimal scenario, the dynamic lift curve is lower than or equal to the kinematic curve due to the flexibility and stiffness of the different parts. To determine the valve separation from the seat, the Valve Separation element was used. It is element, which compares difference between dynamic and kinematic valve lift. The positive value of valve

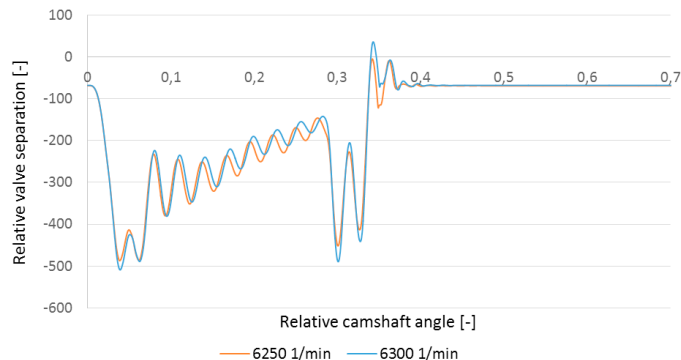


FIGURE 9: Valve separation dependence on relative camshaft RPM
OBRÁZEK 9: Průběh odskoku ventilu od sedla v závislosti na otáčkách vačkové hřídele

separation (exceeding zero value) represents the separation of the valve from the seat. Based on the analysis of this curve, the maximum operating rotation speed of the valve train was determined. The chart below shows the curve of valve separation at the rotation speed limit where no separation occurs yet. After having exceeded this value, separation occurs after valve seating (the critical zone is depicted in red). It is the first identifiable condition where stroke occurs in the valve seat. The valve train, however, can be operated further up to higher speed because the limit value of valve separation is determined by the design limits of the mechanism. For example it means the maximum possible gap between valve and valve seat after valve bounce defined by designers. Valve seating velocity gradient increases with the increasing rotation speed, which is also associated with excitation of the valve spring. As I have stated above, due to the loss of pretensioning of the valve spring by the excitation with natural frequency the valve separation is not absorbed by the spring. This results in increased stress on the entire valve train.

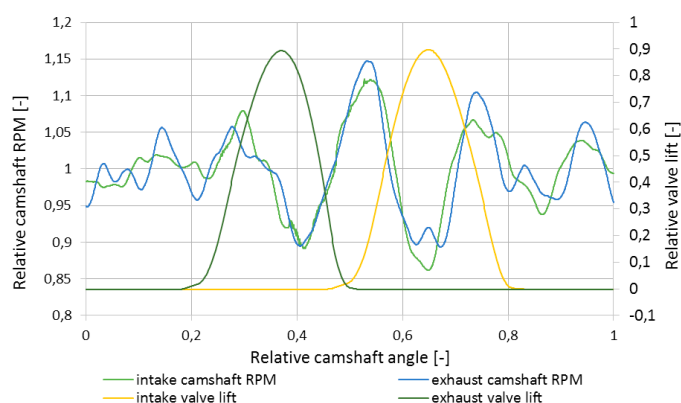


FIGURE 10: Valve lift curves and the impact on the actual rotation speed of the camshaft
OBRÁZEK 10: Průběh zdvihových křivek ventilů a vliv na průběh okamžitých otáček vačkové hřídele



4.2 ACTUAL ROTATION SPEED CURVE

The actual rotation speed curve periodically oscillates around the mean value of relative rotation speed of the camshaft. The action of the exhaust cam on the valve overcomes the pre-tensioning of the valve spring and reduces the actual rotation speed. Upon closure of the valve, the pre-tensioning in the spring increases the rotation speed. The same principle operates in the intake valves. After they have been closed, the actual rotation speed stabilizes around the mean value, which is manifested by decrease of the amplitude thereof. A partial test was performed because of the impact of the oscillation of the actual rotation speed in the region of closing of the valves, whether more significant deviations occur. No greater oscillation of the belt occurs, according to Figure 10, in the deviation of the amplitude of the actual rotation speed from the value of mean rotation speed in the region outside of the valve lift. It means the sufficient value of pretensioning of the toothed belt, which can be used to predict good adjustment thereof.

4.3 INTERRUPTION OF THE SUPPLY OF PRESSURE OIL

One of the possible conditions in which a single-cylinder engine can be found is a condition of certain failure. For example, in an experimental test, the oil circuit may be interrupted and the pressure jumps to a lower value. The mechanism includes a hydraulic cam phaser which is operated by pressure oil. Upon the loss of oil pressure, the valve timing may change, leading to a collision of the piston and valve in the event that the cam phaser rotor is not locked by a pin. Therefore in the design of the mechanism, it is necessary to take this risk into account and set the range of the cam phaser and valve timing such that a collision of the piston and valve can never occur. Decrease in oil pressure in the cam phaser chambers adds a degree of rotor freedom of the system between the stator and blades of the rotor of the cam phaser. The chart below shows the curve of the phase change of the cam phaser in the event of a step change of the oil pressure. The added degree of freedom of the mechanism between the pulley and camshaft causes a phase change due to the momentum transmitted through the pulley and the angular momentum of the system. Decreasing angular speed due to valve springs can cause overturning of the rotor blades against the stator between its walls. This will result in chaotic actual rotation speed of the pulley or, more precisely the camshaft.

The type of failure where the rotor oscillates against the stator due to the sudden drop of oil pressure and, at the same time, the pin locking does not occur is very unlikely. But if it happens, it will have impact on the entire mechanism. According to Figure 11, there is an apparent oscillation of the phase change of the cam phaser after oil pressure loss

in a very short time interval. One of the effects of this cause is the form of the resulting lift curve in comparison with the kinematic curve. This difference is shown on the picture below. The separation of dynamic from kinematic lift means greater valve acceleration than the one for which the mechanism is designed. In the first lift curve we can observe greater separation, which is also associated with the impact of the rocker roller all the way to the base of the cam. The spring does not manage to absorb the impact of the valve, and an additional valve separation occurs.

Therefore, only from mechanical point of view a short-term interruption of oil supply is not dangerous because increased stress of the individual parts, such as valves, valve seats etc., only occurs locally. But on the other hand, total oil pressure interruption is dangerous for whole engine, if engine does not stop as soon as possible. With this phenomenon is connected secondary problem, which is the deviation of the lift curve from the required curve. See Figure 12.

5. CONCLUSION

The article presented the application of a tool for synthesis of engine mechanisms based on DASY. The application includes creation of a computer parametric model of variable valve train with toothed belt, and a thermodynamic model of a single-cylinder engine in the environment of the GT-SUITE software. DASY software with genetic algorithm was used

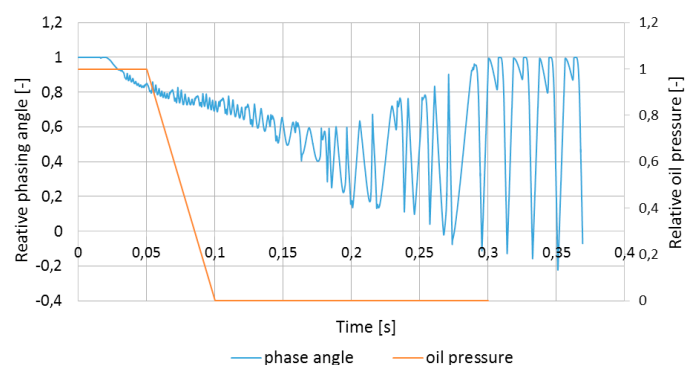


FIGURE 11: Dependence of cam phaser phase angle on oil pressure
OBRÁZEK 11: Závislost fázové změny camphaseru na tlaku oleje

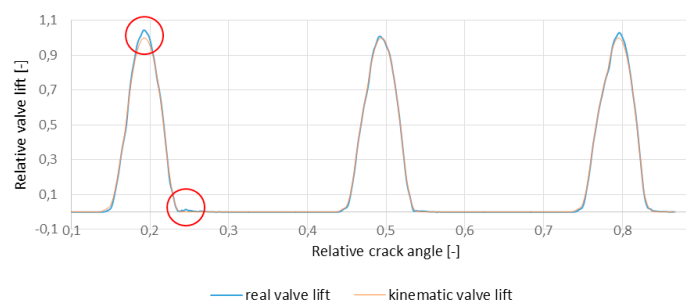


FIGURE 12: Impact of oil pressure loss on valve lift curve
OBRÁZEK 12: Vliv poklesu tlaku oleje na zdvihovou křivku ventilu



for calibration and optimization of the model. The optimal approach seems to be looking for the objective function of the continuous function such as valve acceleration or actual rotation speed curve using a set of reference points and evaluation using the method of minimum value of the sum of the squares of the deviations. Calibration of individual models according to the data measured is more time-intensive also after having used certain simplifications, but a connection thereof leads to the resulting model with a relatively accurate predictability. The holistic approach to the mechanical part of the model seems beneficial in terms of examination of the mutual interactions between the mechanism members. With respect to the uniqueness of the prototype of the experimental engine, the computer model is a useful tool because it makes it possible to simulate conditions which cannot be performed on a test engine because it is still under development. Some design modifications can be made, if applicable. Last but not least, the simulation can prevent conditions where damage could occur to the engine, a fact that has been verified also by several predictive simulations.

ACKNOWLEDGEMENTS

This work was supported by:

- Technological Agency, Czech Republic, programme Centre of Competence, project #TE01020020 Josef Božek Competence Centre for Automotive Industry.
- The Ministry of Education, Youth and Sports program NPU I (LO), project # LO1311 Development of Vehicle Centre of Sustainable Mobility.

LIST OF NOTATIONS AND ABBREVIATIONS

DASY	Design Assistance System
B_D_C	Belt Damping Coefficient
B_E_A	Belt Axial Stiffness
B_E_I	Belt Bending Stiffness
B_S_M	Belt Sectional Mass
B_S_M_I	Belt Sectional Moment of Inertia
B_S_S	Belt Shearing Stiffness
BSFC	Break Specific Fuel Consumption
DOHC	Double Over Head Camshaft
EO	Exhaust Valve Open
IO	Intake Valve Open
RPM	Revolution Per Minute
TQ	Torque
SI	Spark Ignition

REFERENCES

- [1] FISCHER, Thomas a Benjamin SCHAAL. [Holistic Design of a cam phaser](#) [online]. In: 2015, s. 28 [cit. 2017-03-19]. Available from: https://www.gtisoft.com/wp-content/uploads/2015/11/Holistic_Design_Of_A_Cam_Phaser.pdf
- [2] GT-ISE Help, GT-SUITE version 2016, Gamma Technologies Inc., 2015
- [3] TICHÁNEK, Radek. Dasy Based Tool for The Design of Ice Mechanisms. [Journal of Middle European Construction and Design of Cars](#). 2015-01-1, 13(3), doi: 10.1515/mecdc-2015-0013. ISSN 1804-9338.
- [4] RICHTER, David. [Výpočet dynamiky variabilního ventilového rozvodu](#) [Calculation of the variable valve train dynamics]. Praha, 2017. THESIS (by Ing.). Czech Technical University in Prague. Faculty of Mechanical Engineering, Department of Automotive, Combustion Engine and Railway Engineering. Supervisor: Radek Tichánek.



OPTIMIZATION OF 2-STAGE TURBOCHARGED GAS SI ENGINE UNDER STEADY STATE OPERATION

OLDŘICH VÍTEK, JAN MACEK

Czech Technical University in Prague Josef Božek Research Center Technická 4, 166 07 Prague 6, Czech Republic,
Tel.: +420 224 352 507, E-mail: oldrich.vitek@fs.cvut.cz

JIŘÍ KLÍMA, MARTIN VACEK

PBS Turbo Velká Bíteš

ABSTRACT

The proposed paper deals with an optimization of a highly-turbocharged large-bore gas SI engine. Only steady state operation (constant engine speed and load) is considered. The paper is mainly focused on theoretical potential of 2-stage turbocharging concept in terms of performance and limitation. The results are obtained by means of simulation using complex 0-D/1-D engine model including the control algorithm. Different mixture composition concepts are considered to satisfy different levels of NO_x limit – fresh air mixed with external cooled EGR is supposed to be the right approach while optimal EGR level is to be found. Considering EGR circuit, 5 different layouts are tested to select the best design. As the engine control is relatively complex (2-stage turbocharger group, external EGR, compressor blow-by, controlled air excess), 5 different control means of boost pressure were considered. Each variant based on above mentioned options is optimized in terms of compressor/turbine size (swallowing capacity) to obtain the best possible BSFC. The optimal variants are compared and general conclusions are drawn.

KEYWORDS: INTERNAL COMBUSTION ENGINE, MATHEMATICAL MODELING, 0-D/1-D CFD, 2-STAGE TURBOCHARGING, NO_x LIMIT, TA LUFT, EGR, DIFFERENT BMEP CONTROL MEANS

SHRNUTÍ

Práce se zabývá optimalizací vysoce přeplňovaného velkého plynového zážehového motoru. Pouze ustálené režimy (konstantní otáčky a zátěž) jsou uvažovány. Článek je primárně zaměřen na teoretický potenciál dvoustupňového přeplňování z hlediska dosažených parametrů a omezení. Výsledky byly získány pomocí komplexního 0-D/1-D modelu motoru včetně řídicího algoritmu. Různé koncepce složení směsi jsou uvažovány pro dosažení různých limitů pro NO_x – předpokládá se, že správný přístup zahrnuje mísení čerstvé směsi s EGR a hledá se optimální úroveň EGR. Co se týká EGR, tak je testováno celkem 5 variant okruhů EGR, ze kterých se vybírá nejlepší varianta. Protože řízení motoru je relativně komplexní (dvoustupňová plnicí skupina, vnější EGR, přepouštění na straně kompresoru, přebytek vzduchu), je testováno 5 různých způsobů řízení plnicího tlaku. Každá varianta založena na výše uvedených konfiguracích je optimalizována z hlediska velikosti kompresoru/turbíny (hltnost) pro nejlepší měrnou spotřebu. Jsou porovnány optimální varianty a formulovány obecné závěry.

KLIČOVÁ SLOVA: SPALOVACÍ MOTOR, MATEMATICKÉ MODELOVÁNÍ, 0-D/1-D CFD, DVOUSTUPŇOVÉ PŘEPLŇOVÁNÍ, LIMIT NO_x , TA LUFT, EGR, RŮZNÉ ZPŮSOBY ŘÍZENÍ BMEP

1. INTRODUCTION

Large-bore spark-ignited internal combustion engines (SI ICEs) are usually applied as a power source (e.g., electricity). The amount of applications has been increasing significantly in recent decades due to the fact that they can achieve diesel-like efficiency (over 40% of brake efficiency) while keeping pollutant formation at very low level – c.f. [8,24,27,28]. Such performance

is achieved by application of lean mixture concept – air excess is relatively high (more than 1.8 at nominal operating conditions), which lowers both heat losses and NO_x formation while knock resistance is usually improved as well. However, the concept requires that a boost device is able to provide high amount of fresh air. This can be achieved by application



of 2-stage turbocharger group. Theoretical potential of 2-stage turbocharging is relatively high provided that the turbochargers are properly matched with the target engine. Moreover, boost pressure control during fast transient load change is demanding. On top of that, it is expected that future emission limits will (most likely) require application of cooled external EGR concept as it is widely used in passenger cars. All these facts lead to a conclusion that such an engine will be relatively complex from design point of view which requires complex control as well. It is also obvious that close cooperation between ICE manufacturer and turbocharger manufacturer is needed to achieve an optimized design and a proper control.

History of 2-stage turbocharging concept is relatively old due to its application to CI engines (c.f. [5, 6, 10]). Concerning SI engines, it is not the case due to well-known limitations of this engine type (e.g., knocking, uncontrolled auto ignition, high exhaust gas temperature). When considering large-bore SI engines only, the high efficiency single-stage turbochargers, which are able to provide boost pressure over 5.5 bar currently, were a sufficient solution for many decades. However, the recent trend, which requires lowering pollutant (NO_x) formation while improving engine efficiency, enforces the application of the lean-burn concept in combination with non-standard engine cycle (Miller/Atkinson) while increasing engine BMEP (downsizing). This leads to requirement of very high boost pressure, which is beyond the ability of single-stage boost systems. Hence, the worlds first commercial application of 2-stage boost group to a large-bore lean-burn gas SI engine was implemented only recently – in 2010, Jenbacher J624 engine was introduced in a 2-stage configuration (c.f. [28]). There are other 2-stage turbocharged engines being developed by major large-bore SI engine manufacturers (c.f. [3, 8, 24, 27]) while different ignition concepts are considered – classical spark ignition, application of pre-chamber (scavenged version or local fuel enrichment design) or dual fuel approach.

Application of high efficiency boost group (total peak efficiency of 2-stage turbocharger group, which was applied in this paper, is 73% – this value was measured at turbo test rig while running both stages together; moreover, special design HP turbocharger was applied – the design is optimized for 2-stage application) provides high potential for improving both ICE efficiency and engine transient response. It is well-known that turbocharger efficiency is a critical factor in terms of engine BSFC, hence there is always a need to improve it as much as possible c.f. [4, 11, 33, 34, 36]. Moreover, if high values of boost pressure are achievable, non-standard thermodynamic engine cycle can be applied (early/late IVC, which is usually known as Miller/Atkinson thermodynamic cycle). Such cycles allow to decrease effective compression ratio while preserving high expansion ratio –

this has a positive effect on both BSFC and NO_x level of an SI engine (c.f. [9, 12, 23, 24, 26, 27]).

When dealing with requirement to lower NO_x level, there are different technologies available – lowering engine compression ratio, increasing air excess, application of cooled external EGR, advancing combustion towards BDC (late combustion), application of exhaust SCR system, etc. Each of them has its own advantages and disadvantages, moreover there is usually a cost and/or BSFC penalty associated with that. For the case of large-bore gas SI engine, there is an interesting possibility to combine high efficiency boost group with non-standard thermodynamic cycle (early IVC – Miller cycle) and possibly with cooled external EGR to significantly decrease NO_x while preserving low BSFC (very low BSFC penalty).

The presented paper deals with theoretical potential of 2-stage turbocharged gas SI engine in terms of BSFC and NO_x level. The presented work is a part of larger project (national grant of Technological Agency of the Czech Republic, Project TA03011212) which deals with development of 2-stage turbocharger boost group for large-bore ICE applications. The results presented in the paper deal with gas SI engine under steady state operation with fixed valve train parameters.

2. MAIN GOALS

The main target was to evaluate steady state performance of large-bore SI engine in terms of different engine control, different EGR route configurations, different EGR levels and different NO_x levels. The results were obtained by means of detailed thermodynamic simulation. Influence of each factor (engine control, EGR route configuration, applied EGR levels and required NO_x levels) was evaluated by means of sensitivity study – only one parameter was varied while all other ones were kept constant. The evaluation of results is performed by means of relative comparison of tested variants.

Based on that, the following additional goals were set:

- Optimize each variant in terms of turbocharger matching while minimizing BSFC under steady state operation at rated engine load (c.f. Table 1).
- Compare different engine control means in terms of BSFC.
- Compare different configurations of EGR circuit and select the best variant(s).
- Evaluate the influence of required EGR rate with respect to BSFC.
- Evaluate the influence of required NO_x level (defined by means of *TA Luft* norm) in terms of BSFC.
- Propose optimal engine concept in terms of EGR rate and EGR route configuration at different NO_x levels while BSFC is minimal.



TABLE 1: Main engine parameters.
TABULKA 1: Hlavní parametry motoru.

Engine Parameter	Unit	Value
Bore-to-Stroke Ratio	[1]	0.8636
Compression Ratio	[1]	14
Charging	2-stage Turbocharged	
Fuel	Methane	
Number of Intake Valves		2
Number of Exhaust Valves		2
Rated BMEP	[bar]	24
Mean Piston Speed	[m.s ⁻¹]	11

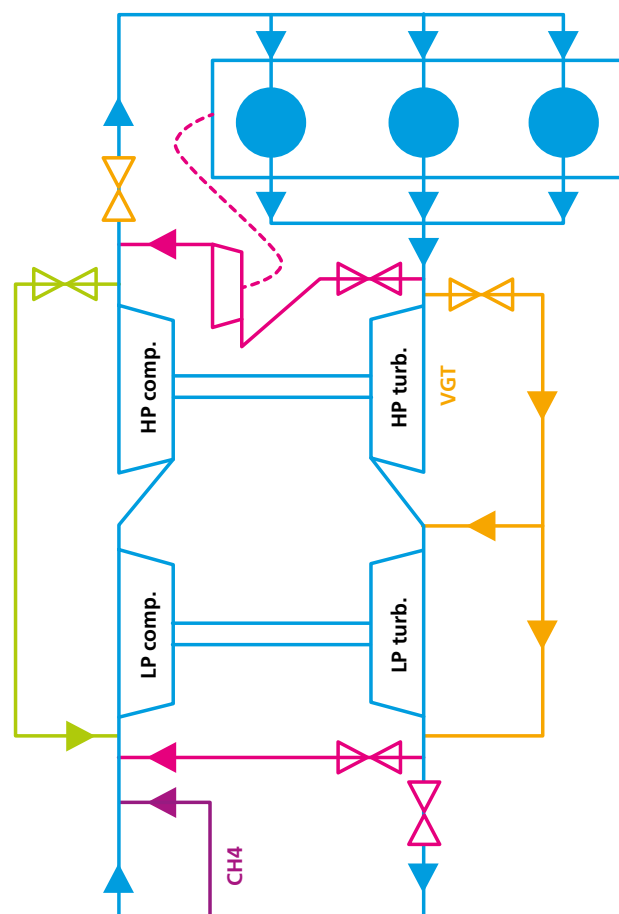
It should be stressed that an optimization/development of a specific engine was not a primary goal of the work. The paper is mainly about theoretical potential of 2-stage turbocharging for the case of lean-burn gas SI engine concept. As the large project has been done in cooperation with a turbocharger manufacturer, the main focus is put on performance and limitation of 2-stage turbocharging concept, hence the interaction between an engine and a boost group is of main interest. It is well-known that selected engine concept, layout of important pipe systems and BMEP control strongly influence a requirement of boost pressure. Extreme cases were tested while maintaining high BMEP requirement (c.f. Table 1) – very high EGR rates, very low NO_x levels. Different EGR configurations and different boost pressure control were analyzed. This enables to evaluate the theoretical potential of the 2-stage turbocharging concept in terms of possible future applications, which is very important for a turbocharger manufacturer.

3. ENGINE MODEL

It was already mentioned that all results presented in the paper were obtained by means of simulation. Sensitivity studies were performed and relative comparison of tested variants was done. Extreme cases in terms of EGR and/or NO_x level were evaluated, which may require very high boost pressure. Such simulation requires a reliable calibrated model as many operating conditions, which were tested by simulation approach, cannot be verified on an existing engine. However, the target engine (c.f. Table 1) does not exist and limited amount of data were available from measurement when similar engine was experimentally verified. All these facts lead to a statement that the applied engine model corresponds to a virtual engine which is defined by means of limited experimental knowledge and experience of the authors with similar engines (i.e., large-bore lean-burn gas SI ICE). This may limit the quality of the prediction in terms of quantities,

however, the qualitative trends are supposed to be captured properly if correct modelling approach was adopted. This mainly concerns the application of predictive submodels. Moreover, the relative comparison of considered variants was done this means that only the differences among tested cases were considered, hence possible modelling errors are compensated. Such approach can provide only qualitative conclusions.

The engine model was build in GT-Power 0-D/1-D code [1] which enables to simulate the whole engine cycle including exhaust gas energy transfer between the cylinders and the turbocharger. Main engine parameters are summarized in



- Air excess control:
 - based on free oxygen (including EGR)
- Compressor blow-by control:
 - customer requirement (tv5%)
 - compressor surge
- BMEP control:
 - intake throttle
 - compressor blow-by ('green' path)
 - waste-gate (2 variants)
 - variable geom. turbine (VGT)
- External cooled EGR control:
 - EGR valve eff. area
 - dedicated EGR compressor driven by electric motor
 - exhaust throttling (if needed)

FIGURE 1: Engine layout with main control circuits (all considered EGR variants are plotted in Figure 5).

OBRAZĚK 1: Konfigurace motoru včetně řídicích okruhů (všechny uvažované EGR varianty jsou vykresleny na Obrázku 5).



Table 1, the engine layout is shown in Figure 1. The engine model is based on existing engine of unspecified manufacturer. Only limited knowledge of the target engine parameters was available, hence unknown information was estimated by the authors using experience with similar engines [15, 25, 29, 32]. The turbocharger manufacturer was able to get some experimental data from engine manufacturer. These data concern the reference engine which is the same as the target engine (Table 1), however, it is equipped with different boost group. Unfortunately, there is not sufficient information to perform a calibration of all important submodels. Moreover, there are some uncertainties regarding important engine operating conditions of the measurement. Based on that, the engine model is based mainly on previous experience with similar engine (internal reports [30, 31] – the model was updated taking into account only reliable information from reference engine measurement. The engine head has 4 valves – 2 intake valves and 2 exhaust valves. The valve lifts and the flow discharge coefficients are based on previous experience (internal reports [30, 31]). The geometry model is based on limited knowledge of the target engine.

Concerning combustion model, no experimental data were available. Simple Vibe function model was applied using the previous experience (internal reports [30, 31]). When not stated otherwise, the combustion duration and timing are constant regardless of engine load, air excess and EGR level. This is obviously simplification, however, results presented in [37] show almost no sensitivity of ROHR with respect to increased external EGR (c.f. Figure 19). On the other hand, it should be stated that relatively low EGR rates were tested (up to 10%) and different ignition system (pre-chamber) was applied. Based on all facts, the authors are convinced that application of non-predictive combustion model has minor influence on optimization of boost group and selection of both proper control and the best EGR configuration. More details to support this statement are presented in *Appendix*.

When performing sensitivity studies, it is necessary to apply models which have predictive ability. Therefore the following models were applied. Simplified finite element (FE) model, which is based on papers [13, 20], is used to calculate combustion chamber temperatures while Woschni formula (c.f. [38]) was applied to estimate the heat transfer coefficient between the in-cylinder gas and the walls (boundary condition for FE model). The simplified FE model is the standard built-in model (labelled 'EngCylTWallSoln') in the commercial code [1] – it calculates temperatures of combustion chamber (liner, piston, head, valves, etc.) based on simplified geometry model and material properties. The advantage of the model is that it can predict wall temperatures based on engine

operating conditions, however, both the FE model and the Woschni one need calibration to provide quantitatively correct results. All necessary model constants were estimated by the authors – they are based on previous experience (internal reports [30, 31]). Mechanical efficiency was calculated using GT-Power formula based on Chen-Flynn model [7], which includes dependency on engine speed, engine square speed and in-cylinder maximum pressure.

Regarding intercooler models (LP and HP), they were built in such a way that outlet fluid temperature was constant (taking into account the temperature of water cooling system dedicated to intake air cooling) while pressure loss at nominal power is approximately 3-5 kPa. By doing this, large and quite efficient intercooler was modelled. EGR cooler model was created in a similar way, however, cooler wall temperature is calculated based on cooler geometry and outer boundary condition (of cooling water temperature).

After a base engine model had been created, the following major modifications were done so that the main targets could be achieved:

- Different EGR systems were added to the model (c.f. Figure 1 and Figure 5). Each EGR circuit consists of EGR valve, piping and EGR cooler. Prescribed EGR rate is of linear dependency on engine load (subFigure (e) of Figure 14) while the label in the text and figures corresponds to maximal EGR requirement (which is for BMEP 24 bar). The expected linear dependency was estimated by the authors to take into account the fact that NO_x formation strongly depends on temperature which is expected to decrease when engine load is decreased.
- Application of NO_x model which considers Zeldovich kinetic mechanism of NO_x formation [39]. Details can be found below in Chapter 3.2.
- Control algorithms of all necessary components which need to be actuated/controlled during the simulations (e.g., compressor by-pass (blow-by), waste-gate, intake throttle, air excess based on experimental data or NO_x level, HP VGT, EGR valve, EGR exhaust throttle, EGR compressor gear ratio). Required air excess is based on experimental data or it is controlled to achieve requested level of NO_x , which is defined by means of TA_{Luft} multiplier – the value of 1.0 means that NO_x level corresponds to the limit defined by TA_{Luft} norm while the value of 0.25 requires that NO_x level has to decrease to 25% of TA_{Luft} norm.

It should be stressed that no knocking or auto-ignition were taken into account. Moreover, little was known about valve timing. It was estimated by means of using limited available experimental data and authors experience. Concerning IVC,



it is expected that Miller cycle is adopted – sensitivity study suggested that relatively strong Miller cycle is applied (IVC, which is defined by 1mm lift, at 55CAdeg BBDC). Many modern large-bore ICEs adopt Miller/Akinson cycle to limit maximum in-cylinder pressure and/or NO_x level while preserving high expansion ratio to obtain low BSFC (c.f. [9, 12, 23, 24, 27, 28]), however, such approach requires high efficiency boost group.

3.1 TURBOCHARGER MODEL

Concerning turbocharger maps, the standard approach was adopted. This means an application of lumped compressor/turbine model(s) using standard maps provided by turbocharger manufacturer. However, the turbocharger manufacturer provided data based on measurement of the whole boost group, which means that both turbochargers were measured simultaneously. It was found that efficiency of HP turbocharger is increased when compared with measurement data of single stage turbocharger only. This is a slightly surprising result, however, the experts from the turbocharger manufacturer explain that by relative decrease of losses when turbocharger is heavily loaded thanks to LP stage, which enables density increase at HP compressor/turbine inlet. This fact, which is based on experimental data, had to be taken into account in the simulation as well. After some discussions with people from the turbocharger manufacturer, it was decided that efficiency multipliers will be applied to HP compressor/turbine using data from experiments this is plotted in Figure 2. At that time, it was not obvious what was a correct parameter which was supposed to determine efficiency scaling. The HP compressor inlet density was selected to be the marker for efficiency

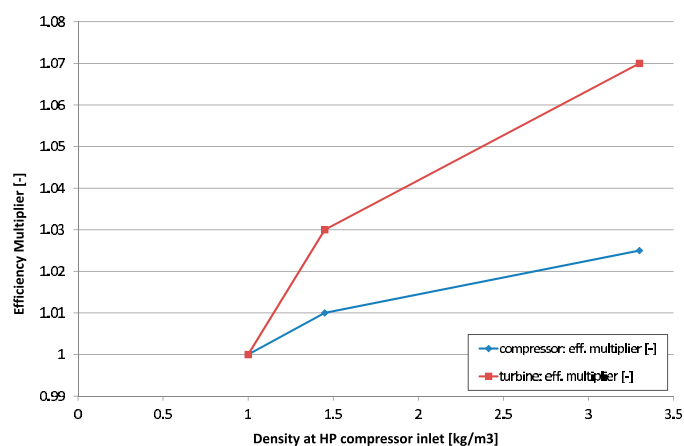


FIGURE 2: Efficiency multipliers of HP turbocharger based on measurements at the turbocharger manufacturer when the whole boost group (HP stage + LP stage) was tested.

OBRÁZEK 2: Násobitele účinnosti pro vysokotlaké turbodmychadlo založené na měřeních u výrobce, kdy byla testována celá plnicí skupina (tj. nízko- i vysokotlaký stupeň).

scaling (it is plotted on horizontal axis of Figure 2). It should be stressed that efficiency increase at high inlet density, which corresponds to high mass flow rate, is relatively significant especially for HP turbine.

Final comment concerns possible application of 1-D radial turbine model which was developed at CTU. The model is based on [14, 16–18] and it was successfully applied in a case of fixed geometry turbine for heavy duty diesel engine and for VGT turbine for medium duty diesel engine. Such model has predictive capability based on 1-D CFD – it can be applied to extrapolate turbine maps or improve turbine model performance under strongly unsteady conditions (including engine transient response). However, the authors doubt that it can predict efficiency increase which was measured (Figure 2). Additional measurements are planned for the future and it would be of advantage if 1-D turbine model can be created and successfully calibrated to improve overall simulation accuracy.

3.2 NO_x MODEL CALIBRATION

Applied NO_x model is a simple model which is based on multi-zone approach and well-known Zeldovich mechanism [39]. The model is a standard built-in one (object 'EngCylNO_x') and it needs to be calibrated with respect to experimental data. The calibration was done using data provided by the turbocharger manufacturer for engine power output in the range from 20% to 100% of rated power (c.f. Figure 3). Reasonable correspondence between measurement and prediction was achieved by means of calibrating only one tuning constant of the model. Similar approach was successfully adopted in previous work (internal report [31] c.f. Figure 4). The NO_x model main calibration parameter (NO_x Calibration Multiplier) is set to the value of 4.448, which is exactly the same value as in the case of internal report [31]. All other calibration parameters remain at their default values. However, it seems that the simple calibration leads to overestimation of NO_x for the low engine load range which leads to a necessity to increase air excess (when compared with measured data) in order to satisfy NO_x limit (*TA Luft* at 100% level).

Predicted engine efficiency is slightly lower and boost pressure is slightly higher when compared with existing experimental data. This is most likely caused by the fact that the boost group is different (the measurement was performed using turbomachinery of another manufacturer) and a lack of experimental results (in-cylinder pressure, intercooler pressure loss, detailed geometry information, intake/exhaust valve lift/discharge coefficient, etc.), which forced the authors to estimate them using the modelling experience with similar



engines. However, the qualitative trends are similar, hence the engine model calibration is considered to be satisfactory taking into account main goals of the paper. On the other hand, the predicted air excess curve has clearly different slope when compared with experimental values – this is not inline with experience gained during previous project (internal report [31] c.f. Figure 4).

Different sensitivity studies were performed to find the reason why NO_x prediction is poor under low engine load conditions. It was found that calibration constants of the model cannot change the slope of predicted air excess (red curve in Figure 3) – they can only shift the curve. The same applies to a case when IVC event was varied – this leads to

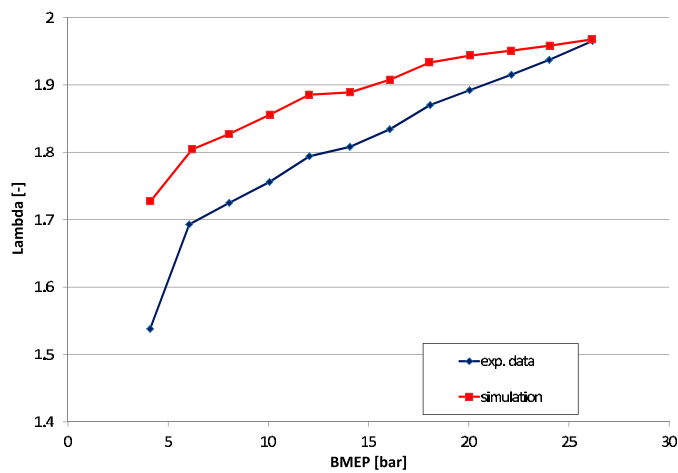


FIGURE 3: Reference engine: comparison of measured and predicted air excess at constant NO_x level (TA Luft = 100%).

OBRÁZEK 3: Referenční motor: srovnání naměřených a vypočtených hodnot přebytku vzduchu pro konstantní úroveň NO_x (TA Luft = 100%).

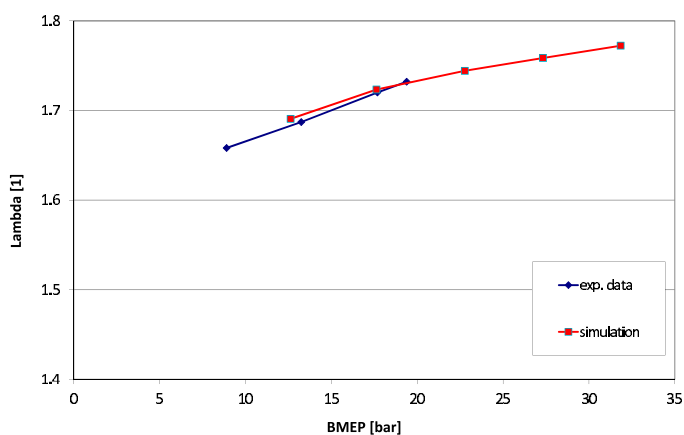


FIGURE 4: Similar large-bore lean-burn gas SI engine: comparison of measured and predicted air excess at constant NO_x level (TA Luft = 100%).

OBRÁZEK 4: Podobný velký plynový zážehový motor: srovnání naměřených a vypočtených hodnot přebytku vzduchu pro konstantní úroveň NO_x (TA Luft = 100%).

curve shifting while the slope is changed only marginally. All the facts indicate that more sophisticated combustion model is needed to properly predict NO_x level at different engine load. Moreover, it is expected that external EGR is supposed to be applied to meet strict emission limits – this also calls for application of advanced combustion model. However, there are not enough experimental data to calibrate such model, hence it was decided not to do that. More details regarding applied combustion model can be found in *Appendix*.

Final comment of NO_x model calibration is that the model is reasonably well calibrated under high engine load (BMEP ≈ 24 bar) and high air excess (≈ 1.9), hence optimizations can be performed at this load/air excess levels while using simple combustion model (constant combustion duration and phasing). The authors also expect that qualitative trends are supposed to be captured properly even for the case of external EGR application. If quantitatively correct prediction is needed, the application of the advanced combustion model is supposed to be necessary – this mainly concerns cases with different engine load and/or different air excess and/or possibly non-zero external cooled EGR level.

4. COMPUTED CASES

The main target of the paper was to optimize boost group (2-stage turbocharger system including its control + external cooled EGR system) of large-bore gas SI engine under steady operation. To achieve that, different types of simulations were performed:

- Standard steady state simulations were carried out at different engine power levels (approximately between 20% and 100% of rated power). The target was to obtain a steady-state solution of all important engine parameters.
- Fine-tuning simulations were carried out to find reasonable constants of the controllers to achieve converged results while all required targets were met. This was actually challenging task as there are usually multiple controllers active during the course of the simulation to achieve different targets simultaneously (BMEP, air excess, compressor blow-by, EGR). Hence, the instability of a single controller leads to oscillations of the remaining ones. Moreover, the dynamic behavior of the whole engine is significantly changed when different turbochargers are applied. Different control strategies are also important. Hence, a lot of simulations were carried out to verify stable model performance so that the optimizations can provide correct answers – in other words: if controller performance leads to instability, the results are not



converged, hence the performance targets are not met which may lead to dropping potentially promising design, which has to be avoided.

- Multi-variable optimizations under steady conditions at maximum required power (Table 1) were performed. Details about the applied optimization procedure can be found below in Chapter 4.3. The target of the optimization was to minimize BSFC while taking into account limiting conditions (e.g. required engine power, air excess, compressor blow-by, EGR). Typically, the following parameters were optimized – 4 multipliers of HP/LP compressor/turbine maps to find the best possible turbocharger combination. Different control strategies, different EGR configurations, different EGR levels and different NO_x levels were considered.

As the paper is mainly focused on theoretical potential of 2-stage boost concept in terms of possible future applications (c.f. Chapter 2), the main outputs of the optimization procedure were mass flow multipliers of HP/LP compressor/turbine. This means that 2-stage boost group performance was verified under extreme cases of high EGR, very low NO_x level while considering different EGR configurations and/or different boost pressure control.

If the engine was the main focus, which was not the case, then important engine design parameters would be optimized – this would concern engine compression ratio, all valve timing events with the special focus on IVC, combustion phasing, etc.

4.1 DIFFERENT ENGINE POWER CONTROL MEANS

The original engine is controlled by means of throttle located downstream of HP intercooler. This control is considered to be the default one, hence if there is no specific label of applied control, the default one was considered. It is labelled in figures and in the paper text as *throttle*. The throttle control is a standard approach to control SI engine power output, however, it is well-known that it is not the optimal one in terms of BSFC. Based on that, other possibilities were considered to quantify potential of BSFC improvement – it should be stressed that the different control means are evaluated from thermodynamic point of view only (no reliability/safety/cost reasons are considered).

The engine was equipped by a compressor by-pass, which is labelled *blow-by*. It connects HP pipe system (the inlet of blow-by system is located downstream of HP intercooler) with the LP one (outlet of blow-by system is positioned upstream of LP compressor). The main reason of the system is to have additional power margin with respect to intake system clogging. Initially the blow-by system is open (the amount of mass flow rate is approx. 5-8% of engine fresh

air flow). Once the intake pipe system pressure losses are increased, the blow-by valve is being closed to keep engine power at the required level. Once the blow-by valve is fully closed, the engine service is required to clean the whole intake pipe system. It is obvious that application of the blow-by is a loss from thermodynamic point of view, however, it is a convenient solution to increase engine service intervals. It is obvious that the system can be applied to control engine power, hence it was considered as a possible engine control mean. From thermodynamic point of view, the compressor blow-by leads to decrease of effective turbocharger efficiency, hence it can easily control boost pressure.

Other possibility is the classical waste-gate approach. The boost pressure is controlled via taking control of turbine power. In the case of 2-stage boost group, there are 2 possibilities. The first one concerns waste-gating of HP stage only – such variant is labelled *WG_HP_only*. The second possibility consists of by-pass of both turbine stages and it is labelled *WG*. It is obvious that waste-gating causes some thermodynamic losses.

Final possibility, which is considered in the report in terms of engine power control, is variable geometry turbine (VGT) at HP stage. Such variant is labelled as *fict_HP_VGT*. The authors are aware of the fact that the turbocharger manufacturer does not consider (at the time of writing the paper) the option to offer HP turbine as a VGT one, hence the label 'fict', which represents fictitious possibility. Moreover, the swallowing capacity of VGT turbine was increased towards higher mass flow rates. This was done due to the fact that certain engine operating conditions require such large turbine, which is not available in reality. This was done to be able to apply the correct HP turbine size in all cases. The *fict_HP_VGT* is considered purely from thermodynamic reasons as it represents the control mean with the lowest thermodynamic loss when compared with all above mentioned control variants.

Based on the text above, 5 different control means are considered. All these variants were fully optimized under different operating conditions to evaluate influence on BSFC. The control stability is also important – certain variants are causing relatively large changes of thermodynamic properties in intake/exhaust HP pipe system(s) which leads to oscillations and possible issues with respect to engine control.

4.2 DIFFERENT EGR ROUTES

The target engine was supposed to be equipped with external cooled EGR system to satisfy more strict limits (*TA Luft*) in terms of NO_x formation. Different EGR routes were examined to evaluate their potential in terms of BSFC penalty due to pressure losses in EGR pipe system. Exhaust gas cooling



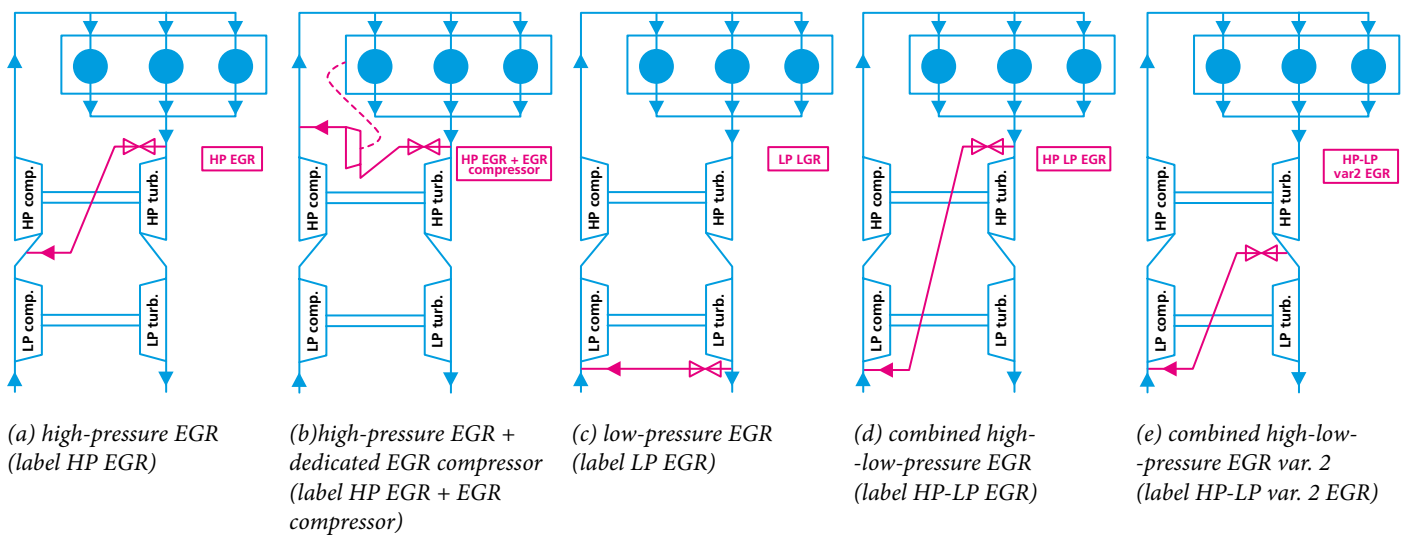


FIGURE 5: Comparison of different EGR configurations and their labelling; there is an exhaust throttle located downstream of LP turbine which is activated whenever the EGR valve is fully opened while EGR requirement is not satisfied.

OBRÁZEK 5: Srovnání různých konfigurací EGR okruhů a jejich označení; za nízkotlakou turbinou je umístěna výfuková škrtící klapka, která se aktivuje kdykoliv je EGR ventil naplno otevřen a přitom není dodržena požadovaná hodnota EGR.

was achieved in EGR cooler. The considered variants are schematically plotted in Figure 5. The EGR rate is controlled via EGR valve – when it is not sufficient, which means that EGR valve is fully opened while EGR requirement is not met, the exhaust throttle flap (located downstream of LP turbine) is being closed to increase pressure level in the exhaust system. It is obvious that such exhaust throttling leads to significant increase of engine BSFC, hence it should be avoided whenever it is possible.

The standard approach is to apply high-pressure EGR circuit which connects HP turbine inlet with HP compressor outlet – this is not possible in this case as boost pressure is significantly higher than exhaust back pressure due to high efficiency of the whole 2-stage boost group. Hence, the high-pressure EGR variant (label *HP EGR*) connects HP turbine inlet with HP compressor inlet – it is plotted in subFigure (a) of Figure 5. The obvious disadvantage of this variant is non-equal mass flow through HP turbocharger as compressor mass flow is higher than turbine one.

Other possibility is to use low-pressure EGR system which connects LP turbine outlet with LP compressor inlet – such variant (labelled *LP EGR*) is shown in subFigure (c) of Figure 5. The advantage of the system is that it uses natural pressure losses in the pipe systems. However, exhaust pressure loss is relatively low for this large-bore SI engine (unlike in the case of automotive ICEs equipped with exhaust gas aftertreatment devices). This leads to low amount of maximum achievable EGR, hence exhaust throttling might be needed when EGR requirement is high. There is one significant advantage of *LP*

EGR system – compressor/turbine mass flow is not negatively affected by required EGR rate.

There are other 2 possibilities of combined EGR systems which connect exhaust pipe with intake one. The variant labelled as *HP-LP EGR* is shown in subFigure (d) of Figure 5 while the variant labelled as *HP-LP var. 2 EGR* is shown in subFigure (e) of Figure 5. Based on experience from automotive applications [36], EGR systems with too high pressure difference are not suitable for low BSFC cases – their advantage is in possibility to achieve high EGR rates while there is high BSFC penalty. This is mainly caused by non-optimal turbocharger performance due to non-equal mass flow rates of compressor/turbine and additional pressure losses caused by throttling in EGR system.

Finally, it was decided to take into account proper HP EGR variant. To achieve that, additional compressor, which is labelled dedicated EGR compressor, is needed to overcome higher pressure in intake system when compared with the pressure of exhaust system. This variant is labelled *HP EGR + EGR compressor* and it is shown in subFigure (b) of Figure 5. The obvious advantage is that compressor/turbine mass flow of both turbochargers is equal and there is no need of throttling at EGR valve as the EGR compressor is supposed to be powered by electrical motor, which is controlled in such a way that required EGR rate is achieved by using the right compressor speed. Disadvantage is the complexity of the system (additional compressor + its control is needed) and higher price. However, such system has potential to provide required very high EGR rate at relatively low BSFC penalty.



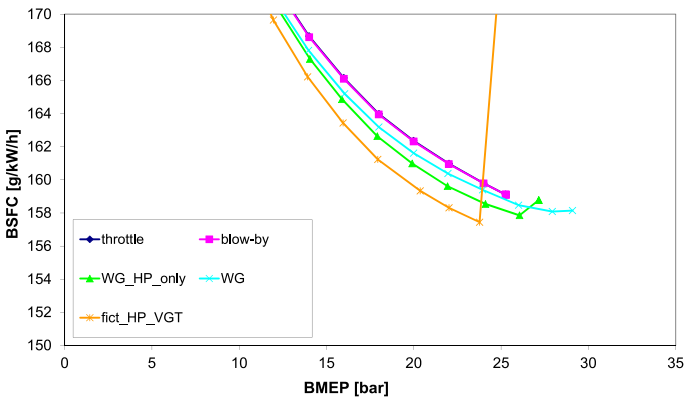
4.3 DESCRIPTION OF OPTIMIZATION PROCEDURE

Optimization is an important target of any simulation project. Properly/reasonably calibrated ICE model can be optimized to achieve improvements in terms of ICE design and/or operation. It is important to create/apply properly designed optimization procedure to achieve required simulation targets.

In this particular case, there are at least 4 independent variables (compressor/turbine swallowing capacity of each turbocharger) and many limits (compressor surge, turbocharger overspeeding checks that required engine operation was reached in terms of BMEP, EGR, NO_x level, air excess). The target is to minimize BSFC. Hence, it is a multi-variable multi-constraint single-target optimization. Genetic algorithm [2] was applied to find the optimal solution.

Once the optimal design is found, ICE load curve (dependency of any parameter on engine load at constant engine speed) is calculated using the optimal setting – this setting is kept constant at any ICE operating point. As the optimization target is to find optimal turbocharger combination in terms of their swallowing capacity to minimize BSFC, the optimization procedure leads to optimal turbocharging matching for the case of considered engine configuration under given operating conditions (BMEP, EGR, blow-by, air excess, etc) – all optimal results presented in the paper concern cases with BMEP=24 bar (c.f. Table 1).

(a) brake specific fuel consumption (detail)



(b) pumping indicated efficiency

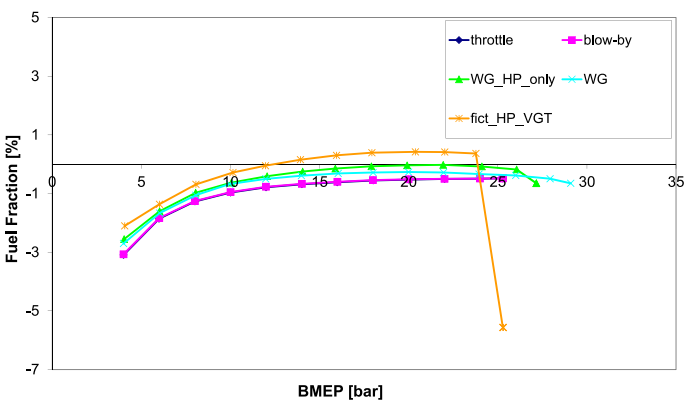
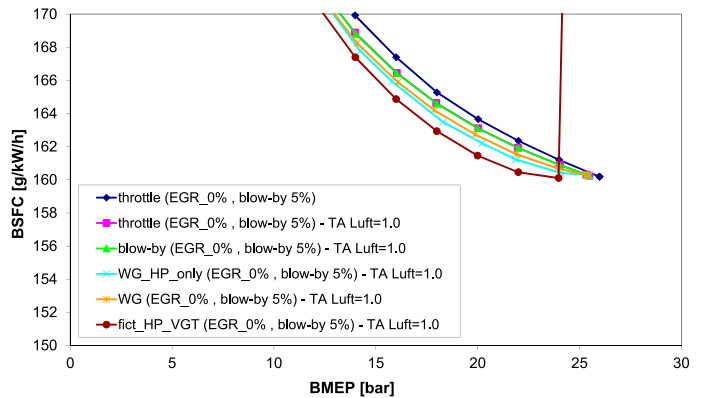


FIGURE 6: Comparison of different control means under steady operation – selected engine output parameters; engine setting: blow-by = 0%, EGR = 0% (at BMEP = 24 bar), prescribed air excess.

OBRÁZEK 6: Srovnání různých způsobů řízení motoru za ustálených podmínek – vybrané výstupní parametry motoru; nastavení: blow-by = 0%, EGR = 0% (pro BMEP = 24 bar), předepsaný průběh přebytku vzduchu.

(a) brake specific fuel consumption (detail)



(b) pumping indicated efficiency

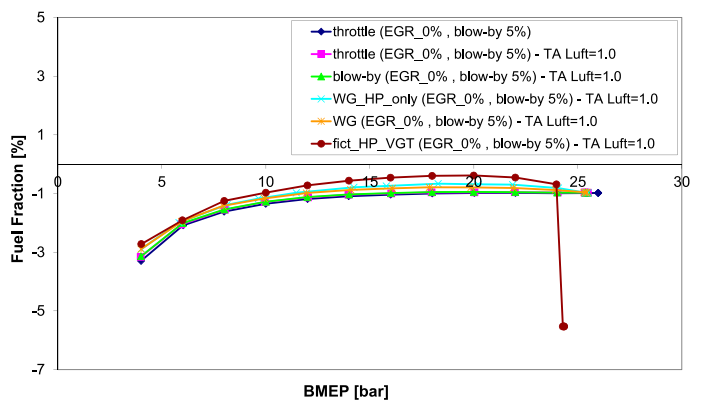
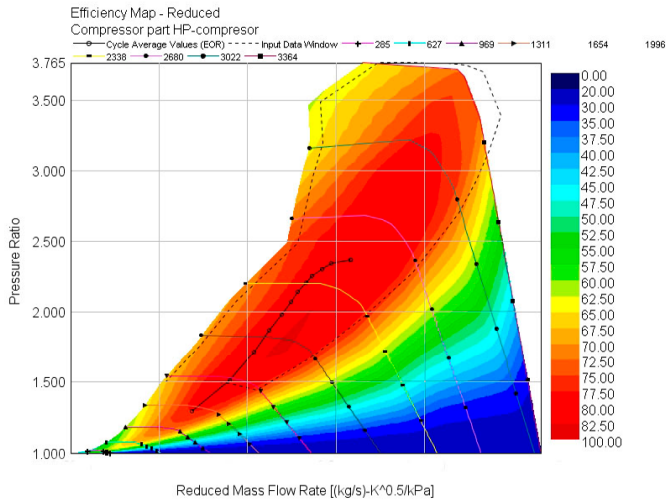


FIGURE 7: Comparison of different control means under steady operation – selected engine output parameters; engine setting: blow-by = 5%, EGR = 15% (at BMEP = 24 bar), prescribed air excess, HP EGR + EGR compressor.

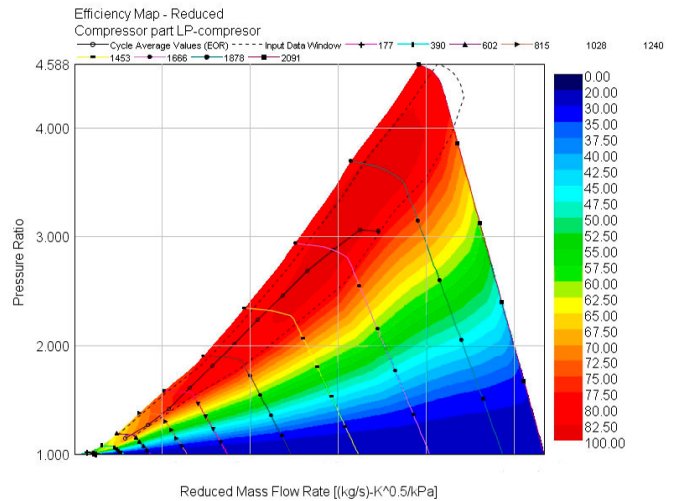
OBRÁZEK 7: Srovnání různých způsobů řízení motoru za ustálených podmínek – vybrané výstupní parametry motoru; nastavení: blow-by = 5%, EGR = 15% (pro BMEP = 24 bar), předepsaný průběh přebytku vzduchu, varianta HP EGR + EGR compressor.



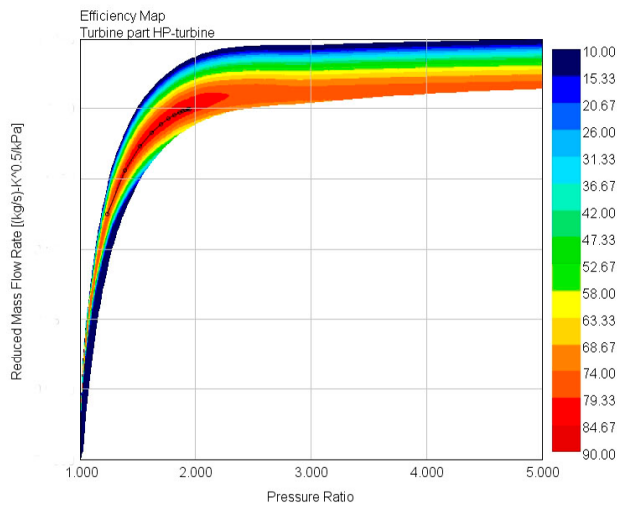
(a) HP compressor



(b) LP compressor



(c) HP turbine



(d) LP turbine

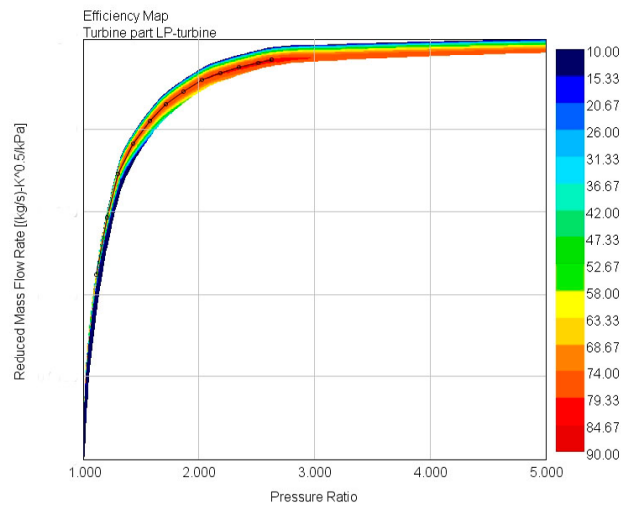


FIGURE 8: HP/LP compressor/turbine maps and operating curves corresponding to engine load curve of the variant throttle in Figure 6 (comment: dark blue curve represents the variant throttle in Figure 6, however, the curve coincide with pink curve of the variant blow-by in terms of BSFC and pumping work).

OBRAZĚK 8: Mapy vysoko- a nízkotlakého kompresoru a turbíny včetně pracovních křivek odpovídajícím zatěžovací charakteristice motoru pro variantu throttle z Obrázku 6 (poznámka: tmavě modrá křivka reprezentuje variantu throttle v Obrázku 6, která je ovšem totožná s růžovou křivkou odpovídající variantě blow-by z hlediska měrné spotřeby paliva a práce na výměnu náplně válce).

5. DISCUSSION OF RESULTS

The presented results are usually based on optimization of turbocharger sizes (mass flow multipliers) at BMEP=24 bar – detailed description of optimization procedure is written above in the Chapter 4.3. After that, engine load data (BMEP is varied between 4 and 30 bar with increment of 2 bar) are calculated keeping constant parameters of the whole engine model while only certain control algorithms are active to satisfy BMEP, air excess, EGR, etc. Maximum calculated BMEP is set to 30 bar to check the potential of a considered variant to reach higher (than requirement in Table 1) power output levels.

Computed cases including labelling of considered variants are briefly described above in the Chapter 4. The most important reasons are commented here to explain trends presented in figures. As there are many considered variants, the Figure description also informs about considered engine configuration (blow-by level, EGR level, NO_x level, etc). The most important information is engine efficiency (BSFC) and the main reason of BSFC differences is usually pumping work, hence these 2 figures are typically shown for each considered case. If needed, additional figures might be presented to



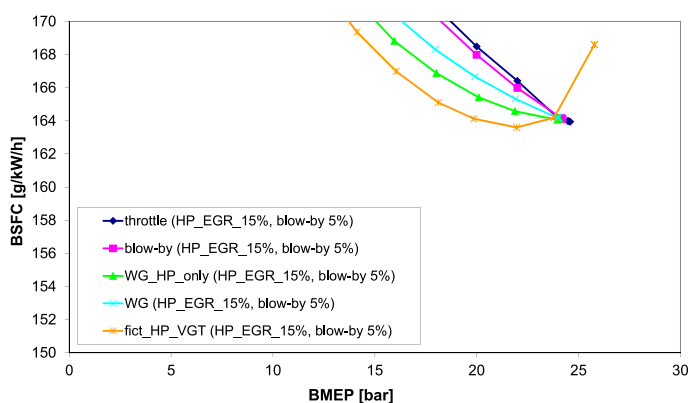
provide additional information. When concerning energy fluxes, they are normalized with respect to total fuel energy – e.g., subFigure (b) of Figure 6 shows *pumping work indicated efficiency* which is pumping work divided by total fuel energy. Positive values represent a gain due to very high efficiency of applied boost group. Detailed description of such normalization procedure of energy fluxes can be found in [33] (Appendix section of that paper).

5.1 INFLUENCE OF ENGINE POWER CONTROL MEANS

Considered means of engine power control are described above in the Chapter 4.1. Optimized results for the case of 0% EGR and 0% blow-by are shown in Figure 6. The difference among the variants in terms of BSFC (subFigure (a) of Figure 6) is small, however, it can be significant and can make a difference when engine is supposed to be run for many years. As expected, the most efficient variant is *fict_HP_VGT* due to the fact that no thermodynamic loss, which is associated with the boost pressure control and it can be quantified by pumping work (c.f. subFigure (b) of Figure 6), is imposed to control HP turbine power. Hence, using VGT means to apply just the right HP turbine size in terms of mass flow to reach boost pressure level which is needed. The main reason for BSFC difference is usually pumping work (subFigure (b) of Figure 6) as high-pressure phase indicated efficiency is very similar for all considered variants. There is almost no difference in heat transfer and mechanical efficiency as well. It is the pumping loss which determines overall brake efficiency. It is interesting to note that the variants *throttle* and *blow-by* are very similar (both variants, i.e., *throttle* and *blow-by*, are very similar in terms of BSFC and pumping losses although the reasons are different – this similarity leads to the fact that both curves, i.e., dark blue for *throttle* and pink one for *blow-by*, coincide) while they are the worst ones in terms of BSFC. Both waste-gate variants are between *fict_HP_VGT* and *throttle* in terms of BSFC while HP waste-gate (variant *WG_HP_only*) is slightly better than waste-gating both turbines (variant *WG*). This is obvious result as exhaust gases, which by-pass HP stage, can be expanded in LP turbine to use some of its internal energy. When using by-pass of both turbines, this is not possible and all the internal energy of by-passing exhaust gases is lost. However, the difference is small due to the fact that optimal turbochargers require only limited waste-gating. There are differences in maximal achievable power. However, this is a side-effect result and it follows expected trend that the variants with higher thermodynamic losses, which are associated with boost pressure control, can reach higher power levels as they have certain amount of a reserve boost pressure (c.f. Figure 8).

Concerning turbocharger performance, the following can be stated. There are relatively small differences of HP turbocharger efficiency which are related to pumping work while LP turbocharger operation is very similar for all variants. Since less efficient variants require higher boost pressure, HP turbocharger speed is higher as well. However, the difference in turbocharger speed and/or efficiency is also related to distribution of PR between HP and LP stage. It was to be expected that LP turbocharger would provide more compression/expansion work as it is more efficient and compressor inlet temperature is not increased (as it is the case for HP compressor due to upstream compression at LP stage). There are significant differences as variants

(a) brake specific fuel consumption (detail)



(b) pumping indicated efficiency

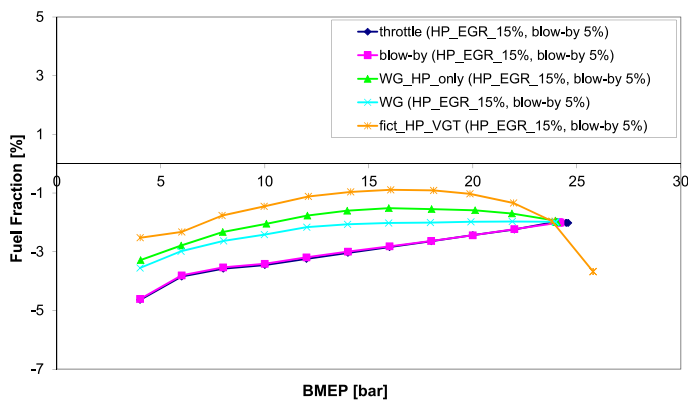


FIGURE 9: Comparison of different control means under steady operation – selected engine output parameters; engine setting: blow-by = 5%, EGR = 0% (at BMEP = 24 bar), TA Luft = 100%, HP EGR + EGR compressor.

OBRAZĚK 9: Srovnání různých způsobů řízení motoru za ustálených podmínek – vybrané výstupní parametry motoru; nastavení: blow-by = 5%, EGR = 0% (pro BMEP = 24 bar), TA Luft = 100%, varianta HP EGR + EGR compressor.



fict_HP_VGT and *WG_HP_only* require more work from LP stage. Concerning compressor surge, it is typical that all variants operate very closely to the surge limit (c.f. Figure 8). The only exception is *blow-by* variant which is much safer in terms of possible surge due to a reason of compressor by-pass application which increases compressor mass flow rate at the same level of PR. The steep increase of most parameters of variant *fict_HP_VGT* for BMEP higher than 24 bar is caused by non-linearity of VGT control.

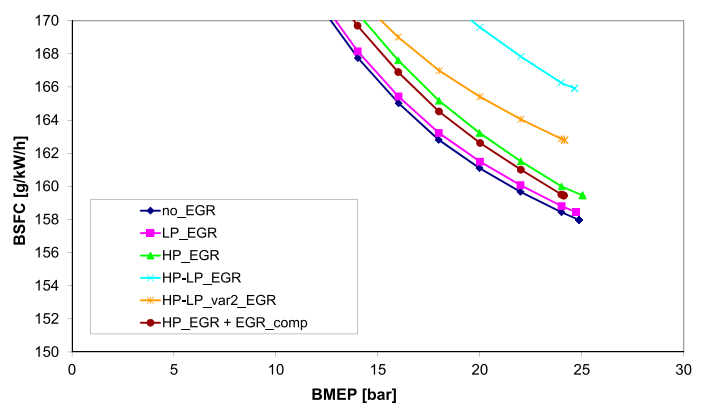
Similar trends can be observed when engine is operated under different conditions in terms of blow-by, EGR and/or air excess (NO_x level) – c.f. Figures 7 and 9. It is usually possible to find suitable turbocharger(s) in terms of their swallowing capacity (realistic mass flow limits of turbocharger(s) were considered as the turbocharger manufacturer provided the maps – these limits are related to design constraints) to provide just the needed boost pressure to achieve required BMEP level – this would lead to the fact that all the variants have the same BSFC at BMEP of 24 bar (c.f. Figure 7). However, such variant (with the exception of *fict_HP_VGT* one) has no boost pressure reserve, hence it would require long time to reach BMEP target, thus being unsuitable for fast engine load changes. The above described differences of BSFC in terms of different control means are magnified when an engine load is decreased, as a boost pressure control is unavoidable. Based on that, the conclusions have general relevance – the most efficient control is the VGT one while the least efficient ones are throttling and compressor blow-by.

5.2 INFLUENCE OF EGR ROUTE CONFIGURATION

Considered EGR variants are summarized above in the Chapter 4.2 and figure 5. The results concerning comparison of all EGR variants are shown in Figure 10. It was expected that the variants with balanced flow (the term *balanced flow* means that mass flow rate through compressor is approximately equal to mass flow rate through turbine) will be better in terms of BSFC – these variants are *LP EGR* (this variant is usually labelled as *LP_EGR* in figures/legend) and *HP EGR + EGR compressor* (this is the default EGR variant, hence no special label is used in figures – it is simply labelled as *EGR* in Figure legend; the only exception is Figure 10, where it is explicitly labelled as *HP EGR + EGR compressor*). The difference between those 2 variants and the one without EGR (labelled as *no_EGR* in the figures) is relatively small, which is caused by low EGR requirement (7.5%). The dominant phenomenon is pumping work. It is significantly worse for variants with non-balanced flow as the turbochargers are not optimized for such operation. Turbine is being overloaded by compressor when the flow is not balanced. The variant

HP EGR + EGR compressor is supposed to be equipped with electrically driven compressor. When dedicated EGR compressor is applied, it requires certain amount of power to pump exhaust gases back into intake system. This energy is supplied from engine crank train taking into account efficiency of electric motor (95%). This energy is related to gas exchange, hence it needs to be considered when analyzing low pressure part of engine work cycle. Based on that, the sum of pumping work and attachment work is plotted in subFigure (b) of Figure 10. The former is related to pressure forces acting on piston during gas exchange, the latter concerns power requirements of dedicated EGR compressor. Hence, such graph (pumping work + attachment power) is shown whenever there is a variant with dedicated EGR compressor.

(a) brake specific fuel consumption (detail)



(b) pumping indicated efficiency + attachment power fuel fraction

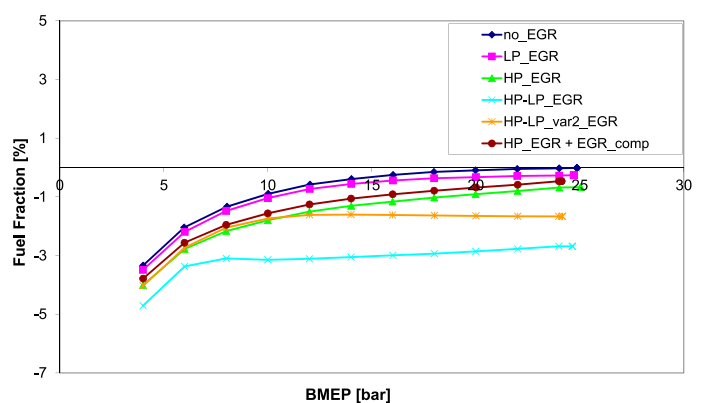
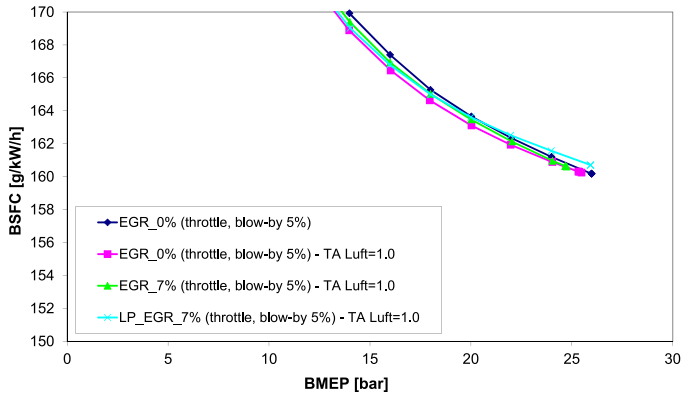


FIGURE 10: Comparison of different EGR variants under steady operation – selected engine output parameters; engine setting: blow-by = 0%, EGR = 7.5% (at BMEP = 24 bar), prescribed air excess.

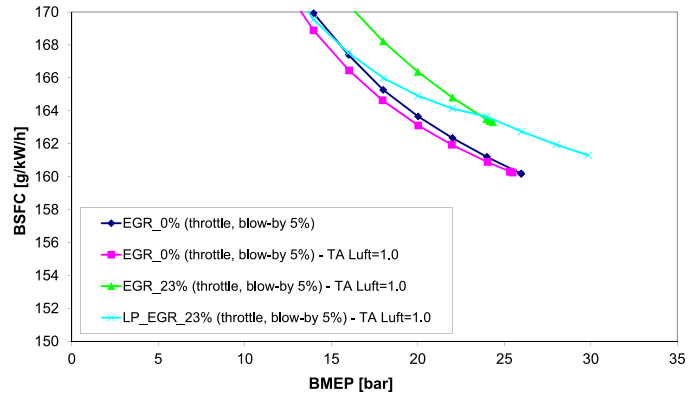
OBRAZĚK 10: Srovnání různých EGR variant za ustálených podmínek – vybrané výstupní parametry motoru; nastavení: blow-by = 0%, EGR = 7.5% (pro BMEP = 24 bar), předepsaný průběh přebytku vzduchu.



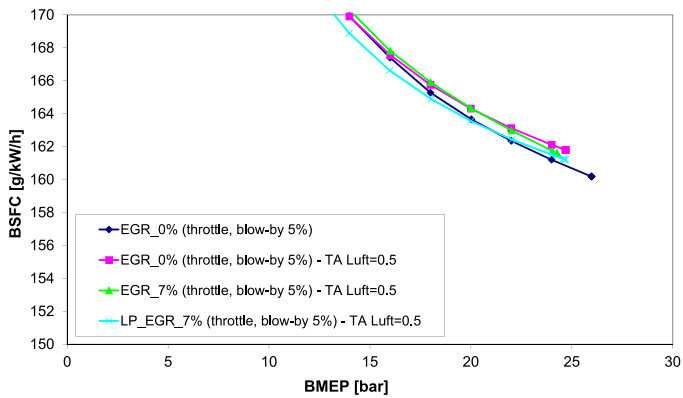
(a) BSFC: req. EGR = 7% at BMEP = 24 bar, TA Luft = 100%



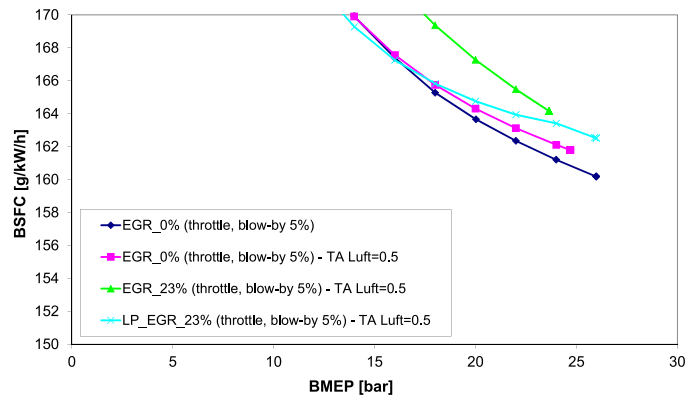
(b) BSFC: req. EGR = 23% at BMEP = 24 bar, TA Luft = 100%



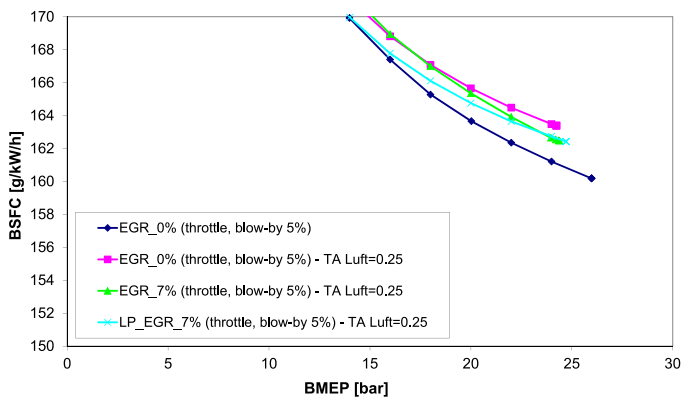
(c) BSFC: req. EGR = 7% at BMEP = 24 bar, TA Luft = 50%



(d) BSFC: req. EGR = 23% at BMEP = 24 bar, TA Luft = 50%



(e) BSFC: req. EGR = 7% at BMEP = 24 bar, TA Luft = 25%



(f) BSFC: req. EGR = 23% at BMEP = 24 bar, TA Luft = 25%

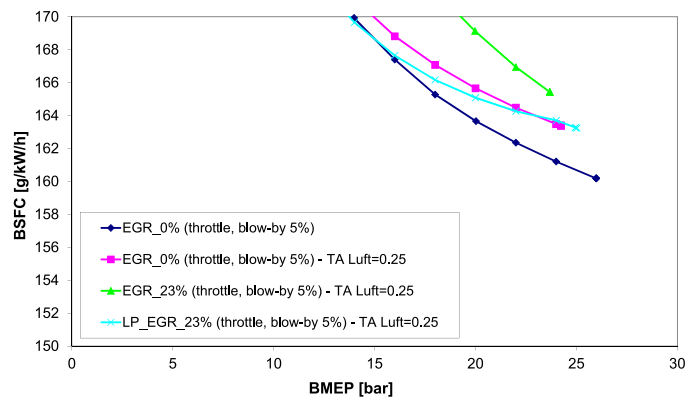


FIGURE 11: Comparison of different EGR configurations at different EGR and/or TA Luft levels under steady operation – selected engine output parameters; engine setting: blow-by = 5%.

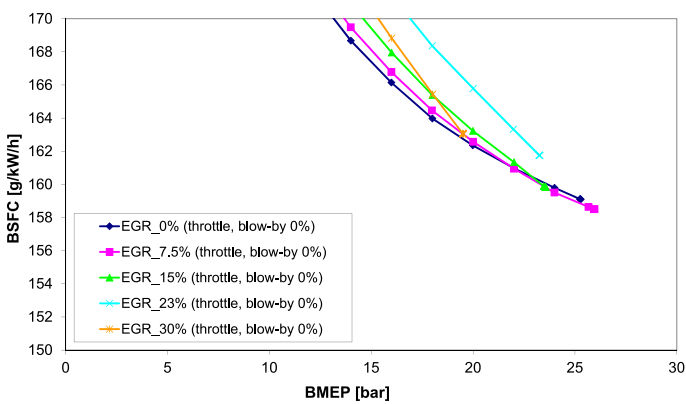
OBRAZĚK 11: Srovnání různých EGR konfigurací pro různé úrovně EGR a/nebo NOx (dle TA Luft) za ustálených podmínek – vybrané výstupní parametry motoru; nastavení: blow-by = 5%.



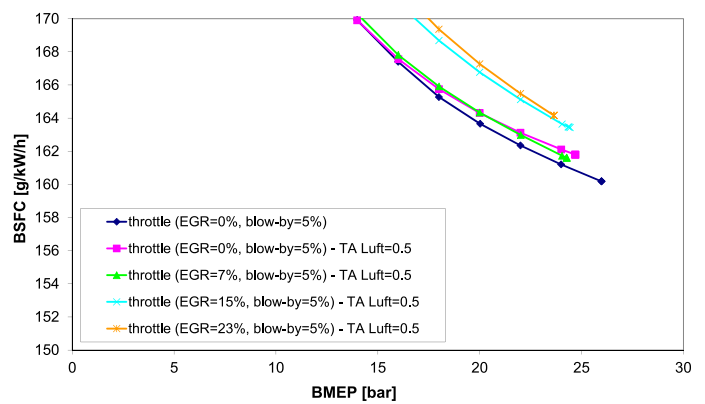
It is no surprise that *LP EGR* is the best variant as it preserves balanced flow while taking advantage of existing pressure losses of exhaust pipe system located downstream of LP turbocharger. Comparison of *HP EGR + EGR compressor* variant with *LP EGR* variant is also presented in Figure 11. This Figure is in-line with the above mentioned facts. Unlike in the previously mentioned cases, where both EGR level and air excess were prescribed, these data concern constant levels of NO_x at different EGR levels. It seems that *LP EGR* variant can satisfy all considered NO_x levels (based on *TA Luft* norm) without additional exhaust throttling, hence it is usually better than *HP EGR + EGR compressor* one. Moreover, as the mass flow increases due to requirement of higher BMEP, natural pressure loss is increased as well, hence *LP EGR*

variant can provide high EGR rate even at very high BMEP levels (≥ 24 bar). On top of that, as the mass flow increases, HP turbine efficiency is increased as well (c.f. Figure 2) which improves both pumping work and maximum achievable power. Both effects are limited in the case of *HP EGR + EGR compressor* application. The higher EGR requirement, the smaller positive effect of HP turbine efficiency increase. Hence, BSFC difference is increased for higher EGR levels making *LP EGR* variant clearly a better one. On the other hand, the variant *LP EGR* is negatively influenced by the fact that LP compressor inlet temperature is increased when non-zero EGR is required which increases compressor work. This effect gets stronger as EGR requirement increases, hence BSFC of *LP EGR* variant might be actually worse (when

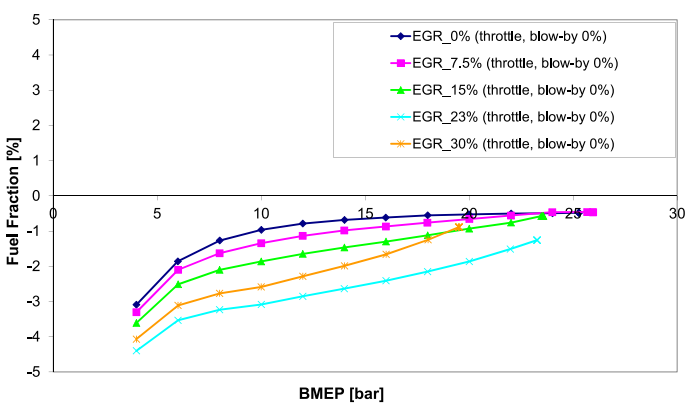
(a) brake specific fuel consumption (detail)



(a) brake specific fuel consumption (detail)



(b) pumping indicated efficiency + attachment power fuel fraction



(b) pumping indicated efficiency + attachment power fuel fraction

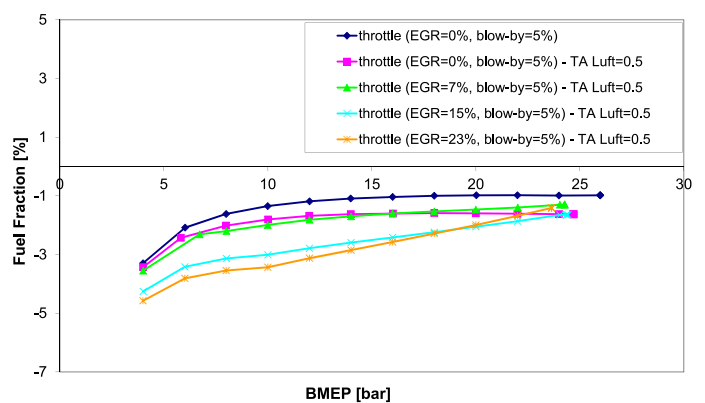


FIGURE 12: Comparison of different amounts of EGR under steady operation – selected engine output parameters; engine setting: blow-by = 0%, prescribed air excess, *HP EGR + EGR compressor*.

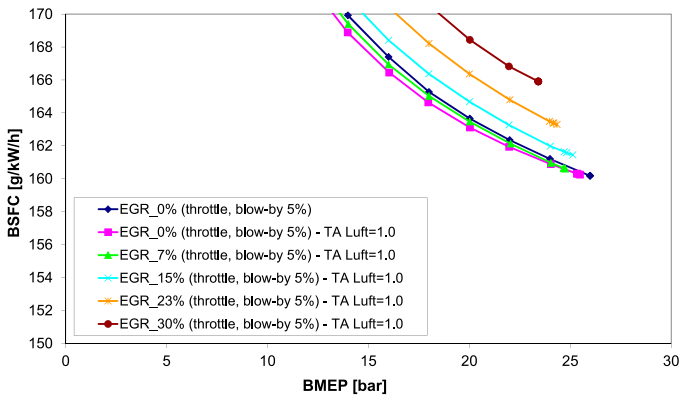
OBRÁZEK 12: Srovnání různých množství EGR za ustálených podmínek – vybrané výstupní parametry motoru; nastavení: blow-by = 0%, předepsaný průběh přebytku vzduchu, varianta HP EGR + EGR compressor.

FIGURE 13: Comparison of different amount of EGR under steady operation – selected engine output parameters; engine setting: blow-by = 5%, TA Luft = 50%, *HP EGR + EGR compressor*.

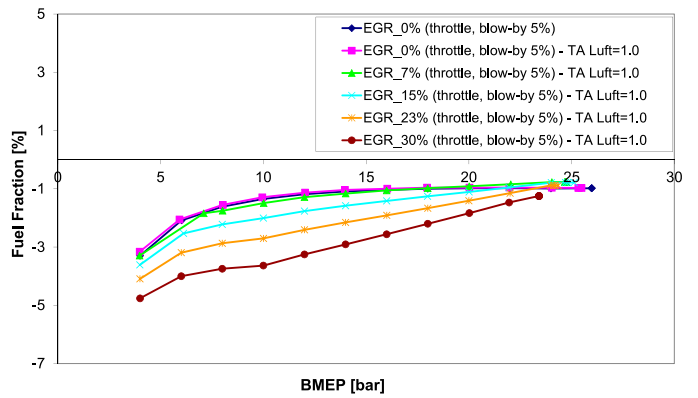
OBRÁZEK 13: Srovnání různých množství EGR za ustálených podmínek – vybrané výstupní parametry motoru; nastavení: blow-by = 5%, TA Luft = 50%, varianta HP EGR + EGR compressor.



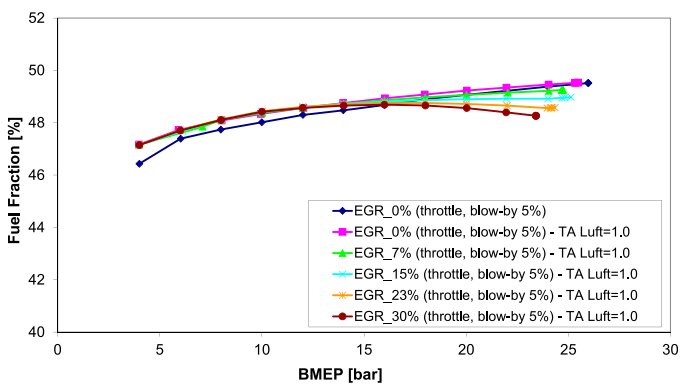
(a) brake specific fuel consumption (detail)



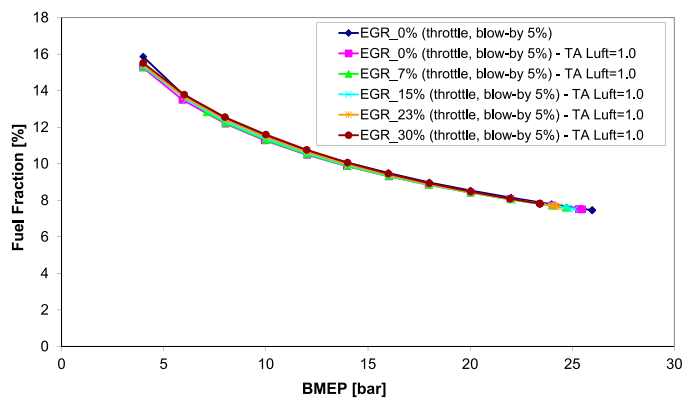
(b) pumping indicated efficiency + attachment power fuel fraction



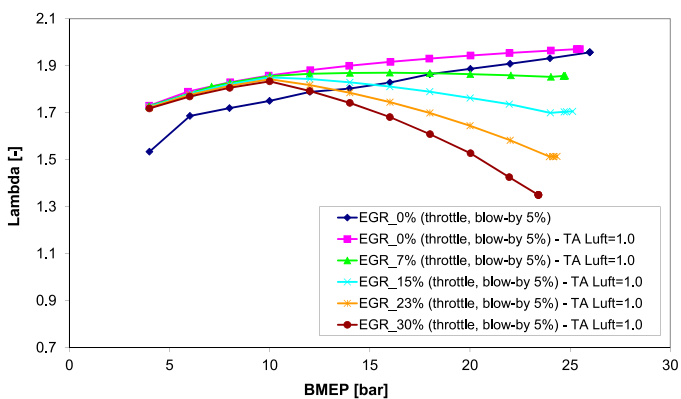
(c) indicated efficiency of HP phase



(d) in-cylinder heat transfer



(e) air excess (based on free oxygen)



(f) total in-cylinder EGR (external + internal)

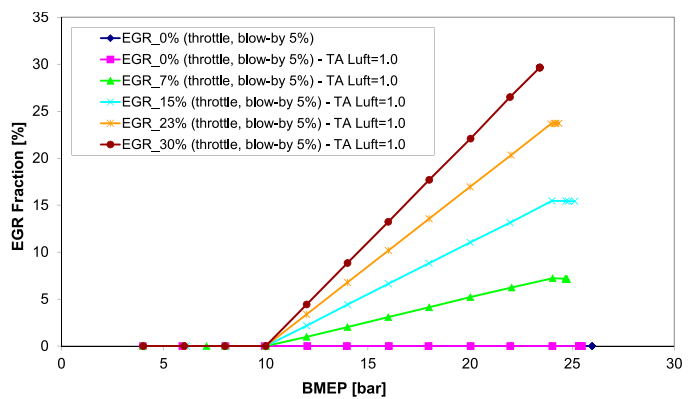


FIGURE 14: Comparison of different amounts of EGR under steady operation – selected engine output parameters; engine setting: blow-by = 5%, TA Luft = 100%, HP EGR + EGR compressor.

OBRÁZEK 14: Srovnání různých množství EGR za ustálených podmínek – vybrané výstupní parametry motoru; nastavení: blow-by = 5%, TA Luft = 100%, varianta HP EGR + EGR compressor.



compared with variant *HP EGR + EGR compressor*) when very high EGR (30%) is required. However, optimal values of EGR rate are in the range between 0 and 10% (c.f. Figure 17). These are low values and the above mentioned effects are relatively small under these conditions.

Based on above mentioned facts, it is expected that both EGR variants are the optimal solution for the target engine while each one has its own advantages and disadvantages. The main advantage of variant *HP EGR + EGR compressor* is the ability to provide almost any EGR requirement. Moreover, it has the shortest geometrical distance for EGR to get from cylinder through exhaust/EGR/intake piping back to cylinder. This is important advantage for transient cases. This enables to minimize transport delays of the system (c.f. [36]). However, large-bore engines are not yet supposed to satisfy pollutant limits under transient operation. The main advantages of variant *LP EGR* are simple design and low BSFC penalty.

5.3 INFLUENCE OF REQUIRED EGR LEVEL

The amount of external EGR is an important factor. It determines engine efficiency and pollutant formation (NO_x). The influence of required EGR level for the case of prescribed air excess is plotted in Figure 12. When EGR requirement is low (0-15%), there is almost no difference in BSFC. Higher EGR rate leads to lower heat transfer losses, hence higher indicated efficiency of engine HP phase (of ICE thermodynamic cycle). Even pumping work is slightly improved due to higher LP stage efficiency and higher boost pressure. However, these positive effects are compensated by power requirement of EGR compressor. The overall effect is that BSFC is very similar at high BMEP level (near 24 bar of BMEP). When EGR requirement is increased, it is more difficult to get enough fresh air into cylinder(s). This

effect was already discussed above and it is related to the fact that the boost group is approaching its limit which causes that boost pressure is limited regardless of exhaust back pressure. This leads to increase of BSFC for higher EGR levels (23 and 30%). Moreover, maximum achievable BMEP is significantly decreased (when EGR requirement is 30%, BMEP target of 24 bar cannot be reached). From thermodynamic point of view, there is an optimum value of EGR for given air excess.

However, the level of NO_x was not considered in the case, which was discussed in the paragraph above. It is obvious that higher EGR level in combination with the same air excess will clearly lead to lower NO_x formation. As the chemical kinetics, which controls NO_x formation, is driven by exponential dependency on temperature, the influence of in-cylinder temperature on NO_x is strongly non-linear. This

effect is supposed to be properly captured by applied multi-zone NO_x model. The comparison of different EGR level cases while NO_x level is constant (*TA Luft* at level of 100%) is shown in Figure 14. From qualitative point of view, the results are the same as for the case of prescribed air excess. The main difference is in air excess and the fact that BSFC increase is already visible for EGR level of 15%. Moreover, BSFC differences are larger due to missing effect of reduced heat transfer, which is visible for the case of prescribed air excess. Hence, the decisive factors are pumping work, which is closely related to the effect of increased HP stage efficiency when mass flow rate is high (more details can be found in Chapter 3.1), attachment work and mixture composition, which influences indicated efficiency of engine HP phase. The effect of mixture composition might be relatively significant as effective mixture LHV and Poisson constant (ratio of specific heat capacity at constant pressure over the capacity at constant specific volume) can change significantly while EGR requirement is varied. This influences in-cylinder pressure pattern which controls piston work. In the case of high EGR rate, Poisson constant is too low, hence pressure increase (due to energy release caused by combustion) is lower when compared with case of low EGR requirement. Concerning heat transfer, there is almost no difference among the variants of different EGR levels. Based on these facts, there is an optimal value of EGR rate in terms of BSFC, which is mainly driven by pumping work and efficiency of engine HP phase.

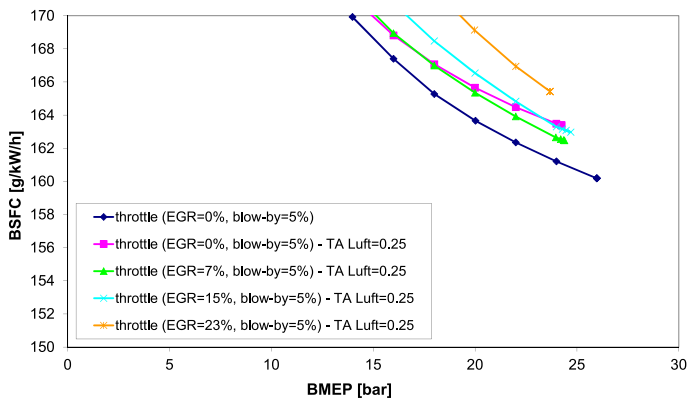
From qualitative point of view, similar trends can be observed for both optimal EGR variants (*LP EGR* and *HP EGR + EGR compressor*) while requiring more strict NO_x limits (at 50% or even 25% of *TA Luft* norm). The influence of required NO_x level is discussed below in Chapter 5.4.

5.4 INFLUENCE OF REQUIRED NO_x LEVEL

The requirement of NO_x level is related to the level of *TA Luft* norm. Hence, 100% of *TA Luft* means that NO_x is just at the limit defined by the norm (500mg of NO_x per cubic meter, recalculated to the level of 5% free oxygen in exhaust gas). The results concerning that (100% of *TA Luft*) are shown in Figure 14. If the limit is set to 50% of *TA Luft*, which is more demanding as the limit is only 50% of original *TA Luft* value, the results are plotted in Figure 13. Finally, even more strict requirement of 25% of *TA Luft* is shown in Figure 15. All these results are plotted in such a way that the lines of different EGR levels are shown. The main reason was to stress that the each requirement of NO_x has its own optimal value of EGR level, which determines fresh air requirement. To get a better idea of the influence of more strict NO_x limit, Figure 16 was created.



(a) brake specific fuel consumption (detail)



(b) pumping indicated efficiency + attachment power fuel fraction

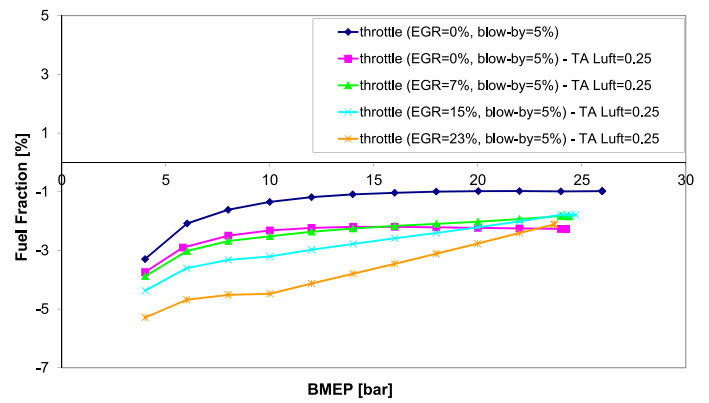
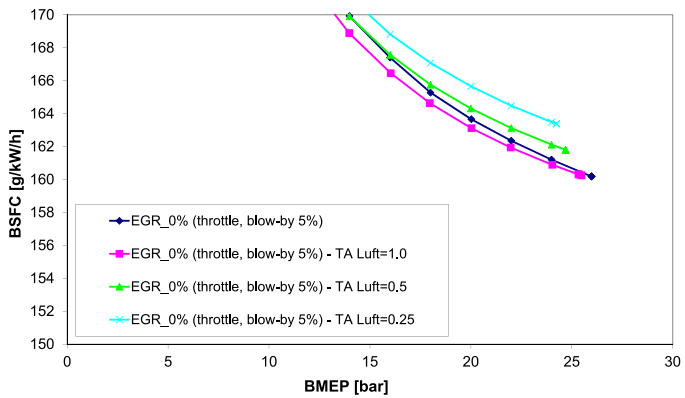


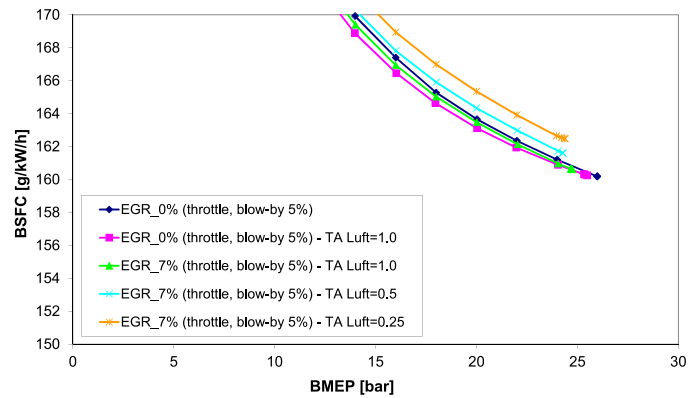
FIGURE 15: Comparison of different amount of EGR under steady operation – selected engine output parameters; engine setting: blow-by = 5%, TA Luft = 25%, HP EGR + EGR compressor.

OBRÁZEK 15: Srovnání různých množství EGR za ustálených podmínek – vybrané výstupní parametry motoru; nastavení: blow-by = 5%, TA Luft = 25%, varianta HP EGR + EGR compressor.

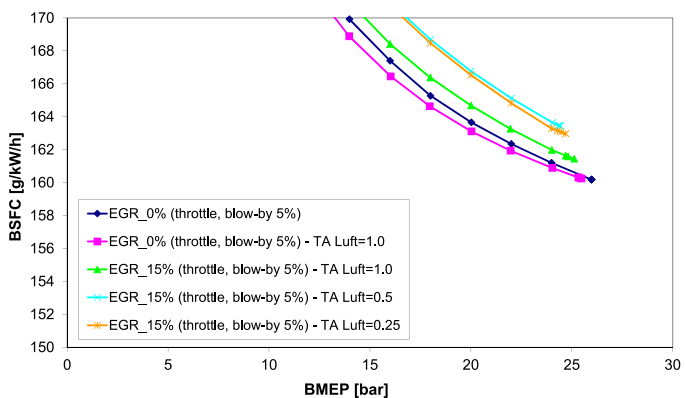
(a) BSFC: required EGR = 0% at BMEP = 24 bar



(b) BSFC: required EGR = 7% at BMEP = 24 bar



(c) BSFC: required EGR = 15% at BMEP = 24 bar



(d) BSFC: required EGR = 23% at BMEP = 24 bar

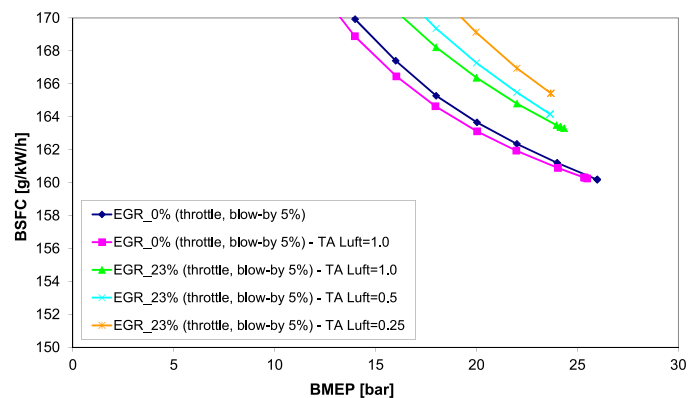
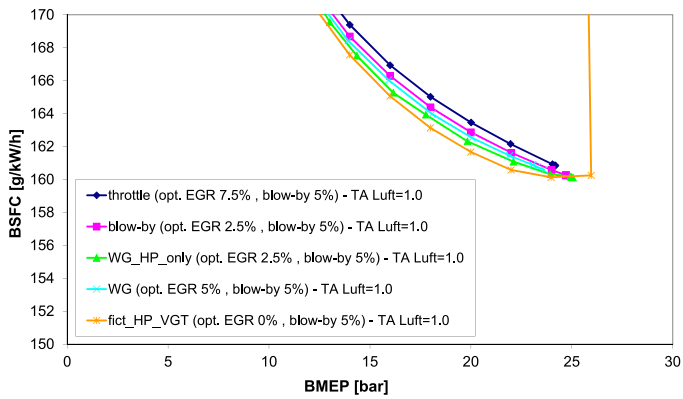


FIGURE 16: Comparison of different NOx levels (based on TA Luft norm) at different EGR levels under steady operation – selected engine output parameters; engine setting: blow-by = 5%, HP EGR + EGR compressor.

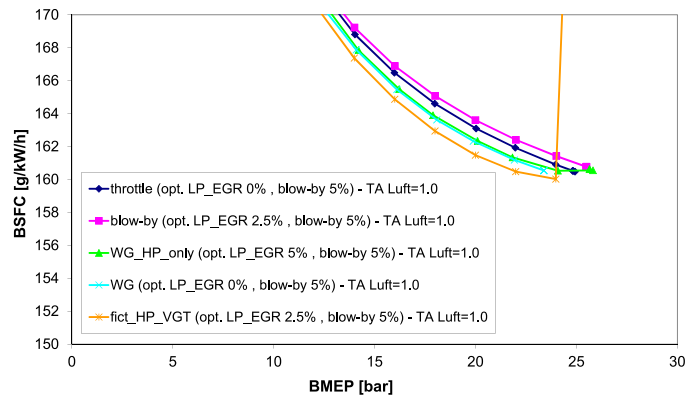
OBRÁZEK 16: Srovnání různých úrovní NOx (dle normy TA Luft) za ustálených podmínek – vybrané výstupní parametry motoru; nastavení: blow-by = 5%, varianta HP EGR + EGR compressor.



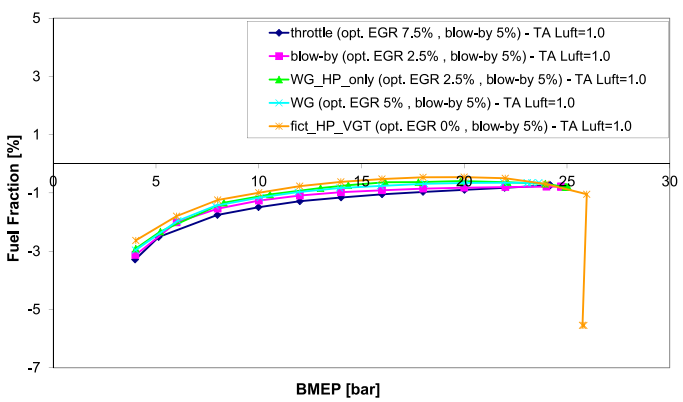
(a) brake specific fuel consumption (detail)



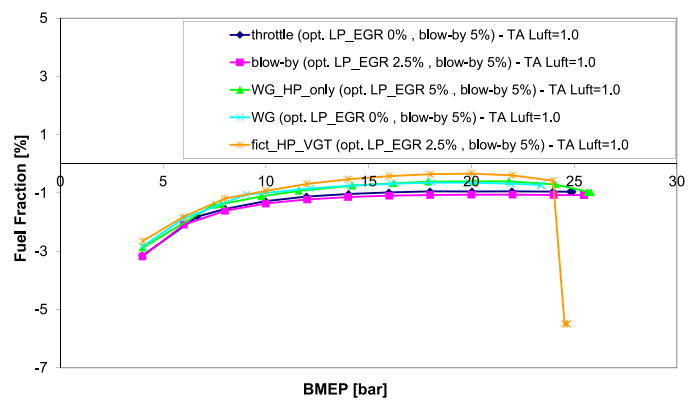
(b) brake specific fuel consumption (detail)



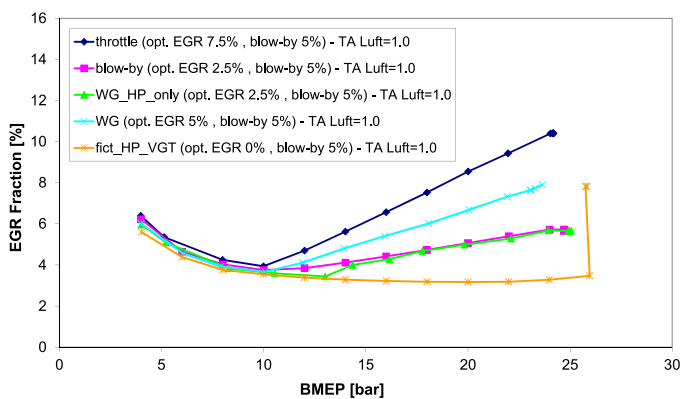
(c) pumping indicated efficiency + attachment power fuel fraction



(d) pumping indicated efficiency + attachment power fuel fraction



(e) total in-cylinder EGR (external + internal)



(f) total in-cylinder EGR (external + internal)

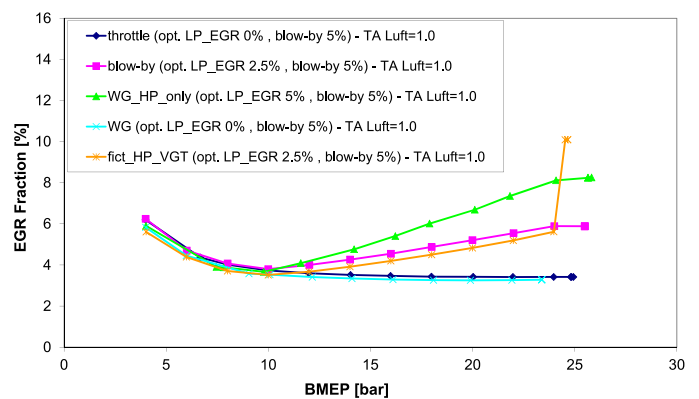


FIGURE 17: Comparison of different control means under steady operation – selected engine output parameters; engine setting: blow-by = 5%, TA Luft = 100%, EGR = optimal, HP EGR + EGR compressor (left column) and LP EGR (right column).

OBRÁZEK 17: Srovnání různých způsobů řízení motoru za ustálených podmínek – vybrané výstupní parametry motoru; nastavení: blow-by = 5%, TA Luft = 100%, EGR = optimální, varianta HP EGR + EGR compressor (levý sloupec) a LP EGR (pravý sloupec).



The subFigure (a) of Figure 16 presents the comparison of all considered variants at external EGR of 0%. For the sake of comparison with other variants, 2 curves of 0% EGR are shown as well – the dark-blue one corresponds to calibrated engine model while pink one was optimized under 100% *TA Luft* requirement. However, there is little difference between those 2 curves in terms of BSFC. Similarly, subFigure (b), subFigure (c) and subFigure (d) corresponds to 7, 15 and 23% of EGR respectively. As expected, more strict requirement leads to higher BSFC as more EGR and/or fresh air is needed to decrease in-cylinder temperature during combustion, hence limiting NO_x formation. It seems that the BSFC penalty is not too high, especially for the case of 7% EGR.

The optimal values of EGR are shown in Figure 17, which concerns the case of NO_x level at 100% of *TA Luft* and different control means. The optimal EGR values are relatively low (typically 5%). Similar trends are observed for lower NO_x levels. If *TA Luft* at 50% is considered, optimal EGR rate varies between 7-10%. If *TA Luft* at 25% is evaluated, optimal EGR requirement is between 10 and 15%. As expected, lower NO_x levels require higher EGR rate, which is also confirmed by Figure 16. When comparing EGR variants (*LP EGR* versus *HP EGR + EGR compressor*), the latter requires slightly higher EGR values. It seems that optimal value of EGR is not higher than 20% even for the case of very low NO_x level (*TA Luft* at 12%). The decisive factor is pumping work which is closely related to the requirement of fresh air. The more strict NO_x limit, the higher air excess. It seems that the best compromise is to use relatively low amount of external EGR in combination with air excess in the range between 1.9 and 2.1. This is related to boost pressure potential of applied boost group, which cannot get much higher due to limits of applied turbochargers, and non-linearity of the whole problem in terms of in-cylinder temperature (NO_x level, heat transfer) and pumping work.

6. CONCLUSIONS

The paper summarizes the results of thermodynamic system simulations of 2-stage turbocharged large-bore lean-burn gas SI engine. The results concern steady state operation of the engine at constant speed. The main goal was to evaluate the potential of 2-stage turbocharging concept in terms of possible future applications, which will require more stringent emission (NO_x) level. This means that sensitivity studies of selected parameters were performed while optimizing boost group configuration in terms of swallowing capacity of HP/LP compressor/turbine. That enables to find an optimal engine concept in terms of mixture quality, EGR circuit configuration and engine control while considering different NO_x levels.

Concerning engine control, the following can be stated. HP stage VGT is the best variant in terms of overall efficiency (BSFC). Classical approach, which is the application of throttle located downstream of HP intercooler, is the worst one. Similar efficiency level can be achieved when engine power is controlled by means of compressor blow-by. Waste-gating is better than throttle control, however, it is worse than VGT one. The differences are not huge, however, they cannot be neglected. The dominant factor is pumping work. As the boost group approaches its limit in terms of maximum achievable boost pressure, which is basically driven by requirement of air excess or/and external EGR, the differences among the variants become smaller at BMEP of 24 bar.

Dealing with optimal configuration of EGR circuit, the variants *HP EGR + EGR compressor* and *LP EGR* are the best ones. Both of them keep balanced flow through turbochargers. This means that compressor mass flow is almost the same as turbine one. This is very important as the turbochargers are designed in that way. When using other options (variants *HP EGR*, *HP-LP EGR*, *HP-LP var. 2 EGR*), this assumption is not satisfied which leads to significantly worse pumping work, hence worse BSFC. When comparing the best EGR variants, there is little difference between them when EGR requirement is low (up to 10%) as negative effects, which are related to application of external EGR, are relatively low. However, when EGR rate is increased, *LP EGR* becomes slightly better. If the requirement of EGR is too high, the pressure difference between exhaust system and intake one is not sufficient and the only way to satisfy EGR requirement is to apply exhaust throttling which leads to exhaust back pressure increase, hence BSFC increase. The final selection of EGR variants is not a clear cut. Under certain operating conditions, *LP EGR* variant is better while *HP EGR + EGR compressor* one is more convenient in all other cases. It should be stressed that the variant *HP EGR + EGR compressor* requires dedicated EGR compressor, the speed of which is supposed to be controlled by electric motor. This increases cost and control complexity.

Regarding the influence of required NO_x level, the dependency is obvious – the more strict requirement, the higher BSFC. Moreover, each NO_x level has its own optimal combination of EGR and air excess. To satisfy *TA Luft* of 100%, it seems that no external EGR is needed as optimal EGR rate is low, which is typically 2.5-5% depending on applied BMEP control. When *TA Luft* of 50% is required, EGR level about 7–10% is the optimal value while at *TA Luft* of 25%, EGR level between 10 and 15% is expected to be the best choice. Simulation results also suggest that significant lowering of a NO_x limit leads to relatively low BSFC penalty. This is caused by non-linearity effects and by the fact that HP turbine efficiency increases when mass flow is increased. Based on these facts, the optimal strategy seems to



be a combination of relatively low external EGR with relatively high air excess. That is enabled by high efficiency 2-stage boost group which is able to provide very high boost pressure. This is needed to achieve both low NO_x level and high thermodynamic efficiency due to application of Miller cycle.

When evaluating the potential of 2-stage turbocharging approach for the case of large-bore lean-burn gas SI engine, the following can be stated. It can provide very high boost pressure, hence extreme cases of required EGR and/or NO_x level can be satisfied while meeting high BMEP requirement. Moreover, strong Miller cycle (early IVC) was applied in all tested cases, which increases requirement of boost pressure even more. Although the efficiency of applied 2-stage boost group is relatively high as the considered turbochargers have state-of-the-art performance parameters, it has its limits. Once these limits are approached, engine BSFC starts to increase significantly. This negative phenomenon has to be avoided. This can be achieved by careful optimization of the whole engine. Not only turbochargers, but other important parameters should be taken into account as well including EGR configuration, engine compression ratio, intake/exhaust valve timing, etc. This was not done – the paper primarily focuses on optimization of boost group while evaluating different concepts in terms of EGR level, EGR circuit configuration, engine control and NO_x level. Concerning boost pressure control, it is definitely more demanding when compared with single-stage boost group. Especially the variants, which change pressure distribution between stages (i.e., *fict_HP_VGT* and *WG_HP_only*), can be tricky in terms of stable BMEP control.

Final comment concerns optimal size of applied compressor/turbine of each turbocharger. Regarding compressors (both HP and LP stage), the optimal size is very similar for all considered variants regardless of BMEP control, EGR route configuration or NO_x level. This is not a surprise as the engine geometry parameters are fixed. This mainly concerns valve timing (especially IVC). Dealing with HP turbine, its optimal size changes relatively strongly. When NO_x level is decreased, HP turbine size is decreased as well and it is always slightly smaller for the EGR variant *HP EGR + EGR compressor*. This statement is also predictable as lower NO_x requires higher boost pressure. When comparing both EGR variants, it is obvious that *HP EGR + EGR compressor* variant needs smaller HP turbine as its mass flow rate is smaller due to EGR. Optimal LP turbine size varies only slightly – typically it is within 10%. Moreover, it was verified that its influence on BSFC is very low, hence the same turbine can be applied to all optimal cases without any significant BSFC penalty. It also follows expected trend that slightly larger LP turbine is needed for the variant *LP EGR*. Based on all available facts, the most dominant factor is HP turbine size.

REFERENCES

- [1] *GT-Power User's Manual, GT-Suite version 7.3*. Gamma Technologies Inc., 2012.
- [2] *modeFRONTIER – Multi-Objective Design Environment, version 4.4.3*. [CD-ROM], 2012.
- [3] Behr, T., Kahi, M., Reichl, A., and Hubacher, M. *Second Generation of Two-stage Turbocharging Power2 Systems for Medium Speed Gas and Diesel Engines*. Proceedings: Conseil International Des Machines A Combustion (CIMAC) Congress 2013, Shanghai, May 2013. Paper No.: 134.
- [4] Bogomolov, S., Doleček, V., Macek, J., Mikulec, A., and Vitek, O. *Combining Thermodynamics and Design Optimization for Finding ICE Downsizing Limits*. SAE Technical Paper Series, April 2014. Paper 2014-01-1098, doi: 10.4271/2014-01-1098.
- [5] Bozung, H. G. *Zweistufige Aufladeaggregate – Wirkungsgrade und Gefälleaufteilung im Hinblick auf Vollastund Teillastbetrieb*. MTZ, 39(5):209–215, 1978.
- [6] Bozung, H. G. *Die M.A.N.-Turboladerbaureihe NA und NA-VP für ein- und zweistufige Aufladung*. MTZ, 41(4): 125–133, 1980.
- [7] Chen, S. and Flynn, P. *Development of a Single Cylinder Compression Ignition Research Engine*. SAE Technical Paper Series. Paper 650733, doi: 10.4271/650733.
- [8] Christen, C. and Brand, D. *IMO Tier 3: Gas and Dual Fuel Engines as a Clean and Efficient Solution*. Proceedings: Conseil International Des Machines A Combustion (CIMAC) Congress 2013, Shanghai, May 2013. Paper No.: 187.
- [9] Fiedler, M., Fiedler, H., and Boy, P. *Experimental Experience Gained with a Long-Stroke Medium-Speed Diesel Research Engine using Two Stage Turbo Charging and Extreme Miller Cycle*. Proceedings: Conseil International Des Machines A Combustion (CIMAC) Congress 2013, Shanghai, May 2013. Paper No.: 253.
- [10] Izumi, S. and Hirayama, Y. *Two-Stage Turbocharged MITSUBISHI UE-E Type Diesel Engine*. Journal of the Japan Society of Mechanical Engineers, 79(694):864–869, 1976.
- [11] Kesgin, U. *Effect of Turbocharging System on the Performance of a Natural Gas Engine*. Energy Conversion and Management, Vol. 46(1):11–32, January 2005. ISSN 01968904, doi: 10.1016/j.enconman.2004.02.006.
- [12] Kesgin, U. *Efficiency Improvement and NO_x Emission Reduction Potentials of Two-Stage Turbocharged Miller Cycle for Stationary Natural Gas Engines*. International Journal of Energy Research, Vol. 29(3):189–216, March 2005. ISSN 0363907X, doi: 10.1002/er.1048.



- [13]Lowe, A. and Morel, T. *A New Generation of Tools for Accurate Thermo-Mechanical Finite Element Analyses of Engine Components*. SAE Technical Paper Series, March 1992. Paper 920681, doi: 10.4271/920681.
- [14]Macek, J., Vávra, J., and Vítek, O. *1-D Model of Radial Turbocharger Turbine Calibrated by Experiments*. SAE Technical Paper Series, March 2002. Paper 2002-01-0377, doi: 10.4271/2002-01-0377.
- [15]Macek, J. and Vítek, O. *Contribution to Thermodynamic Design of Highly Turbocharged Engines*. In: KoKa 2007, Bratislava, SR [CD-ROM], 2007.
- [16]Macek, J. and Vítek, O. *Simulation of Pulsating Flow Unsteady Operation of a Turbocharger Radial Turbine*. SAE Technical Paper Series, April 2008. Paper 2008-01-0295, doi: 10.4271/2008-01-0295.
- [17]Macek, J., Vítek, O., Burič, J., and Doleček, V. *Comparison of Lumped and Unsteady 1-D Models for Simulation of a Radial Turbine*. SAE Technical Paper Series, April 2009. Paper 2009-01-0303, doi: 10.4271/2009-01-0303.
- [18]Macek, J., Vítek, O., and Žák, Z. *Calibration and Results of a Radial Turbine 1-D Model with Distributed Parameters*. SAE Technical Paper Series, April 2011. Paper 2011-01-1146, doi: 10.4271/2011-01-1146.
- [19]Millo, F., Bernardi, M. G., and Delneri, D. *Computational Analysis of Internal and External EGR Strategies Combined with Miller Cycle Concept for a Two Stage Turbocharged Medium Speed Marine Diesel Engine*. SAE International Journal of Engines, Vol. 4(1):1319–1330, 2011. Paper 2011-01-1142, doi: 10.4271/2011-01-1142.
- [20]Morel, T., Rackmil, C., Keribar, R., and Jennings, M. *Model for Heat Transfer and Combustion in Spark Ignited Engines and its Comparison with Experiments*. SAE Technical Paper Series, March 1988. Paper 880198, doi: 10.4271/880198.
- [21]Škarohlíd, M. *Modelling of Influence of Biogas Fuel Composition on Parameters of Automotive Engines*. In: *Modeling of SI and Diesel Engines*, April 2010. ISBN 978-0-7680-3418-9.
- [22]Škarohlíd, M. *The Positive Influence of CO₂ in Fuel on Engine Parameters*. Journal of Middle European Construction and Design of Cars (MECCA), (01/2011): 26–31, 2011. ISSN 1214-0821.
- [23]Okamoto, K., Zhang, F.-R., Shimogata, S., and Shoji, F. *Development of a Late Intake-Valve Closing (LIVC) Miller Cycle for Stationary Natural Gas Engines – Effect of EGR Utilization*. SAE Technical Paper Series, March 1997. Paper 972948, doi: 10.4271/972948.
- [24]Sander, U., Menzel, S., and Raindl, M. *The New MTU Type L64 of Series 4000 Gas Engines*. Proceedings: Conseil International Des Machines A Combustion (CIMAC) Congress 2013, Shanghai, May 2013. Paper No.: 67.
- [25]Takats, M. and Macek, J. *Vehicle Lean Mixture Gas Engines*. Proceedings: Conseil International Des Machines A Combustion (CIMAC) Congress 1993, London, May 1993.
- [26]Tinschmann, G., Birgel, A., Trapp, C., Schnessl, E., Redtenbacher, C., and Wimmer, A. *Large Gas Engines – 75 mg/Nm³@15%O₂ NO_x 'Engine-Internal Measures or Exhaust Aftertreatment?'*. Proceedings: Conseil International Des Machines A Combustion (CIMAC) Congress 2013, Shanghai, May 2013. Paper No.: 296.
- [27]Trapp, C., Birgel, A., Spyra, N., Kopecek, H., and Chvatal, D. *GE's All New J920 Gas engine – a Smart Accretion of Two-stage Turbocharging, Ultra Lean Combustion Concept and Intelligent Controls*. Proceedings: Conseil International Des Machines A Combustion (CIMAC) Congress 2013, Shanghai, May 2013. Paper No.: 289.
- [28]Trapp, C., Klausner, J., and Lang, J. *J624 – der weltweit erste Gasmotor mit zweistufiger Aufladung*. MTZ, 2011.
- [29]Vítek, O. and Macek, J. *The Influence of Ambient Conditions on a Turbocharged Gas Internal Combustion Engine*. In: KoKa 2001, Brno, 2001.
- [30]Vítek, O. and Macek, J. *2-stage Turbocharger Matching for Largebore Gas SI Engine*. Internal report for Project FI-IM3/213: Z 06-17, CTU in Prague, Prague, 2006.
- [31]Vítek, O. and Macek, J. *Study on 2-stage Turbocharging of Gas SI Engine*. Internal report for Project FI-IM3/213: Z 07-05, CTU in Prague, Prague, 2007.
- [32]Vítek, O. and Macek, J. *Optimization of 2-stage Turbocharged Large Bore SI Engine*. In: KoKa 2008, Brno, [CD-ROM], 2008.
- [33]Vítek, O. and Macek, J. *Feasibility of 2-stroke SI Engine Concept using Stoichiometric Mixture*. Journal of Middle European Construction and Design of Cars (MECCA), Volume VIII. (01/2010):11–30, 2010. ISSN 1214-0821.
- [34]Vítek, O., Macek, J., Doleček, V., Bogomolov, S., Mikulec, A., and Barák, A. *Realistic Limits of ICE Efficiency*. In: Proceedings of FISITA 2014 [CD-ROM], June 2014. Paper Code: F2014-CET-051.
- [35]Vítek, O., Macek, J., and Polášek, M. *Simulation of Pre-Chambers in an Engine Combustion Chamber Using Available Software*. SAE Technical Paper Series, March 2003. Paper 2003-01-0373, doi: 10.4271/2003-01-0373.
- [36]Vítek, O., Macek, J., Polášek, M., Schmerbeck, S., and Kammerdiener, T. *Comparison of Different EGR Solutions*. SAE Technical Paper Series, April 2008. Paper 2008-01-0206, doi: 10.4271/2008-01-0206.



- [37]Wimmer, A., Pirker, G., Zelenka, J., Chmela, F., Zurlo, J., and Trapp, C. *The Potential of Exhaust Gas Recirculation in Large Gas Engines*. Proceedings: Conseil International Des Machines A Combustion (CIMAC) Congress 2013, Shanghai, May 2013. Paper No.: 271.
- [38]Woschni, G. *An Universally Applicable Equation for the Instantaneous Heat Transfer Coefficient in the Internal Combustion Engine*. SAE Transactions, Vol. 76:3065, 1967.
- [39]Zeldovich, Y. B. *The Oxidation of Nitrogen in Combustion and Explosions*. In: Acta Physicochim, USSR, 21:557–628, 1946.

ACKNOWLEDGMENTS

This research has been realized using the support of Technological Agency, Czech Republic, Project *TA03011212*: "Vývoj dvoustupňové plnicí skupiny pro velké spalovací motory".

This research has been realized using the support of EU Regional Development Fund in OP R&D for Innovations (OP VaVpl) and The Ministry of Education, Youth and Sports, Czech Republic, project *CZ.1.05/2.1.00/03.0125*: 'Acquisition of Technology for Vehicle Center of Sustainable Mobility'.

This research has been realized using the support of Technological Agency, Czech Republic, programme Centres of Competence, project *TE01020020*: 'Josef Božek Competence Centre for Automotive Industry'.

This research has been realized using the support of The Ministry of Education, Youth and Sports program NPU I (LO), project *LO1311*: 'Development of Vehicle Centre of Sustainable Mobility'.

All the help has been gratefully appreciated.

DEFINITIONS/ABBREVIATIONS

BBDC	Before Bottom Dead Center
BDC	Bottom Dead Center
BMEP	Brake Mean Effective Pressure
BSFC	Brake Specific Fuel Consumption
BTDC	Before Top Dead Center
degCA	Degree of Crank Angle
DoE	Design of Experiments
ECU	Electronic Control Unit
EGR	Exhaust Gas Recirculation
EV	Exhaust Valve
EVO	Exhaust Valve Opening
FE	Finite Element
HP	High-Pressure
ICE	Internal Combustion Engine
IMEP	Indicated Mean Effective Pressure
IV	Intake Valve
IVC	Intake Valve Closing
IVO	Intake Valve Opening
LP	Low-Pressure
MBF	Mass Burned Fraction
MEP	Mean Effective Pressure
PID	Proportional-Integral-Derivative controller
PMEP	Pumping Mean Effective Pressure
PR	Pressure Ratio
ROHR	Rate of Heat Release
SI	Spark Ignition
SCR	Selective Catalytic Reduction
TA Luft	legislative norm to limit emission of NO _x ; the air excess was controlled in such way that NO _x should satisfy the <i>TA Luft</i> requirement
TDC	Top Dead Center
VGT	Variable Geometry Turbine/Turbocharger (the same as VTA, which is used in some papers and reports)
WG	Waste-Gate



APPENDIX

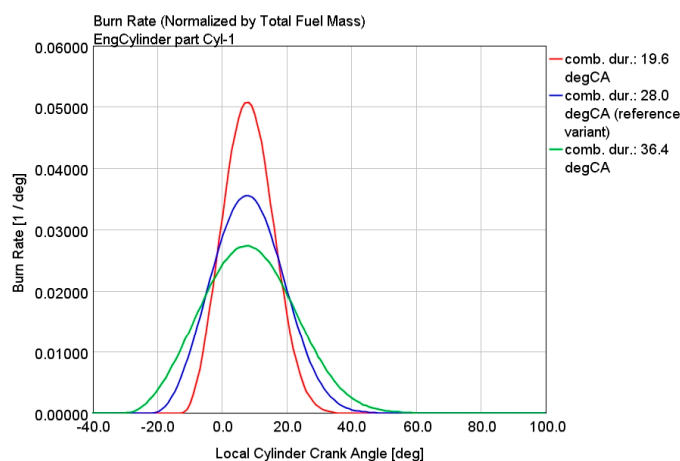
INFLUENCE OF COMBUSTION DURATION

The main goal of presenting this section is to support the statement from Chapter 3, that 'the authors are convinced that EGR rate has minor influence on optimization of boost group and selection of both proper control and EGR configuration'. Three different combustion duration cases were tested (c.f. Figure 18). The reference combustion duration (blue curve in Figure 18), which was applied in all cases presented in the paper (Figures 6–17). The combustion duration is 28 degCA from MBF10% to MBF90% and Vibe exponent is 2.0, which corresponds to duration of 43.6 degCA to burn 90% of the fuel in the cylinder. Such combustion duration is in-line with the authors experience with similar engines. Moreover it corresponds well to measured data from [37] (c.f. Figure 19), when very similar engine was experimentally investigated under similar operating conditions (BMEP 22 bar at TA_{Luft} 100%). To show sensitivity of predicted results with respect to combustion duration, 30% faster combustion (red curve in Figure 18) and 30% slower combustion (green curve in Figure 18) were tested.

The first step was to perform the whole optimization procedure (c.f. Chapter 4.3) for faster/slower combustion cases as well. The optimal values of HP/LP compressor/turbine multipliers, which are always the outputs of the optimization procedure, are shown in Figure 21 – different cases in terms of required EGR/ TA_{Luft} level and/or applied EGR configuration (LP_{EGR} or $HP_{EGR} + EGR_{compressor}$) were tested. Optimal turbocharger configuration in terms of mass-flow multipliers is usually independent of combustion duration. This is especially valid for reference and slower combustion duration (c.f. Figure 21).

This statement is verified in Figure 22, which shows the influence of applied turbocharger group in terms of BSFC. Each subFigure in Figure 22 presents 4 curves. The dark-blue curve corresponds to a case when HP/LP compressor/turbine multipliers are optimized for each considered combustion duration (label opt_{MF_mult}) using information from Figure 21, while combustion phasing is constant (label $const_{comb_pos}$) corresponding to subFigure (b) of Figure 18 – this means that angle location of MBF50% is 8 degCA. The pink curve represents a case when constant mass-flow multipliers are applied – the applied multiplier values correspond to reference combustion duration from Figure 21. Concerning the combustion timing, the same constant approach ($const_{comb_pos}$) was adopted. The light-green curve shows a case when optimal turbochargers are applied for each combustion duration (opt_{MF_mult}), however, combustion timing was optimized as well (label opt_{comb_pos}) to obtain the lowest possible BSFC. Finally, the light-blue curve represents a case when constant mass flow multipliers are applied ($const_{comb_pos}$), while optimized combustion timing approach (opt_{comb_pos}) was adopted. The relative difference between 2 selected curves in Figure 22 shows the specific influence. For example, the difference between the dark-blue curve and the pink one confirms that applying reference optimal turbocharger configuration, which corresponds to a reference combustion duration, leads to a BSFC difference in order of 0.1 g/kWh when compared with optimal configurations of faster/slower combustion duration. Another example shows, that applying

(a) rate of heat release



(b) heat release

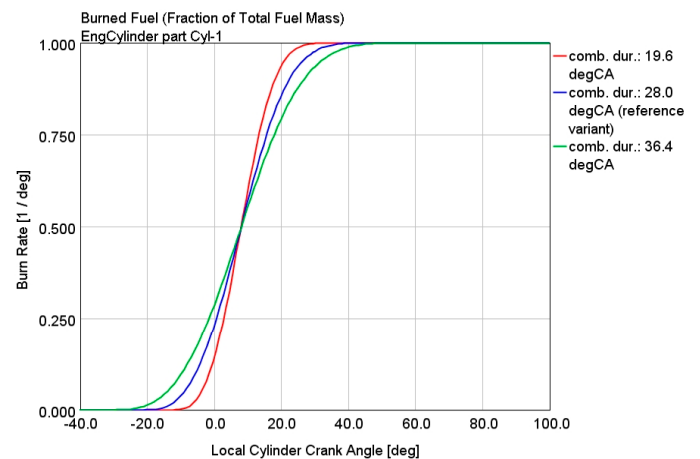
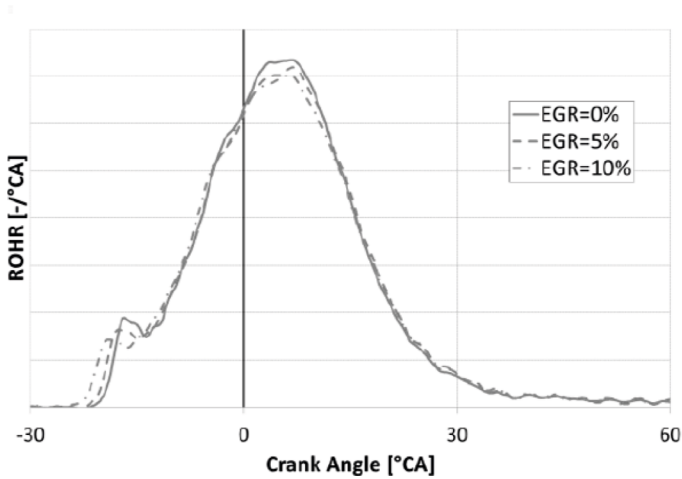


FIGURE 18: Comparison of different ROHR patterns (dark-blue curve corresponds to reference variant).

OBRÁZEK 18: Porovnání různých tvarů vývinů tepla (tmavě modrá barva reprezentuje referenční variantu).



(a) rate of heat release



(b) NOx formation (right y-axis)

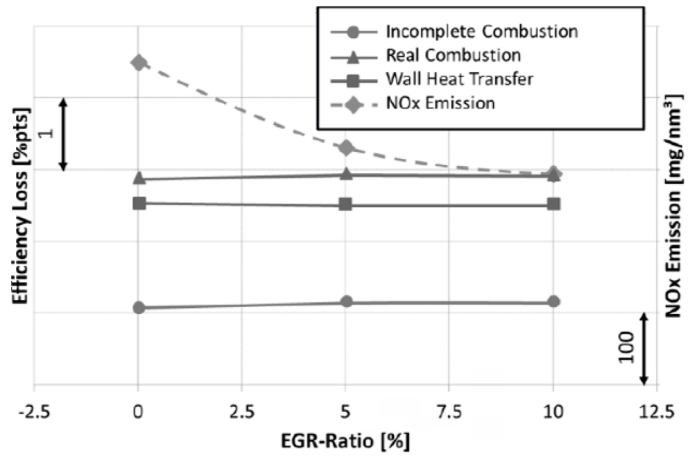
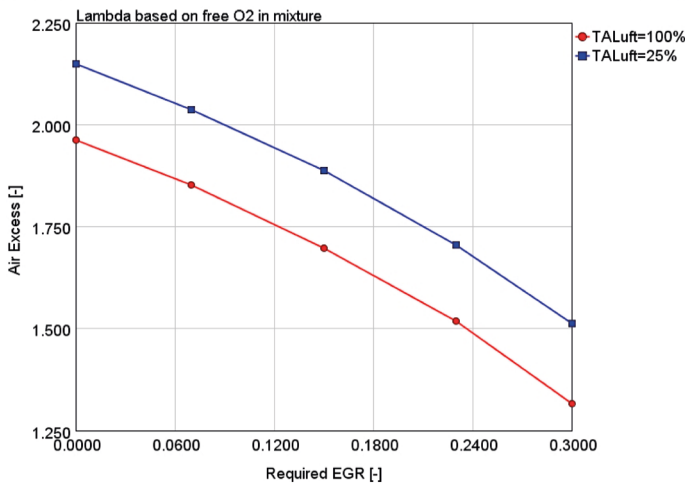


FIGURE 19: Influence of external EGR on ROHR and NOx formation – experimental data from single-cylinder research engine (the plots were reprinted from [37]).
OBRAZEK 19: Vliv vnější recirkulace (EGR) na vývin tepla (ROHR) a tvorbu NOx – experimentální data z výzkumného jednoválce (obrázky převzaty z [37]).

(a) air excess at constant NOx levels



(b) air excess at constant EGR levels

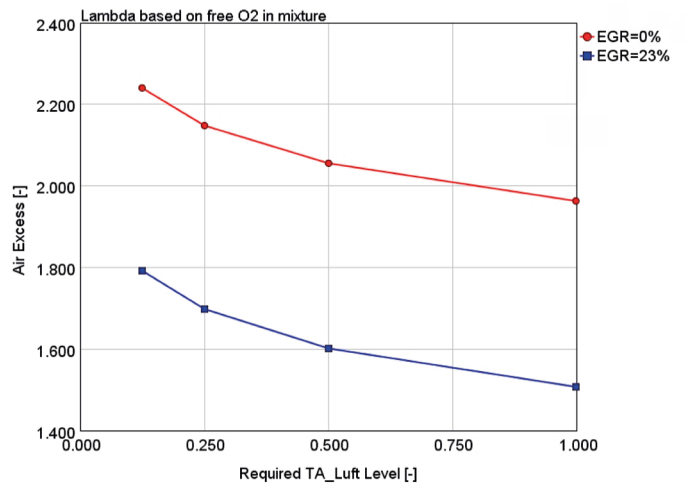


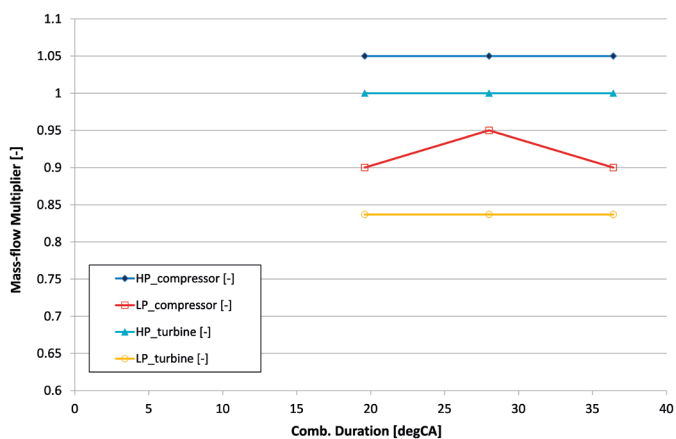
FIGURE 20: Air excess based on free O₂ mass – the plots correspond to data presented in Figure 23.
OBRAZEK 20: Přebytek vzduchu založen na volném kyslíku – grafy odpovídají datům z Obrázku 23.

constant combustion timing leads to almost no BSFC difference when compared with optimal one (compare dark-blue curve with light-green one). Based on data from Figure 21 and Figure 22, there is very little influence of combustion duration and combustion timing on optimal values of HP/LP compressor/turbine mass-flow multipliers. Of course, there is always a BSFC penalty (c.f. Figure 22) associated with increased combustion duration – this penalty is almost independent of required EGR/TA Luft level and/or applied EGR configuration. It should be stressed that there are certain cases in Figure 22 when there is a sudden increase in BSFC when faster combustion duration is considered – light-green curve in subFigure (c) or pink curve

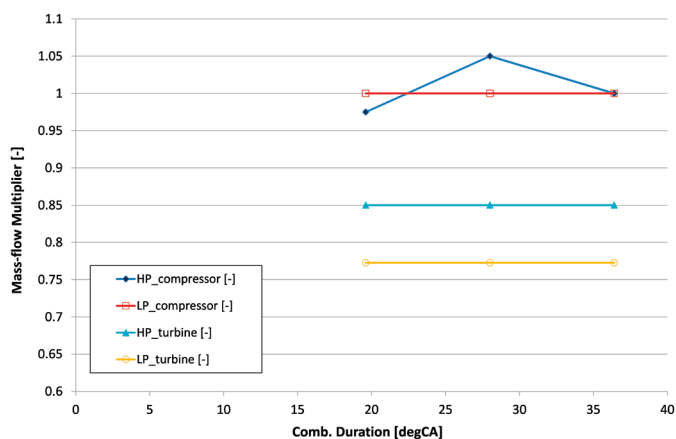
in subFigure (e). This corresponds to a fact that required BMEP of 24 bar cannot be reached, hence additional BSFC penalty is applied. Additionally, there is an open issue if combustion duration is really supposed to be increased when changing requirement of EGR/TA Luft level. There is an experimental evidence from [37] (c.f. subFigure (a) of Figure 19) that combustion duration and its shape is almost independent of applied external EGR level. However, the pre-chamber concept is applied in [37] – the first little peak of ROHR in subFigure (a) of Figure 19 is caused by combustion in pre-chamber. Concerning ignition system, there were no specific assumptions concerning



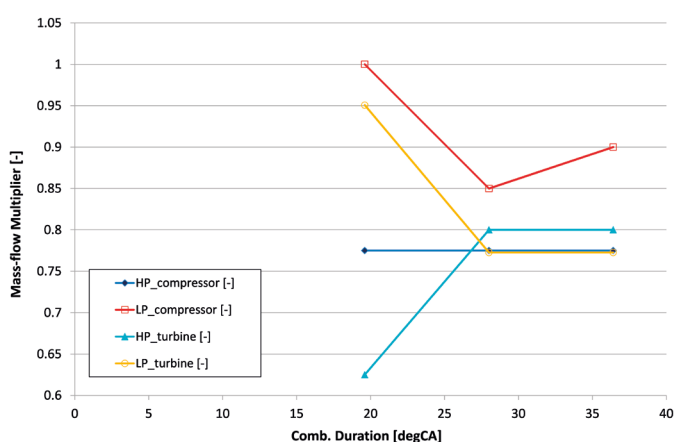
(a) $TA_{Luft} = 100\%$, $EGR = 0\%$



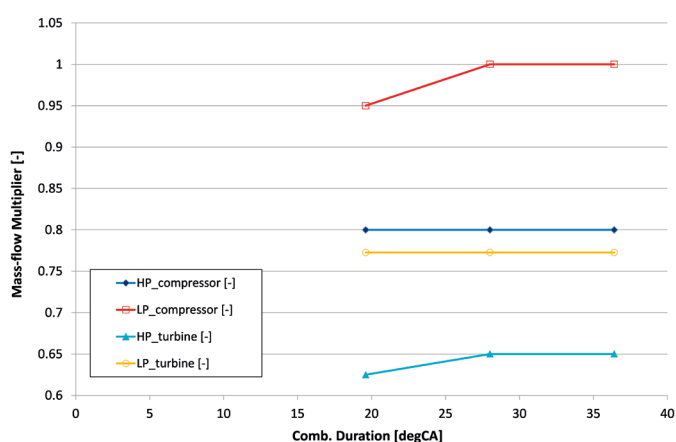
(b) $TA_{Luft} = 25\%$, $EGR = 0\%$



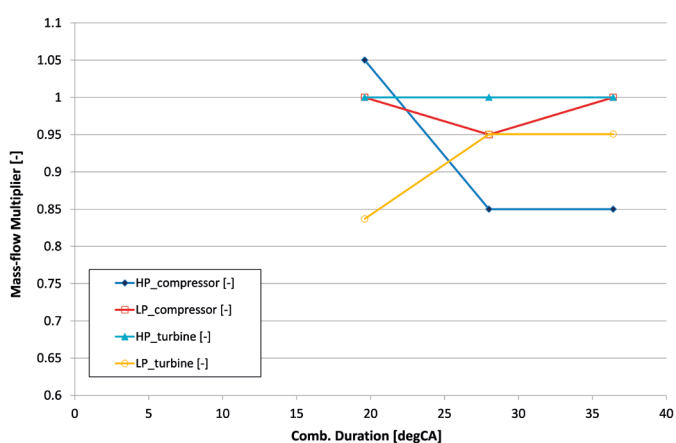
(c) $TA_{Luft} = 100\%$, HP EGR + EGR compressor, $EGR = 23\%$



(d) $TA_{Luft} = 25\%$, HP EGR + EGR compressor, $EGR = 23\%$



(e) $TA_{Luft} = 100\%$, LP EGR, $EGR = 23\%$



(f) $TA_{Luft} = 25\%$, LP EGR, $EGR = 23\%$

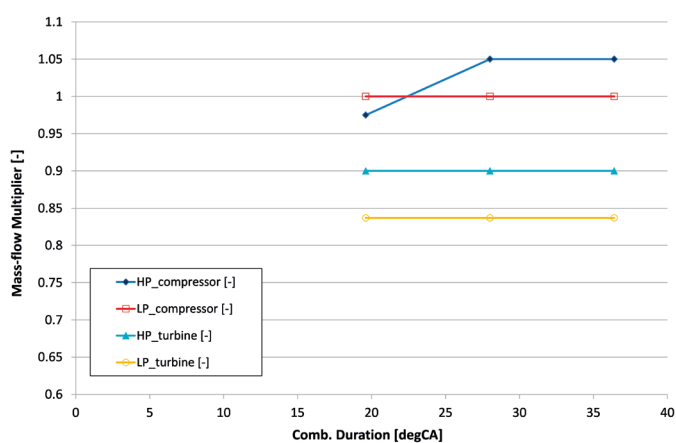


FIGURE 21: Influence of combustion duration under steady operation – optimal mass-flow multipliers of HP/LP compressor/turbine; engine setting: blow-by = 5%, BMEP = 24bar, const comb. timing (MBF50% at 8 degCA after TDC).

OBRÁZEK 21: Vliv délky hoření za ustálených podmínek – optimální velikost vysoko- a nízkotlakého kompresoru a turbíny; nastavení: blow-by = 5%, BMEP = 24 bar, konstantní časování hoření (50% bod je v 8 stupních za horní úvratí).



the target engine (Table 1). The large-bore SI gas engines, which are operated under lean-burn conditions, have to be equipped with high-energy ignition system to enable reliable mixture ignition. It is wellknown that application of pre-chamber concept can provide that (c.f. [24–27, 37]), especially if there is a possibility to add additional fuel into the pre-chamber [35]. In any case, large-bore SI gas engines are less sensitive to mixture composition changes due to application of high-energy ignition system.

Based on the above mentioned facts, it was decided to plot important in-cylinder quantities for different engine operating conditions – this is shown in Figure 23. Different conditions were tested to take into account different EGR/*TA Luft* levels. For each operating condition, there are 2 subfigures in Figure 23 – the left one shows mass fractions of selected in-cylinder species while the right one presents total in-cylinder mass of these species.

The virtual measurement was done at 60 degCA before TDC. The influence of both required EGR level and *TA Luft* are shown. When considering the case of constant *TA Luft* level and varying EGR level, the following can be stated. As EGR increases, the mass fraction of CO₂ is increased while O₂ decreases, the same applies to mass amount of both considered species. The mass fraction of N₂ is almost constant while N₂ mass slightly decreases. This is caused by the fact that total in-cylinder mass slightly decreases. The fuel mass fraction/amount is almost constant due to the fact that required BMEP is the same (24 bar) and BSFC is very similar for all presented cases. The air excess, which is based on free O₂, is shown in subFigure (a) of Figure 20. Regarding the case of constant EGR level and varying *TA Luft* level, the trends are the following. The mass fraction of CO₂, O₂ and N₂ is constant while fuel mass fraction decreases as *TA Luft* requirement gets stricter (lower value of *TA Luft* parameter, which is plotted on x-axis) – this leads to higher air excess (c.f. subFigure (b) of Figure 20). In-cylinder mass increases for all considered species.

Considering all presented information, it seems that keeping *TA Luft* requirement constant while varying EGR level leads to relatively similar in-cylinder conditions in terms of important species. Certain amount of free O₂ is replaced by CO₂, however, its mass fraction is less than 5% due to relatively high air excess. Although air excess changes significantly (c.f. subFigure (a) of Figure 20), the mixture is still very lean and the amount of the mass-dominant specie, which is N₂, is changed only slightly. Hence, the negative effect of high EGR is compensated by lower air excess. This suggests that laminar flame front propagation speed may be changed slightly as well. If the ignition system is able to ignite the mixture reliably, then the main combustion

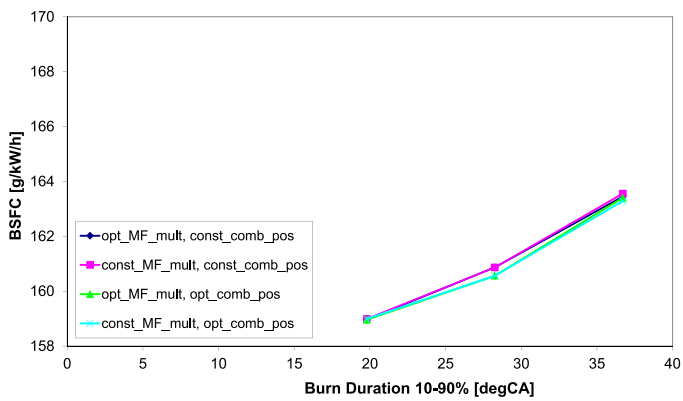
phase is expected to proceed normally – this is driven by turbulent flame front propagation. Hence, no major changes of ROHR duration/shape can be expected – this is confirmed by results in [37]. Moreover, the work presented in [21, 22], which is available at the authors' department, provides similar suggestions. However, the data, which were used for creating a correction functions to recalculate a ROHR model parameters, do not cover a region of very high air excess and high EGR rate. Hence the application of the model [21, 22] for the case of the target engine is not directly possible due to the fact that extrapolation outside of the calibration data is necessary. On the other hand, the author of [21, 22] is convinced that the qualitative trend is predicted correctly – the model suggests that the combustion duration is supposed to be changed only slightly for the cases of constant *TA Luft* and varying EGR level (subFigure (a) of Figure 20 and subfigures (a), (b), (c) and (d) of Figure 23). When dealing with the case of constant EGR level while varying *TA Luft* requirement, the following can be stated. The mass fraction of major species (CO₂, O₂, N₂) is almost constant while fuel fraction decreases when *TA Luft* requirement gets stricter. This leads to significant increase in air excess (c.f. subFigure (b) of Figure 20). This fact together with increased total mass leads to conclusion that such case is more likely to exhibit slower combustion. This is also confirmed by the model based on [21, 22].

When applying ROHR with constant parameters (duration, phasing and shape), there is one important advantage which is difficult to achieve on a real engine. Constant ROHR actually means that the predicted BSFC is not directly influenced by combustion model, hence the influence of all other phenomena is highlighted. This is actually desired as the influence of different operating conditions is of main interest (c.f. Chapter 2).

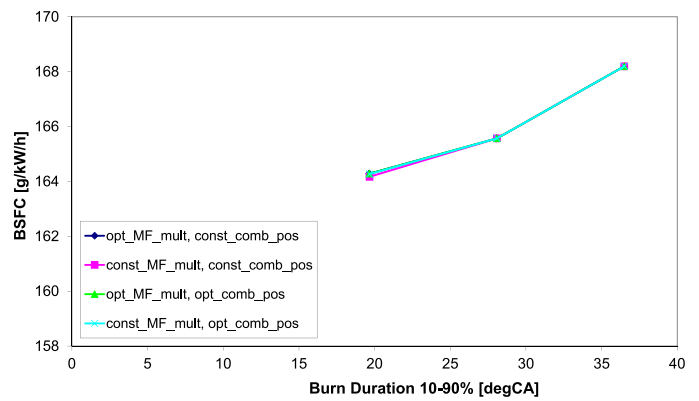
Final comment concerns the results presented in the paper, which corresponds to Figures 6–17. Based on the above mentioned facts, the combustion duration may be important when comparing the results with different NO_x levels (different *TA Luft* requirements). This is only shown in Figure 16. However, the qualitative trends remain unchanged as stricter NO_x leads to higher BSFC even if constant ROHR is assumed. Hence, possibly longer combustion would result in greater BSFC differences only – the qualitative comparison would be the same. There is a possibility that high EGR cases (EGR>15%) might be also influenced by slower combustion. If it is the case, the qualitative trends (c.f. Figure 11–16) would also be unchanged as the optimal EGR levels are relatively low (below 10% – c.f. Figure 17).



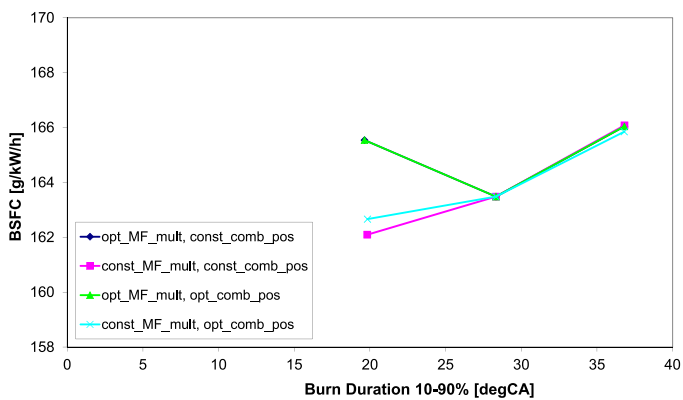
(a) TA Luft = 100%, EGR = 0%



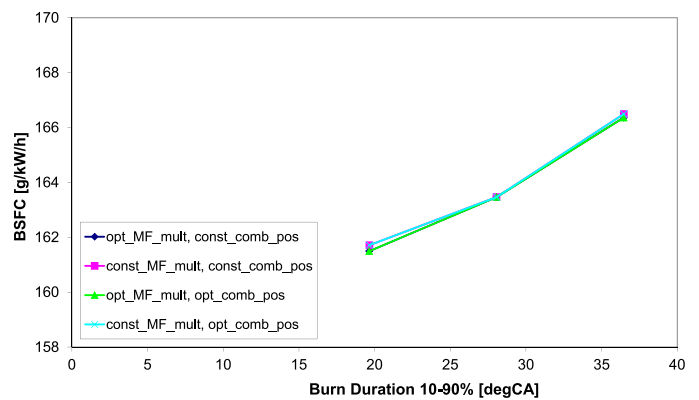
(b) TA Luft = 25%, EGR = 0%



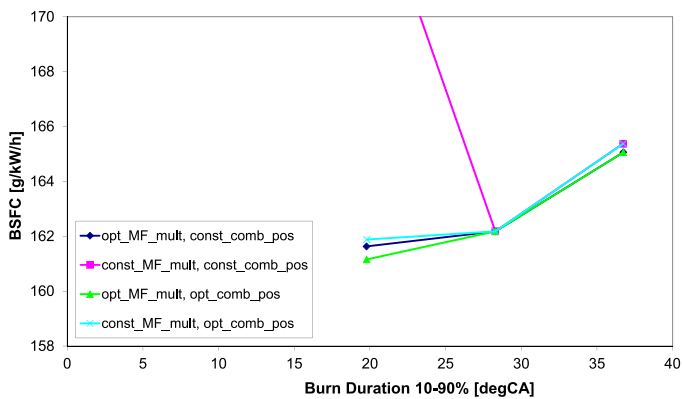
(c) TA Luft = 100%, HP EGR + EGR compressor, EGR = 23%



(d) TA Luft = 25%, HP EGR + EGR compressor, EGR = 23%



(e) TA Luft = 100%, LP EGR, EGR = 23%



(f) TA Luft = 25%, LP EGR, EGR = 23%

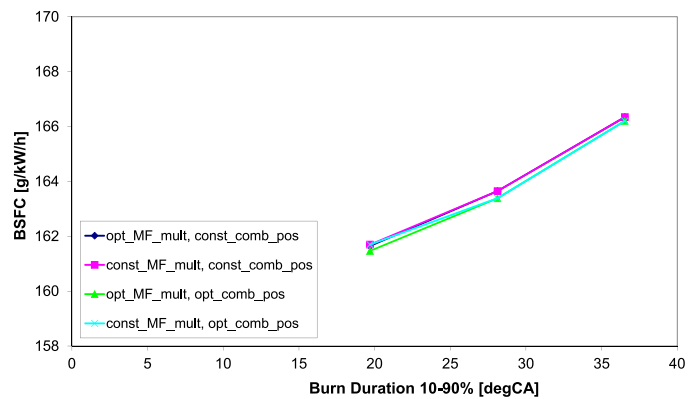
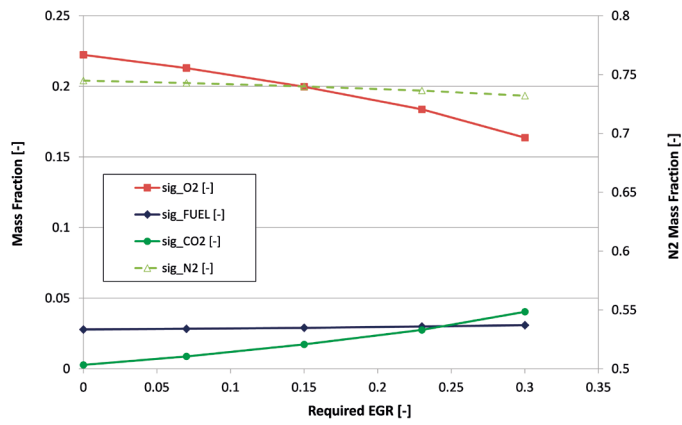


FIGURE 22: Influence of combustion duration under steady operation – BSFC for different cases of applied mass-flow multipliers (Figure legend: ‘opt_MF_mult’ – mass-flow multipliers of HP/LP compressor/turbine optimized for each combustion duration – c.f. Figure 21; ‘const_MF_mult’ – constant mass-flow multipliers corresponding to optimal values at combustion duration of 28.2 degCA; ‘opt_comb_pos’ – combustion timing optimized for best BSFC; ‘const_comb_pos’ – constant combustion timing: MBF50% at 8 degCA after TDC); engine setting: blow-by = 5%, BMEP = 24 bar.

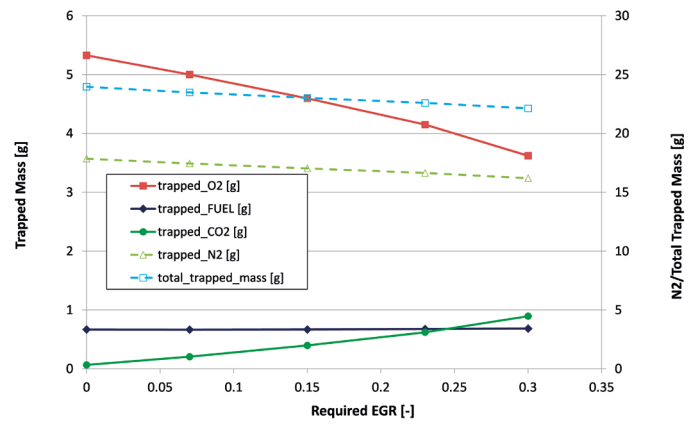
OBRAZEK 22: Vliv délky hoření za ustálených podmínek – měrná spotřeba paliva pro různé hlnosti (legenda: ‘opt_MF_mult’ – velikosti odpovídající Obrázku 21; ‘const_MF_mult’ – konstantní hlnost odpovídající délce hoření 28.2 stupně; ‘opt_comb_pos’ – optimalizovaná poloha hoření pro nejlepší spotřebu; ‘const_comb_pos’ – konstantní poloha hoření: 50% bod v 8 stupních za horní úvratí); nastavení: blow-by = 5%, BMEP = 24 bar.



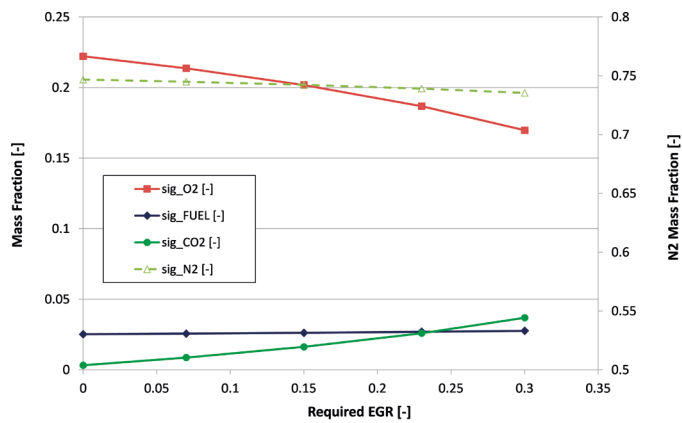
(a) TA Luft = 100%: mass fraction



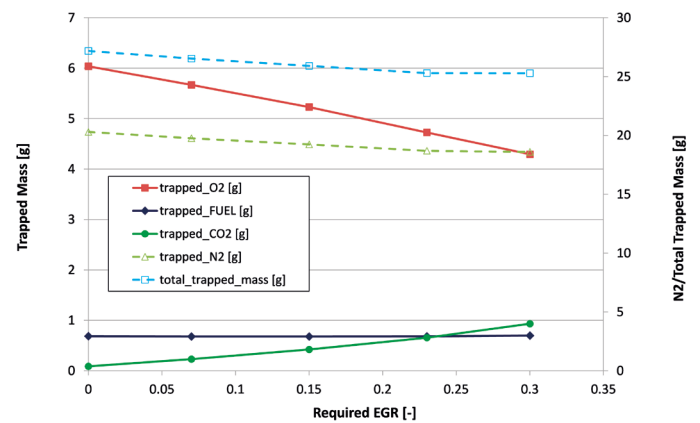
(b) TA Luft = 100%: mass



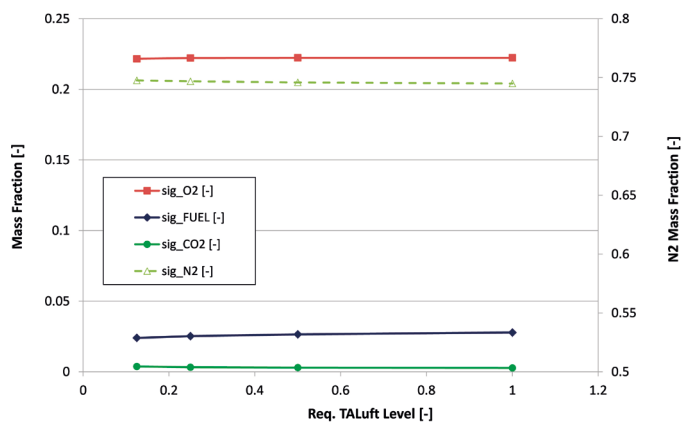
(c) TA Luft = 25%: mass fraction



(d) TA Luft = 25%: mass



(e) EGR = 0%: mass fraction



(f) EGR = 0%: mass

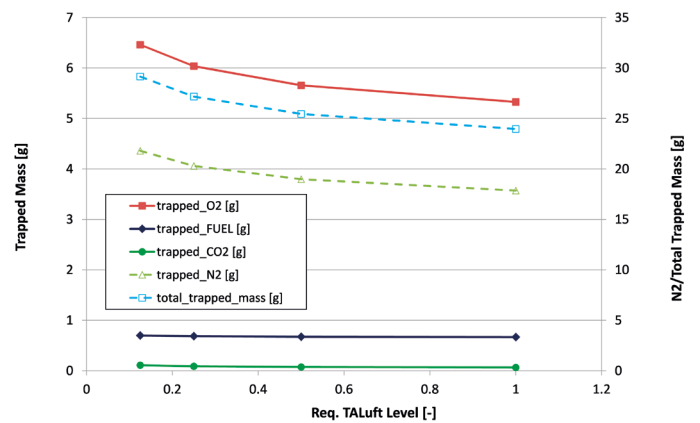


FIGURE 23: Comparison of in-cylinder species content with respect to different EGR level or TA Luft level; engine setting: blow-by = 5%, LP EGR. OBRÁZEK 23: Srovnání složení vybraných složek ve válci pro různé úrovně EGR nebo různé úrovně NOx (dle TA Luft); nastavení: blow-by = 5%, varianta LP EGR.



EVALUATION OF THE PREDICTIVE CAPABILITIES OF A PHENOMENOLOGICAL COMBUSTION MODEL FOR NATURAL GAS SI ENGINE

RASTISLAV TOMAN, JAN MACEK

CTU in Prague, Faculty of Mechanical Engineering; Technická 4, Praha 6, 166 07, Czech Republic

E-mail: rastislav.toman@fs.cvut.cz, jan.macek@fs.cvut.cz

ABSTRACT

The current study evaluates the predictive capabilities of a new phenomenological combustion model, available as a part of the GT-Suite software package. It is comprised of two main sub-models: 0D model of in-cylinder flow and turbulence, and turbulent SI combustion model.

The 0D in-cylinder flow model (EngCylFlow) uses a combined K - k - ε kinetic energy cascade approach to predict the evolution of the in-cylinder charge motion and turbulence, where K and k are the mean and turbulent kinetic energies, and ε is the turbulent dissipation rate. The subsequent turbulent combustion model (EngCylCombSITurb) gives the in-cylinder burn rate; based on the calculation of flame speeds and flame kernel development. This phenomenological approach reduces significantly the overall computational effort compared to the 3D-CFD, thus allowing the computation of full engine operating map and the vehicle driving cycles.

Model was calibrated using a full map measurement from a turbocharged natural gas SI engine, with swirl intake ports. Sensitivity studies on different calibration methods, and laminar flame speed sub-models were conducted. Validation process for both the calibration and sensitivity studies was concerning the in-cylinder pressure traces and burn rates for several engine operation points achieving good overall results.

KEYWORDS: PREDICTIVE PHENOMENOLOGICAL MODEL; INTERNAL COMBUSTION ENGINE; SPARK-IGNITION; K - k - ε KINETIC ENERGY CASCADE; 0D IN-CYLINDER FLOW MODEL; TURBULENT SI COMBUSTION MODEL; NATURAL GAS ENGINE; GENETIC ALGORITHM; GT-SUITE

SHRNUTÍ

Predkladaný článok hodnotí prediktívne schopnosti nového fenomenologického modelu horenia, ktorý je k dispozícii ako súčasť softvérového balíka GT-Suite. Skladá sa z dvoch hlavných sub-modelov: 0D modelu prúdenia a turbulencie vo valci a zážihového turbulentného modelu horenia.

0D model prúdenia a turbulencie vo valci (EngCylFlow) používa kombinovaný prístup K - k - ε kaskády kinetickej energie na predpoveď pohybu zmesi a turbulencie vo valci, kde K a k sú stredné a turbulentné kinetické energie a ε je turbulentná rýchlosť disipácie. Následný model turbulentného horenia (EngCylCombSITurb) určuje rýchlosť horenia vo valci na základe výpočtu rýchlosti čela plameňa a vývoja jadra plameňa. Tento fenomenologický prístup výrazne znižuje celkovú výpočtovú náročnosť v porovnaní s 3D-CFD, čo umožňuje výpočet úplnej charakteristiky spaľovacieho motora a jazdných cyklov vozidla. Model bol kalibrovaný pomocou meraní úplnej charakteristiky preplňovaného zážihového motora na zemný plyn so swirlovými vstupnými kanálmi. Boli vykonané štúdie citlivosti na rôzne kalibračné metódy a na rôzne sub-modely laminárnej rýchlosti čela plameňa. Validáčny proces pre kalibrácie a štúdie citlivosti sa týkal tlaku vo valci a rýchlostí horenia pre niekoľko pracovných bodov motora, dosahujúc dobré celkové výsledky.

KLÍČOVÁ SLOVA: PREDIKTÍVNY PHENOMENOLOGICKÝ MODEL; ZÁŽIHOVÝ SPAĽOVACÍ MOTOR; K - k - ε KASKÁDA KINETICKEJ ENERGIE; 0D MODEL PRÚDENIA VO VALCI; TURBULENTNÝ ZÁŽIHOVÝ MODEL HORENIA; MOTOR NA ZEMNÝ PLYN; GENETICKÝ ALGORITMUS; GT-SUITE



1. INTRODUCTION

Current development of the internal combustion engines (ICE) is focused on the overall efficiency improvement and emissions reduction. To fulfil these goals, downsizing of the ICE presents one of the most valuable options. But the increasing boost levels also lead to an increase in the knock likelihood, requiring spark timing retardation or mixture enrichment. Moreover, current engines use progressively also additional advanced control systems, such as advanced gas exchange systems, cylinder deactivation, or variable compression-ratio systems. With many iterations needed, accurate and robust modelling of the combustion process have become essential during the ICE development process, with an emphasis on the overall simulation time of one engine operating cycle.

A detailed 3D Computational Fluid Dynamics (3D-CFD) analysis of the in-cylinder flows, charge motion and combustion leads to accurate prediction of burn rate (if set-up properly), but with the obvious drawback of its high computational demands [1]. 3D-CFD is therefore used mostly for the analysis of separate engine operating points.

Empirical combustion models usually use an approximation of a measured burn rate. The most common empirical model is a Vibe formula [2]. However, if the user wants to obtain correct burn rate values in changed ICE operating conditions, reference burn rate pattern must be adjusted by additional formulas [3], [4]. In general, empirical models are simple and work well inside the calibrated region, but their extrapolation abilities are poor [5].

Multi-zone models of combustion and heat transfer in SI engines present a fast, accurate, stable and above all physical-based solution. A general theory of zone models based on the laws on conservation is described in [6], with a comparison of Lagrangian and Eulerian approaches. Recent paper of Hvezda [7] presents a specific adaptive approach to the chemical transformation. Multi-zone model of Hvezda models in detail the flame velocities using a turbulent coefficient, and accounts for the real geometry of the combustion chamber.

Finally, phenomenological combustion models also respect the combustion chamber geometry and obtain a burn rate by the calculation of turbulent flame speed and instantaneous flame area [8]. These models need an information on in-cylinder flow quantities as well. Several 0D turbulence models aim to reproduce the complex 3D phenomena, mainly by $k-\varepsilon$ approach [9], [10], [11] or $K-k$ approach recently studied in [12] and [13].

Both, the multi-zone and phenomenological models show very good extrapolation capabilities and low computational demands, allowing for the fast simulation of vehicle driving cycles.

A combustion model evaluated in this study consists of two main sub-models: 0D in-cylinder flow model EngCylFlow (or *Flow*) and turbulent combustion model EngCylCombSITurb (or *SITurb*). Gamma Technologies is currently developing both sub-models as a part of GT-Suite software package [14]. The *Flow* model combines the $k-\varepsilon$ approach of Morel et al. [9], [10] with the $K-k$ into combined $K-k-\varepsilon$ kinetic energy cascade model. Fogla et al. [15] describes the current *Flow* model, comparing with 3D-CFD and former model version, using two similar turbocharged gasoline ICEs, with tumble intake ports.

The *SITurb* model – originally developed by Wahiduzzaman, Morel and Sheard [8] – uses a turbulent flame concept, directly linked to the in-cylinder flow and turbulence calculation. Mirzaeian et al. [16] assessed the predictive capability of the current model version adding the equation system description. They also proposed a calibration method starting with DoE calibration of the *Flow* model against the 3D-CFD data and continuing with the *SITurb* calibration using the Genetic Algorithms (GA) with the objective to match the burn rate against the measurement data (turbocharged gasoline ICE with tumble intake port).

More detail on the combustion model follows in Section 2.

1.1 MAIN GOALS

The main objectives of this paper are:

- First, to calibrate the current combustion model, obtaining a single set of optimal model parameters;
- Second, to test its predictive capabilities.

Already mentioned papers [15] and [16] evaluated the model capabilities on turbocharged gasoline engines, with tumble intake ports. This study uses a full engine map measurement set with EGR variations and stoichiometric conditions of the ICE fueled by natural gas, with swirl intake ports.

The additional goals of the paper are following:

- to summarize the main features of the predictive combustion model;
- to compare different calibration approaches;
- to test the sensitivities of the combustion model on the laminar flame speed.

2. PREDICTIVE COMBUSTION MODEL

2.1 IN-CYLINDER FLOW MODEL

The main equation system of the *Flow* model contains three differential equations (equations 1-3) that govern the mean kinetic energy $K=(1/2)U^2$ (U is the mean velocity inside the cylinder), turbulent kinetic energy $k=(3/2)u'^2$ (u' is the mean fluctuating turbulent velocity inside the cylinder), and the



turbulent dissipation rate ϵ . The model assumes homogeneous and isotropic turbulent field [15].

$$\frac{d(mK)}{dt} = C_{in}(1 - \alpha_{in})E_{in} + K\dot{m}_{out} - P_k \quad (1)$$

$$\frac{d(mk)}{dt} = C_{in}\alpha_{in}E_{in} + k\dot{m}_{out} - P_k + C_{tumb}T - m\epsilon \quad (2)$$

$$\begin{aligned} \frac{d(m\epsilon)}{dt} = & C_{in}E_{in} \frac{\sqrt{k}}{L_g} + \epsilon\dot{m}_{out} - P_\epsilon + C_{tumb}T \frac{\sqrt{k}}{L_g} - \\ & - 1.92 \frac{m\epsilon^2}{k} \end{aligned} \quad (3)$$

First right-hand side terms in all three equations represent the production of each flow quantity, with the inflow energy E_{in} . Parameter α_{in} indicates the fraction of inflow energy entering the cylinder directly as turbulence, although not generated by the kinetic energy cascade process.

The second right-hand side term in the main equations, describes the energy out-flow through the valves, with the mass flow rate of the cylinder exit flow \dot{m}_{out} .

Production terms P_k and P_ϵ (equations 4-5) model the production of the turbulent kinetic energy and a dissipation rate from the large scale mean flows via the kinetic energy cascade process; v_T represents a turbulent viscosity, ρ a density and $\dot{\rho}$ a rate of change of density inside the cylinder. The appendix of [15] describes the evolution of these terms.

$$P_k = C_\beta v_T \frac{2mK}{L_g^2} - \frac{2}{3}mk \left(\frac{\dot{\rho}}{\rho}\right) - \frac{2}{3}mv_T \left(\frac{\dot{\rho}}{\rho}\right)^2 \quad (4)$$

$$P_\epsilon = \frac{\epsilon}{k} \left[5.76C_\beta v_T \frac{mK}{L_g^2} - 2mk \left(\frac{\dot{\rho}}{\rho}\right) - \frac{2.64}{3}mv_T \left(\frac{\dot{\rho}}{\rho}\right)^2 \right] \quad (5)$$

The last right-hand side term in each of the three main equations is a sink term for its respective quantity. The terms with the quantity T model the production of turbulence by the decay of the tumble macro-vortex during the compression [15].

Simple equation systems for the time rate change of the angular momentum dL/dt model the rotational components of the flow – tumble and swirl – as a single macro-vortex undergoing stretching and compression during the engine intake and compression.

Swirl and tumble are produced by the incoming charge, accounting for the measured swirl and tumble coefficients, and reduced by the cylinder out-flow. Equation systems for both rotational motions contain a proper decay functions. Paper [15] does not discuss the swirl decay function, but provides further information on the tumble decay function.

Former *Flow* model ([10], [11]) accounted for the squish motion (inside the swirl model) and injection event kinetic energy and so does the current *Flow* model. However, the exact equation systems are not available in [15].

Since the current *Flow* model calculates the kinetic energy and the dissipation rate, the evolution of integral length scale L_t over time is then obtained directly with the equation 6 ($C_\mu = 0.09$ is a standard $k-\epsilon$ model constant) [15].

$$L_t = C_\mu^{3/4} \frac{k^{3/2}}{\epsilon} \quad (6)$$

Equations 1-5 contain four calibration parameters that can be used to match the in-cylinder *Flow* model with 3D-CFD results and to enhance the predictive abilities of the consecutive turbulent combustion model. These parameters are following:

- Intake term multiplier C_1 multiplies the intake term $C_{in} = 0.18C_1$ and thus accounts for the actual flow velocities through the valves, since these are not equal to the isentropic values assumed by the E_{in} ;
- Production term multiplier C_2 adjusts the magnitudes of the production terms (equations 4-5) directly through the Production term C_β with $C_\beta = 0.38 C_2$;
- Geometrical length scale multiplier C_3 adjust the magnitudes of the production terms indirectly, through the scaling of Geometrical length scale $L_g = C_{len} \times \min(s, 0.5B)$, with B being the cylinder bore, s the instantaneous piston stroke, and $C_{len} = 0.19C_3$;
- Tumble term multiplier C_{tumb} controls the intensity of the tumble decay contribution to the production of turbulence.

2.2 TURBULENT COMBUSTION MODEL

Turbulent combustion model *SITurb* predicts the burn rate for the homogeneous charge, respecting the geometry of the combustion chamber, spark location and timing, mixture motion and fuel properties. The model simulates the development of the flame as a turbulent entrainment process followed by a burnup process in a region behind the flame front [8].

$$\frac{dM_e}{dt} = \rho_u \cdot A_f \cdot (S_L + S_T) \quad (7)$$

The entrainment mass rate of unburned gas dM_e/dt is determined by the equation 7; with the flame front area A_f , laminar and turbulent flame speeds S_L and S_T and finally the unburned gas density ρ_u .

Dedicated sub-model evaluates the instantaneous flame front area from the combustion chamber geometry assuming



the flame front spherical in shape [8]. A model parameter SS_{init} (initial spark size) determines the initial flame front size. For a typical spark plug, its value should be the same as the gap between the spark plug electrodes. However, the real spark size can slightly differ, especially with high-energy spark plugs. Therefore, we use the SS_{init} as a model tuning parameter also, in a reasonable range of sizes.

$$S_L = (B_m + B_\phi \cdot (\phi - \phi_m)^2) \cdot \left(\frac{T_u}{T_0}\right)^\alpha \cdot \left(\frac{p}{p_0}\right)^\beta \cdot (1 - 2.06 \cdot Dil^{0.77 \cdot DEM}) \quad (8)$$

$$S_T = C_S \cdot u' \cdot \left(1 - \frac{1}{1 + C_K \cdot R_f^2 / L_t^2}\right) \quad (9)$$

During the initial flame kernel development, when the size of the flame kernel is still small, the unburned gas entrainment rate is limited by the laminar flame speed S_L (equation 8). Then, the equation 9 accounts for the transition to the turbulent flame speed, with u' representing the mean fluctuating turbulent velocity, R_f the flame radius and L_t the turbulent length scale [16].

The rate of burnup dM_b/dt behind the flame front is proportional to the unburned mass behind the flame front, resulting in the rate equation 10 for the burned mass M_b .

$$\frac{dM_b}{dt} = \frac{M_e - M_b}{\tau} \quad (10)$$

Model assumes that the burnup phase takes place in the laminar flame speed and over the Taylor microscale of turbulence λ , with time constant τ (equation 11). Other assumption is that the turbulence is isotropic and therefore the Taylor microscale of turbulence λ can be obtained from the integral length scale L_t (equations 12).

$$\tau = \frac{\lambda}{S_L} \quad (11)$$

$$\lambda = \frac{C_\lambda \cdot L_t}{\sqrt{Re_t}} \quad (12a)$$

$$Re_t = \frac{\rho_u \cdot u' \cdot L_t}{\mu} \quad (12b)$$

Parameters in the laminar flame speed equation 8 depend on the fuel type and its composition. Since the composition of the natural gas differs, GT-Suite offers two different parameter sets (summed-up in Table 1):

- First set $S_{L_{NG1}}$ from Hernandez et al. [17];
- The second one $S_{L_{NG2}}$ by the work of Lio, Jiang, and Cheng [18]

There are five different calibration parameters in the *SITurb* model that we use to match the measured burn rate. These parameters are following:

- Turbulent flame speed multiplier C_S scales the turbulent flame speed S_T in equation 9;
- Flame kernel growth multiplier C_K scales the flame front evolution from the initial laminar smooth surface to a distorted turbulent flame front (equation 9);
- Taylor length scale multiplier C_λ scales the Taylor microscale of turbulence λ in equation 12
- Dilution exponent multiplier DEM accounts for the dilution by the exhaust residuals and EGR, affecting the laminar flame speed in the equation 8;
- Initial spark size SS_{init} parameter determines the size of the initial flame front.

3. EXPERIMENTAL SET-UP AND TEST MATRIX

The set of experimental data used in this study originates from a steady state engine test bed measurements with a four-cylinder turbocharged SI engine rebuilt from a CI variant and fueled by natural gas. The usual average composition of the natural gas is 98.39 [%vol] CH_4 , 0.44 [%vol] C_2H_6 , 0.26 [%vol] higher hydrocarbons and 0.84 [%vol] N_2 . Table 2 summarizes the main geometrical parameters of the experimental engine. One of the necessary inputs for the *Flow* model is the swirl (or tumble) characteristic of the experimental ICE. Such measurements were conducted in 2005 but only the swirl

TABLE 1: Laminar flame speed sub-model parameters

TABUŁKA 1: Parametre sub-modelu pre výpočet laminárnej rýchlosti čela plameňa

Parameter	Description	$S_{L_{NG1}}$ [17]	$S_{L_{NG2}}$ [18]
B_m [m/s]	Maximum laminar speed	0.490	0.397
B_ϕ [m/s]	Laminar speed roll-of value	-0.590	-1.649
ϕ_m [-]	Fuel/air equivalence ratio at maximum laminar flame speed	1.390	1.061
α [-]	Temperature exponent	$0.68 \times \phi^2 - 1.70 \times \phi + 3.18$	$5.75 \times \phi^2 - 12.15 \times \phi + 7.98$
β [-]	Pressure exponent	$-0.52 \times \phi^2 + 1.18 \times \phi - 1.18$	$-0.925 \times \phi^2 + 2 \times \phi - 1.473$



TABLE 2: Basic experimental ICE features

TABUĽKA 2: Základné charakteristiky experimentálneho spaľovacieho motora

Bore	102 [mm]
Stroke	120 [mm]
Compression ratio	12:1
Number of Cylinders	4
Valves per Cylinder	4
I/O/IVC	342/595 [°CA aTDC] @ 0.1 mm lift
EVO/EVC	123/377 [°CA aTDC] @ 0.1 mm lift
Maximum Torque	600 Nm @ 1600-1800 RPM
Maximum Power	120 kW @ 2000 RPM

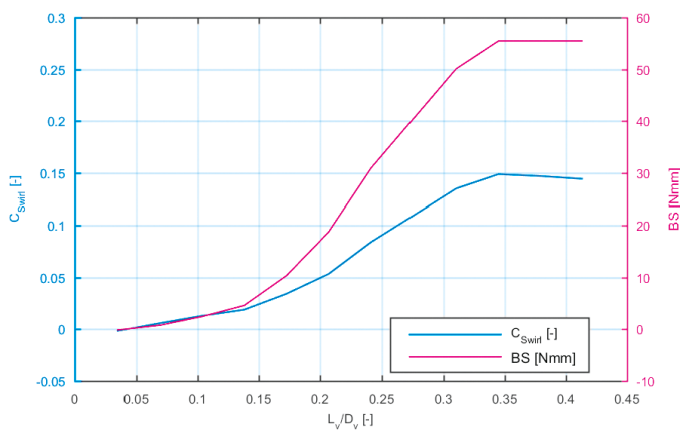


FIGURE 1: Intake port swirl characteristics of the experimental ICEs

OBRAZOK 1: Swirlová charakteristika sacích kanálov experimentálneho spaľovacieho motora

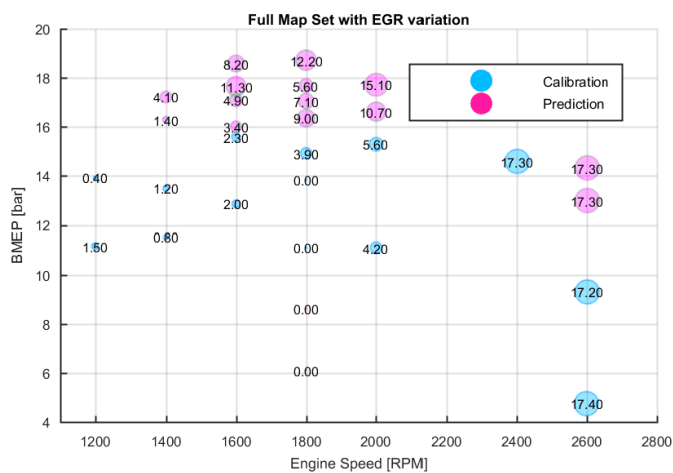


FIGURE 2: Test matrix from the full map measurement set with stoichiometric mixture and EGR ratio variation.

OBRAZOK 2: Testovacia matica z merania úplnej charakteristiky so stechiometrickou zmesou a variáciou pomeru EGR

characteristic is available – shown in Figure 1, where C_{Swirl} represents the swirl coefficient (definition from [14]), BS the swirl torque, and L_v/d_v a ratio of valve lift to its diameter.

The experimental ICE is equipped with a central mixer for metering and delivery of the gaseous fuel mixture downstream the compressor inlet. The fuel flow control is either manual or automatic by a closed loop lambda control. ICE features also a cooled low-pressure EGR system, with the EGR rate adjusted by a servo driven butterfly valve. Variable turbine geometry performs the boost pressure control and the conventional throttle, located downstream from the intercooler, controls the mixture inflow. High-energy ignition system ensures the sufficient spark energy, with the possibility of the spark discharge angle adjustment or closed-loop CA50 control.

Automated data acquisition system records the engine speed and torque, fuel flow, airflow, exhaust gas composition and average temperatures in the intake and exhaust manifolds. Uncooled piezoelectric transducer installed in the glow plug hole of the first cylinder measures the in-cylinder pressure and two piezo resistive pressure transducers measure the intake and exhaust pressures to get a full three-pressure-analysis (TPA). Details on the experimental set-up can be found in [5] and [19].

We used a measurement set containing 83 steady state operation points, representing the full engine map with the stoichiometric mixture and EGR ratio variations (BMEP 4.75-19.30 bar; 1200-2600 RPM). Figure 2 shows the reduced test matrix with model calibration points (in blue) and prediction points (in red). The size of a circle and the number indicate the EGR content. Most of the calibration points represent medium ICE loads; low to medium speeds; EGR rates 0-5.6%. Only three ICE operating points contain high EGR rate of 17% and high ICE speeds. The prediction points then cover low load/high load parts of the map, generally with high EGR rates (except two low load points @ 1800 RPM with 0% EGR rate), to really test the predictive capabilities of the combustion model.

4. CALIBRATION PROCEDURE

4.1 BASIS TPA MODEL

A proper function of the basis thermodynamic model must be ensured to allow for the calibration of the predictive combustion model. Therefore, we have calibrated the basis TPA model beforehand, correcting some model uncertainties and measurement errors, namely: effective compression ratio, convection multiplier of the heat transfer model [20], TDC position error, intake and exhaust ports pressure shifts.

$$\Delta p = \frac{1}{\alpha_{end} - \alpha_{start}} \int_{\alpha_{start}}^{\alpha_{end}} |p_{meas} - p_{sim}| d\alpha \quad (13)$$



The determination of the optimal set of calibrated parameters implies the formulation of the objective functions for the whole calibration. In the case of this calibration, these are derived from following model parameters:

- Absolute pressure difference Δp between the measured and simulated in-cylinder pressures (equation 13);
- $\Delta LHV_{Multiplier}$ evaluated from the GT-Suite output parameter $LHV_{Multiplier}$.

The fuel energy $LHV_{Multiplier}$ represents a multiplier of total fuel energy. When its value differs from unity, it indicates, that the input energy in the simulation system is different from the energy needed to follow exactly the measurement in-cylinder pressure trace. Then, $\Delta LHV_{Multiplier} = |LHV_{Multiplier} - 1|$.

Both variables are calculated for each engine operation point from the calibration set (Figure 2). The average and maximum values from all calibration points serve as the objective functions (leading to four objective functions X_k in total). GA [21] then minimizes these objective functions.

$$F = \sum_{i=1}^k \alpha_k \frac{X_k}{X_{k,max}} \quad (14)$$

The result of a multi-parameter and multi-criterial optimization is a set of non-dominated optimal solutions on a so-called Pareto Frontier. A single optimal solution from the Pareto set is obtained by a criterial function (equation 14), whose value is calculated for each Pareto set solution. The fraction $X_k / X_{k,max}$ then represents a normalization, so that different objective functions X_k can be combined into a single equation. $X_{k,max}$ is a maximum value from all Pareto set solutions, for the respective objective function X_k and parameter α_k is a criterial function weight factor. Table 3 summarizes the objective functions X_k and values of weight factors α_k ; Table 4 the selected optimal settings for the basis TPA model. Figure 3 displays a Pareto Frontier for this specific calibration (optimum point in red); Figure 4 the values of Δp and $\Delta LHV_{Multiplier}$ for each calibrated ICE operating point.

TABLE 3: Objective functions and weight factors for the basis TPA model calibration

TABUĽKA 3: Objektívne funkcie a váhové faktory pre kalibráciu základného modelu TPA

Objective function X_k	Weight factor α_k
Average Δp	0.35
Maximum Δp	0.15
Average $\Delta LHV_{Multiplier}$	0.35
Maximum $\Delta LHV_{Multiplier}$	0.15

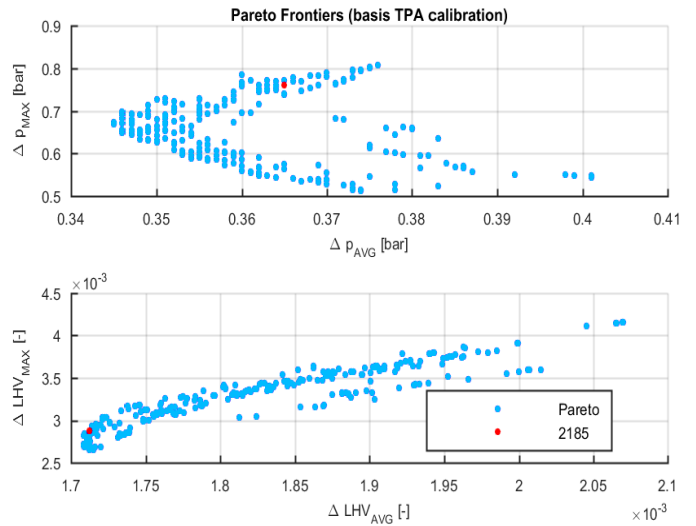


FIGURE 3: Pareto Frontiers with the optimum point for the basis TPA model calibration.

OBRAZOK 3: Pareto hranice s optimálnym bodom pre kalibráciu základného modelu TPA

TABLE 4: Selected optimal settings of the basis TPA model

TABUĽKA 4: Vybrané optimálne nastavenie základného modelu TPA

	Full Map set
Effective compression ratio	12.36:1
Convection multiplier	1.33
TDC position error	0.1 [°CA]
Intake port pressure shift	-0.021 [bar]
Exhaust port pressure shift	0.041 [bar]

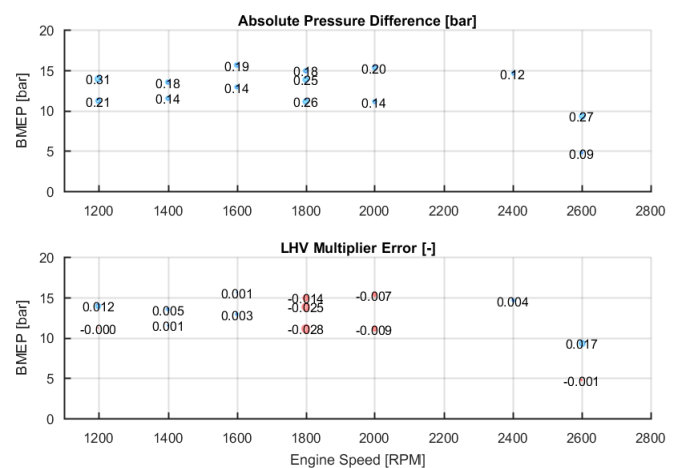


FIGURE 4: Values of Δp and $\Delta LHV_{Multiplier}$ errors for the full map calibration set and optimal settings of the basis TPA model.

OBRAZOK 4: Hodnoty Δp a $\Delta LHV_{Multiplier}$ základného modelu TPA pre jednotlivé pracovné body experimentálneho spaľovacieho motora a vybrané optimálne nastavenie parametrov.



4.2 MAIN CALIBRATION AND PREDICTIONS

Main calibration of the combustion model is conducted on the calibration part of the full map measurement set, combining in total nine *Flow* and *SITurb* parameters (Sections 2.1 and 2.2) and using the $S_{L_{NG1}}$ parameters for the laminar flame speed sub-model.

The objective functions for *Main calibration* of the combustion model are derived from two output parameters:

- Absolute pressure difference Δp between the measured and simulated in-cylinder pressures, but now for the *SITurb* model (equation 13);
- Burn Rate RMS Error (GT-Suite output parameter).

The GA then minimizes four objective functions X_k : two averages and two maxima. Regarding, the values of weight factors α_k in the criterial function (equation 14), $\Delta LHV_{Multiplier}$ is exchanged for Burn Rate RMS Error.

After the calibration of the combustion model, additional prediction points are also simulated.

It is worth noting, that the optimal set of model parameters is universal for the whole ICE map, without any dependencies on variables such as ICE speed or ICE load. The same applies for the following optimized set for both sensitivity studies.

4.3 SENSITIVITY STUDIES

Apart from the main calibration, we have conducted two different sensitivity studies:

- *Sensitivity 1* on calibration inputs, where we calibrated only the *SITurb* parameters, with *Flow* parameters fixed at default values ($def = 1$);
- *Sensitivity 2* on laminar flame speed sub-model, changing its settings to $S_{L_{NG2}}$.

The calibration procedure, objective functions, and weight factors of the criterial function are the same for the *Sensitivity 1* and *Sensitivity 2* as for the *Main calibration*.

5. RESULTS AND DISCUSSION

5.1 MAIN CALIBRATION

After the main calibration of the *Flow* and *SITurb* models, we kept constant the optimized parameters (Table 5, first column) and simulated both the 14 calibration operating points and additional 16 prediction points. Table 6 then summarizes the average and maximum values (*Note*: the average errors are evaluated from absolute values for the individual operating points).

Figure 5 shows the IMEP percentage error between the experimental and simulated values; Figure 6 displays the CA50 error; Figure 7 the 10%-90% Burn Duration (MFB10-90) error; Figure 8 maximum firing pressure error; Figure 9 the error of maximum firing pressure CA position.

TABLE 5: Optimal values of the calibration parameters for the combustion model (*Main calibration, Sensitivity 1, Sensitivity 2*)

TABUĽKA 5: Výsledné optimálne hodnoty kalibračných parametrov pre model horenia (*Hlavná kalibrácia, Citlivosť 1, Citlivosť 2*)

Parameter	Main calibration	Sensitivity 1	Sensitivity 2
Turbulent Flame Speed Multiplier C_s	1.060	0.370	1.600
Flame Kernel Growth Multiplier C_K	9.040	4.210	0.080
Taylor Length Scale Multiplier C_λ	7.510	2.650	8.970
Dilution Exponent Multiplier DEM	0.830	0.830	0.710
Initial Spark Size SS_{mit}	3.500	3.560	4.810
Intake Term Multiplier C_1	1.640	$def = 1$	0.010
Production Term Multiplier C_2	3.690	$def = 1$	0.946
Geometrical Length Scale Multiplier C_3	0.070	$def = 1$	0.050
Tumble Term Multiplier C_{tumb}	0.300	$def = 1$	1.410

TABLE 6: *Main calibration* average and maximum errors (calibration/prediction points)

TABUĽKA 6: Priemerné a maximálne odchýlky *Hlavnej kalibrácie* (kalibračné/predikčné body)

Parameter	Avg. error	Max. error
IMEP	1.35/0.95 [%]	4.75/2.84 [%]
CA50	0.44/0.45 [°CA]	1.28/0.68 [°CA]
MFB10-90	0.52/0.82 [°CA]	2.18/1.14 [°CA]
MFB10-75	1.17/2.17 [°CA]	-2.46/0.53 [°CA]
Maximum Pressure	1.20/2.46 [bar]	3.94/5.78 [bar]
CA @ Maximum Pressure	0.42/0.54 [°CA]	1.10/1.10 [°CA]

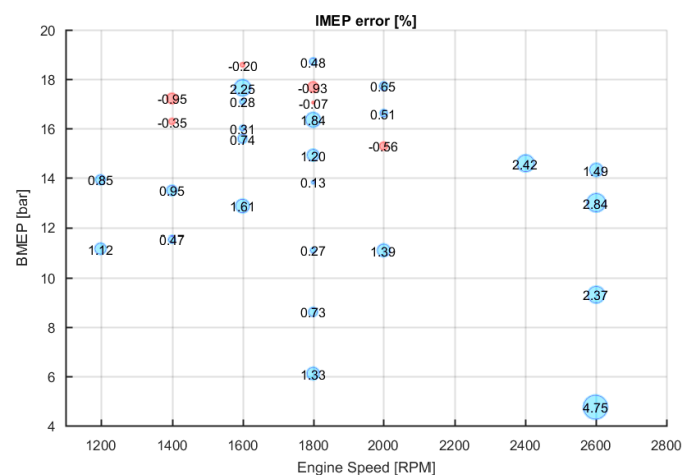


FIGURE 5: IMEP percentage errors of the experimental versus simulation values, *Main calibration*

OBRAZOK 5: Percentuálna chyba IMEP, experiment verzus simulácia



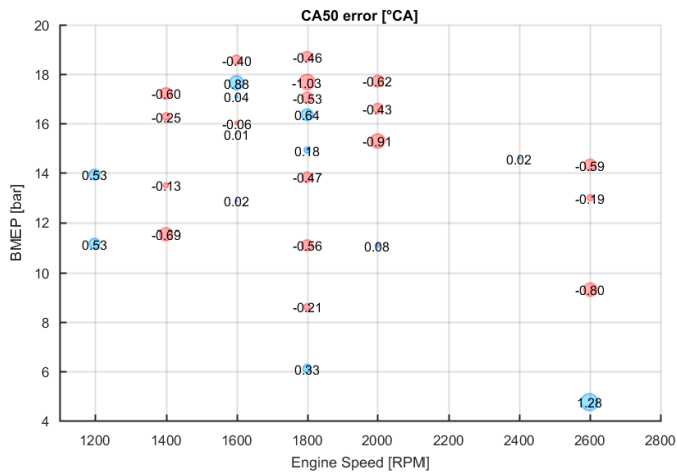


FIGURE 6: CA50 errors of the experimental versus simulation values, *Main calibration*
OBRAZOK 6: Chyba CA50, experiment verus simulácia, *Hlavná kalibrácia*

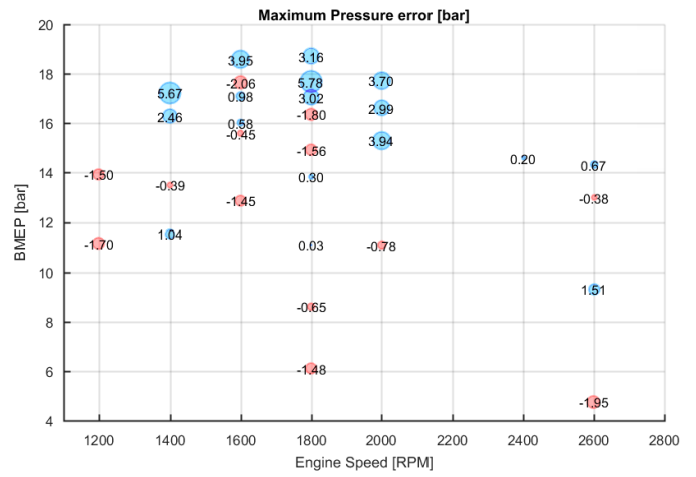


FIGURE 8: Maximum firing pressure errors of the experimental versus simulation values, *Main calibration*
OBRAZOK 8: Chyba maximálneho tlaku, experiment verus simulácia, *Hlavná kalibrácia*

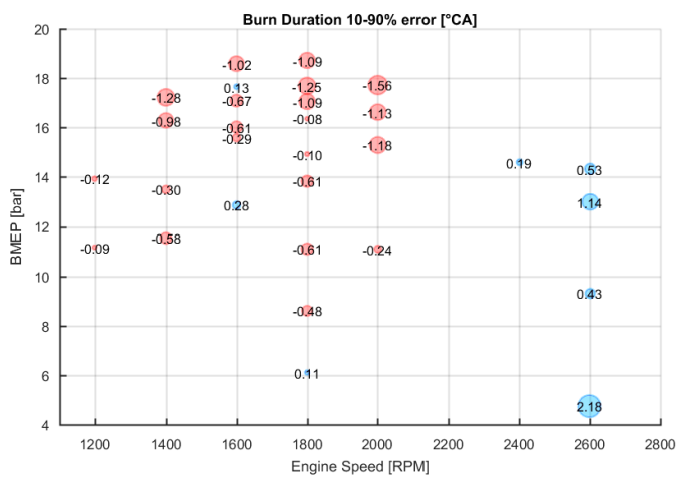


FIGURE 7: Burn Duration 10%-90% errors of the experimental versus simulation values, *Main calibration*
OBRAZOK 7: Chyba dĺžky horenia 10-90% zhoreného paliva, experiment verus simulácia, *Hlavná kalibrácia*

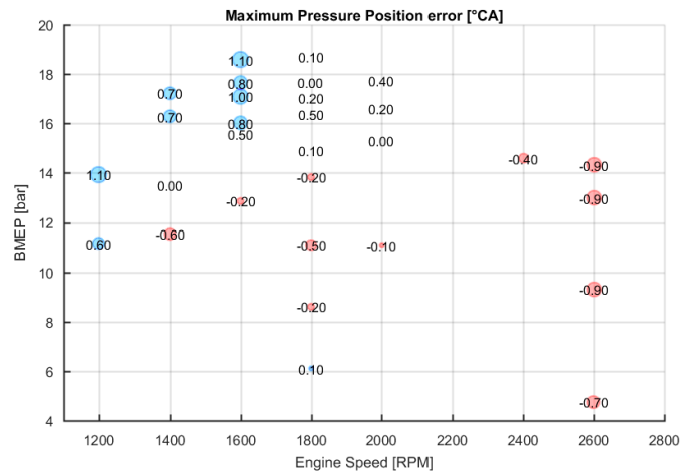
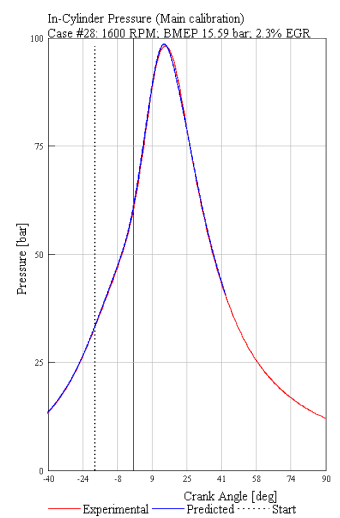
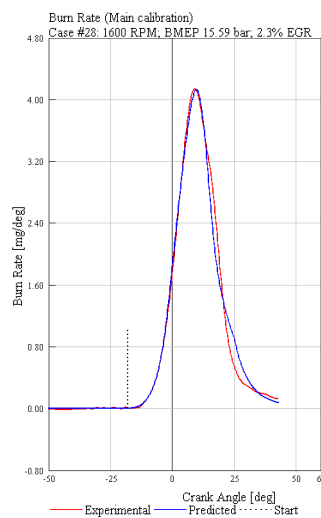
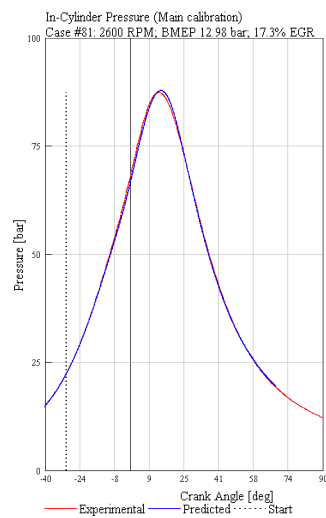
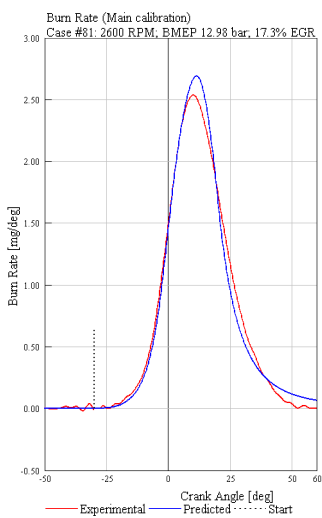


FIGURE 9: Maximum firing pressure crank angle position errors of the experimental versus simulation values, *Main calibration*
OBRAZOK 9: Chyba polohy maximálneho tlaku, experiment verus simulácia, *Hlavná kalibrácia*



Both, calibration and prediction operating points show very good overall agreement, supported by the visual comparison of the burn rate and in-cylinder pressure traces (e.g. Figure 10 and Figure 11). Figure 10 shows the burn rate and in-cylinder pressure comparison for the operating point 81 (prediction set) with the worst IMEP error (2.84%) and Figure 11 for operating point 28 (calibration set).

In conclusion, Table 5 shows that values for some model parameters, such as C_{K_r} , C_{λ} , and C_1 are quite high, on the other hand the value of C_3 is low. This means, that although the agreement of the overall parameters (in-cylinder pressure, IMEP burn rate) is very good, a comparison with 3D-CFD is necessary. The value for the initial spark size SS_{init} is reasonable.

5.2 SENSITIVITY 1: CALIBRATION INPUTS

The first sensitivity compares the *Main calibration* to reduced calibration set, with *Flow* model parameters fixed on default values ($def = 1$). GA was only optimizing the *SITurb* values. Optimal *SITurb* parameters are summarized in the second column of Table 5. It is important to note that the optimal values for both sets (*Main Calibration* and *Sensitivity 1*) are comparable to each-other, with a possible trade-off effect between the *SITurb* parameter C_s (Turbulent Flame Speed Multiplier) and *Flow* parameter C_2 (Production Term Multiplier). Table 7 sums-up the average and maximum error values. The overall agreement is also very good, but compared to the *Main Calibration* results (Table 6), both the average and maximum errors are higher.

To illustrate the effects of the *Flow* model parameters, Figure 12 shows the difference between the turbulent kinetic energy and turbulent flame speeds. The *Flow* model parameters in the *Main Calibration* actually dampen the in-cylinder flow motion, which is compensated by the turbulent velocities.

<<

FIGURE 10: Comparison between the experimental and simulation burn rate and in-cylinder pressure at 2600 RPM, BMEP 12.98 bar, 17.3% EGR (operating point 81 maximum IMEP error for the prediction set)

OBRÁZOK 10: Porovnanie experimentálneho a simulačného priebehu rýchlosti horenia a tlaku vo valci pri 2600 RPM, BMEP 12.98 bar, 17.3% EGR (pracovný bod 81 s maximálnou percentuálnou chybou IMEP, z predikčného setu)

<

FIGURE 11: Comparison between the experimental and simulation burn rate and in-cylinder pressure at 1600 RPM, BMEP 15.59 bar, 2.3% EGR (operating point 28, calibration set)

OBRÁZOK 11: Porovnanie experimentálneho a simulačného priebehu rýchlosti horenia a tlaku vo valci pri 1600 RPM, BMEP 15.59 bar, 2.3% EGR (pracovný bod 28, kalibračný set)

TABLE 7: Sensitivity 1 average and maximum errors (calibration/prediction points)

TABUĽKA 7: Priemerné a maximálne odchýlky Citlivosti 1 (kalibračné/predikčné body)

Parameter	Avg. error	Max. error
IMEP	1.15/1.08 [%]	5.62/2.71 [%]
CA50	0.49/0.59 [°CA]	-1.74/-1.52 [°CA]
MFB10-90	0.79/1.03 [°CA]	2.50/-1.72 [°CA]
MFB10-75	3.04/3.71 [°CA]	-4.49/-5.44 [°CA]
Maximum Pressure	1.30/3.13 [bar]	4.49/6.96 [bar]
CA @ Maximum Pressure	0.55/0.72 [°CA]	-1.40/-1.40 [°CA]

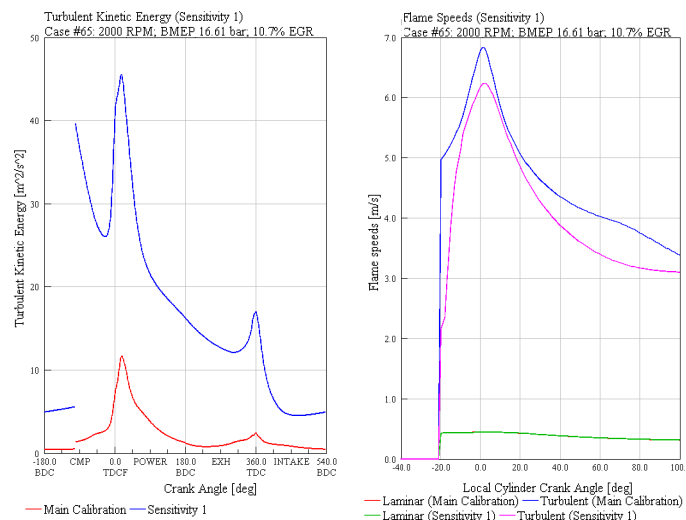


FIGURE 12: Comparison between the experimental and simulation of turbulent kinetic energy and turbulent flame speed at prediction operating point 65 (2000 RPM, BMEP 16.61 bar, 10.7% EGR)

OBRÁZOK 12: Porovnanie experimentálneho a simulačného priebehu turbulenciej kinetickej energie a turbulenciej rýchlosti čela plameňa pre predikčný pracovný bod 65 (2000 RPM, BMEP 16.61 bar, 10.7% EGR)

5.3 SENSITIVITY 2: LAMINAR FLAME SPEED MODEL

Sensitivity 2 deals about the effect of the laminar flame speed model, which is set to $S_{L_{NG2}}$ values. The third column of Table 5 shows the optimized values for both the *Flow* and *SITurb* sub-models. In this case, compared to the *Main Calibration* outputs, the differences are notable.

Table 8 summarizes the average and maximum error values. The average and maximum error values are higher than in the *Sensitivity 1*. And especially those for MFB10-75% show the effect of the different laminar flame speed models.

Figure 13 then depicts the burn rate and in-cylinder pressure comparison of experimental values, *Main Calibration*, and *Sensitivity 2*. The selected low load operating point 41 is taken from the prediction set (achieves a low overall error in the *Main Calibration*).



TABLE 8: Sensitivity 2 average and maximum errors (calibration/prediction points)

TABUĽKA 8: Priemerné a maximálne odchýlky Citlivosti 2 (kalibračné/predikčné body)

Parameter	Avg. error	Max. error
IMEP	0.69/0.92 [%]	-1.97/-1.93 [%]
CA50	0.67/0.68 [°CA]	2.60/1.93 [°CA]
MFB10-90	0.37/0.41 [°CA]	0.84/0.97 [°CA]
MFB10-75	2.10/3.03 [°CA]	-5.71/-5.38 [°CA]
Maximum Pressure	1.48/2.08 [bar]	-3.69/-5.63 [bar]
CA @ Maximum Pressure	0.64/0.92 [°CA]	1.50/1.90 [°CA]

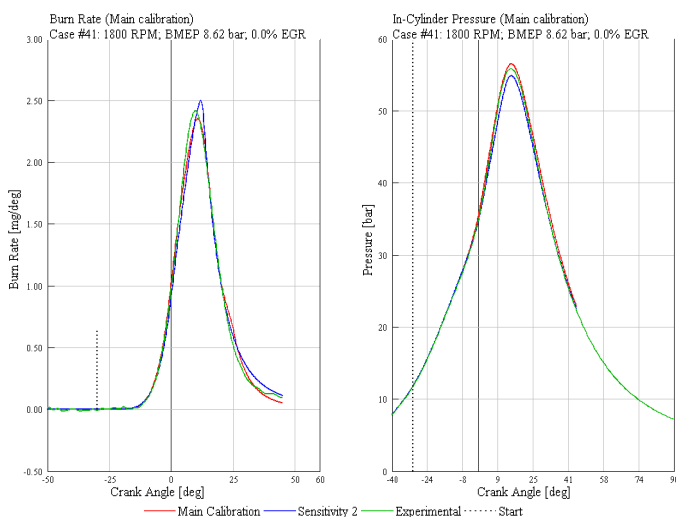


FIGURE 13: Comparison between the experimental and simulation burn rate and in-cylinder pressure at prediction operating point 41 (1800 RPM, BMEP 8.62 bar, 0.0% EGR)

OBRAZOK 13: Porovnanie experimentálneho a simulačného priebehu rýchlosti horenia a tlaku vo valci pre predikčný pracovný bod 41 (1800 RPM, BMEP 8.62 bar, 0.0% EGR)

6. CONCLUSION

We have evaluated the predictive capabilities of a 0D phenomenological in-cylinder flow model, based on the $K-k-\varepsilon$ kinetic energy cascade approach and coupled with a turbulent combustion model, using a turbocharged natural gas SI engine. First, we did a detailed model calibration using GA and then added two model sensitivity studies: regarding the calibration procedure and the laminar flame speed sub-model.

The main detailed model calibration shows that:

- Very good agreement with the experimental data can be achieved on the side of in-cylinder pressure traces and burn rate;
- The combustion model is capable of prediction outside of its calibration range, achieving good results;
- Some of the calibration parameters in the optimal set are high, which has to be further studied (e.g. comparison with 3D-CFD)

The results from the first sensitivity on the calibration inputs (calibrating only the turbulent combustion model; the flow model set to default values) only strengthen the conviction of the necessary comparison with 3D-CFD:

- The available results from the flow model are different than those in the main calibration;
- However, if the flow model is not included in the calibration, the combustion model still shows good agreement with the experimental data and prediction abilities.

The second calibration – concerning the laminar flame speed model – shows the importance of a correct model values:

- We have tested two different sets of laminar flame speed sub-model values and both showing differences;
- The overall effect on the burn rate and in-cylinder pressure traces is greater than in the first sensitivity.

In conclusion, our work shows the importance of the in-cylinder flow model verification with the 3D-CFD, and the importance of a correct laminar flame speed model, especially for the natural gas fueled ICE.

Future development concerning the natural gas ICE will focus on a comparison of the 0D phenomenological in-cylinder flow model with a 3D-CFD and further extension of the test matrix. The extended test matrix will include the air dilution and spark-timing sweeps. After the studies on the natural gas engine, the work will move to a gasoline SI ICE also.

ACKNOWLEDGEMENTS

This work was supported by the Grant Agency of the Czech Technical University in Prague, grant No. SGS16/213/OHK2/3T/12

LIST OF ABBREVIATIONS

0D/3D	Zero/Three-Dimensional
BMEP	Brake Mean Effective Pressure
CA	Crank Angle
CFD	Computational Fluid Dynamics
DoE	Design of Experiments
EGR	Exhaust Gas Recirculation
EVC	Exhaust Valve Close
EVO	Exhaust Valve Open
GA	Genetic Algorithms
ICE	Internal Combustion Engine
IMEP	Indicated Mean Effective Pressure
IVO	Intake Valve Open
IVC	Intake Valve Close
MFB	Mass Fraction Burned
RMS	Root Mean Square
SI	Spark Ignition
TDC	Top Dead Center
TPA	Three-Pressure-Analysis



LIST OF SYMBOLS

A_f	Flame Front Area
B	Cylinder Bore
B_m	Maximum Laminar Speed
B_ϕ	Laminar Speed Roll-off Value
C_1	Intake Term Multiplier
C_2	Production Term Multiplier
C_3	Geometrical Length Scale Multiplier
C_{in}	Intake Term
C_K	Flame Kernel Growth Multiplier
C_S	Turbulent Flame Speed Multiplier
C_{Swirl}	Intake Port Swirl Coefficient
C_{tumb}	Tumble Term Multiplier
C_β	Production Term
C_λ	Taylor Length Scale Multiplier
C_μ	k - ϵ Model Constant
DEM	Dilution Exponent Multiplier
D_{il}	Mass Fraction of the Residuals in the Unburned Zone
E_{in}	Intake Energy
F	Criterial Function
k	Turbulent Kinetic Energy
K	Mean Kinetic Energy
L	Angular Momentum
L_g	Geometrical Length Scale
L_t	Integral Length Scale
m	In-cylinder Mass
\dot{m}_{out}	Cylinder Exit Mass Flow Rate
M_b	Burned Mass
M_e	Entrained Mass
p	Pressure
p_0	Reference Pressure
P_k	Turbulence Production Term
P_ϵ	Dissipation Rate Production Term
R_f	Flame Front Radius
Re	Reynolds Number
s	Piston Stroke
S_L	Laminar Flame Speed
S_T	Turbulent Flame Speed
SS_{init}	Initial Spark Size
T_u	Temperature of Unburned Gas
T_0	Reference Temperature
T	Tumble Contribution to Turbulence
u'	Mean Fluctuating Turbulent Velocity
U	Mean Velocity inside the Cylinder
X_k	Objective Function
α	Temperature Exponent
α_{in}	Intake Energy Fraction Converted Directly into Turbulence

α_k	Weight Factor
β	Pressure Exponent
Δ	Difference
ϵ	Turbulent Dissipation Rate
λ	Taylor Microscale of Turbulence
ν_T	Turbulent Viscosity
ρ	Density
$\dot{\rho}$	Density Rate of Change
ρ_u	Density of Unburned Gas
ϕ	Fuel/air Equivalence Ratio
ϕ_m	Fuel/air Equivalence Ratio at Maximum Laminar Flame Speed

REFERENCES

- [1] Vitek, O., Macek, J., Tatschl, R., Pavlovic, Y., Priesching, P. (2012). LES Simulation of Direct Injection SI-Engine In-Cylinder Flow. [SAE Technical Paper 2012-01-0138](#), doi: 10.4271/2012-01-0138
- [2] Vibe, I.I. (1956). Semi-empirical expression for combustion rate in engines, In: [Proc. Conference on Piston Engines](#), USSR Academy of Sciences, Moscow
- [3] Csallner, P., Woschni, G. (1982). Zur Vorausberechnung des Brennverlaufes von Ottomotoren bei geänderten Betriebsbedingungen, [MTZ](#), No.5
- [4] Vavra, J., Takats, M. (2004). Heat Release Regression Model for Gas Fuelled SI Engines, [SAE Technical Paper 2004-01-1462](#), doi: 10.4271/2004-01-1462
- [5] Skarohlid, M. (2010). Modeling of Influence of Biogas Fuel Composition on Parameters of Automotive Engines, [SAE Technical Paper 2010-01-0542](#), doi: 10.4271/2010-01-0542
- [6] Macek, J., Steiner, T. (1995). Advanced Multizone Multidimensional Models of Engine Thermodynamics. In: [21st CIMAC Congress](#), London, p. D10/1-D10/18
- [7] Hvezda, J. (2014). Multi-Zone Models of Combustion and Heat Transfer Processes in SI Engine. [SAE Technical Paper 2014-01-1067](#), doi: 10.4271/2014-01-1067
- [8] Wahiduzzaman, S., Morel, T., Sheard, S. (1993). Comparison of Measured and Predicted Combustion Characteristics of a Four-Valve S.I. Engine, [SAE Technical Paper 930613](#), doi: 10.4271/9306
- [9] Morel, T., Mansour, N. N. (1982). Modeling of turbulence in Internal Combustion Engines, [SAE Technical Paper 820040](#), doi: 10.4271/820040
- [10] Morel, T., Keribar, R. (1985). A Model for Predicting Spatially and Time Resolved Convective Heat Transfer in Bowl-in-Piston Combustion Chambers, [SAE Technical Paper 850204](#), doi: 10.4271/850204



- [11] Morel, T., Rackmil, C. I., Keribar, R., Jennings, M. J. (1988). Model for Heat Transfer and Combustion in Spark Ignited Engines and Its Comparison with Experiments, *SAE Technical Paper* 880198, doi: 10.4271/880198
- [12] Bozza, F., Gimelli, A. (2004). A Comprehensive 1D Model for the Simulation of a Small-Size Two-Stroke SI Engine. *SAE Technical Paper* 2004-01-0999, doi: 10.4271/2004-01-0999
- [13] Vitek, O., Macek, J., Poetsch, Ch., Tatschl, R. (2013). Modeling Cycle-to-Cycle Variations in 0-D/1-D Simulation by Means of Combustion Model Parameter Perturbations based on Statistics of Cycle-Resolved Data. *SAE Int. J. Engines*, Vol. 6, No. 2, doi: 10.4271/2013-01-1314
- [14] GT-POWER Engine Performance Application Manual. [Manual] Westmont: Gamma Technologies, Inc., 2015
- [15] Fogla, N., Bybee, M., Mirzaeian, M., Millo, F. et al. (2017). Development of a $K-k-\varepsilon$ Phenomenological Model to Predict In-Cylinder Turbulence, *SAE Int. J. Engines*, Vol. 10, No. 2, doi: 10.4271/2017-01-0542
- [16] Mirzaeian, M., Millo, F., and Rolando, L. (2016). Assessment of the Predictive Capabilities of a Combustion Model for a Modern Downsized Turbocharged SI Engine, *SAE Technical Paper* 2016-01-0557, doi: 10.4271/2016-01-0557
- [17] Hernandez, J., Lapuerta, M., Serrano, C. (2005) Estimation of the Laminar Flame Speed of Producer Gas from Biomass Gasification, *Energy Fuels*, Vol. 19, No. 5, p. 2172-2178, doi: 10.1021/ef058002y
- [18] S.Y. Liao, D.M. Jiang, and Q. Cheng. (2004) Determination of laminar burning velocities for natural gas, *Fuel*, Vol. 83, Issue 9, p.1247-1250. doi: 10.1016/j.fuel.2003.12.001
- [19] Vavra, J., Takats, M., Klir, V., Skarohlid, M. (2012). Influence of Natural Gas Composition on Turbocharged Stoichiometric SI Engine Performance, *SAE Technical Paper* 2012-01-1647, doi: 10.4271/2012-01-1647
- [20] Woschni, G. (1967). A Universally Applicable Equation for the Instantaneous Heat Transfer Coefficient in the Internal Combustion Engine, *SAE Technical Paper* 880198, doi: 10.4271/670931
- [21] modeFRONTIER – Multi-Objective Design Environment, version 4.4.3. [CD-ROM], 2012



STUDY OF THE EFFECTS OF ETHANOL AS AN ADDITIVE WITH A BLEND OF POULTRY LITTER BIODIESEL AND ALUMINA NANOPARTICLES ON A DIESEL ENGINE

RAMESHA D K, NISHAD RAJMALWAR, T SREEHARSHA VARMA

Department of Mechanical Engineering, University Visvesvaraya College of Engineering, Bangalore University, Bangalore, Karnataka, India-560001, dkramesha@bub.ernet.in

MRITHYUNAJAYA SWAMY K M

Department of Mechanical Engineering, Vemana Institute of Technology, Visvesvaraya Technological University, Bangalore, Karnataka, India

ABSTRACT

With the increasing population and rise in industrialization, the demand for petroleum reserves is increasing almost daily. This is causing depletion of the non-renewable energy resources. This work aims to find an alternative fuel for diesel engines. The use of poultry litter oil biodiesel obtained from poultry industry waste, which is a non-edible source for biodiesel, is very encouraging as an alternative fuel for diesel engines. The aim of this study is to observe and maximize the performance of poultry litter oil biodiesel by adding alumina nanoparticles and ethanol. The biodiesel is prepared with acid and the base catalysed transesterification of poultry litter oil with methanol using concentrated sulphuric acid and potassium hydroxide as catalysts. The experimentation is carried out on a CI engine with three different blends – B20 biodiesel blend, B20 biodiesel blend with 30 mg/L alumina nanoparticles, and B20 biodiesel blend with 30 mg/L alumina nanoparticles and 15 ml/L ethanol. The performance, combustion and emission characteristics of all three blends are compared with neat diesel. The results of the experiment show that ethanol as an additive improves the combustion and performance characteristics. It increases the brake thermal efficiency and peak cylinder pressure. It also reduces CO and UBHC emissions and there is a marginal increase in NO_x emissions as compared to neat diesel.

KEYWORDS: DIESEL ENGINE; POULTRY LITTER OIL METHYL ESTER; BIODIESEL; ALUMINA NANOPARTICLES; TRANSESTERIFICATION; ETHANOL; PERFORMANCE; COMBUSTION; EMISSION.

SHRNUTÍ

S rostoucím počtem obyvatel a nárůstem industrializace se den za dnem zvyšuje poptávka po ropných rezervách. To způsobuje vyčerpávání neobnovitelných zdrojů energie. Tato práce si klade za cíl nalézt alternativní palivo pro diesellové motory. Použití bionafty získané z oleje z použité podestýlky z chovů drůbeže, která představuje nekonzumovatelný zdroj pro výrobu bionafty jako alternativní palivo pro diesellové motory, je velmi slibné. Cílem této studie je pozorovat a maximalizovat výkon bionafty z oleje z použité drůbeží podestýlky přidáním nanočástic oxidu hlinitého a etanolu. Bionafta je připravována kyselinou a zásadou katalyzovanou transesterifikací oleje z použité drůbeží podestýlky a metanolem, kde jsou jako katalyzátory použity koncentrovaná kyselina sírová resp. draselný louh. Experimentace se provádí na vznětovém motoru s třemi různými druhy směsi – směs bionafty B20, směs bionafty B20 s 30 mg/L nanočástic oxidu hlinitého a směs bionafty B20 s 30 mg/L nanočástic oxidu hlinitého a 15 ml/L etanolu. Parametry výkonu, spalování a emisí všech tří směsí jsou srovnávány diesellovým palivem (naftou) bez přísad. Výsledky experimentu ukazují, že etanol jako aditivum zlepšuje parametry spalování a výkonu. Zvyšuje brzdnou tepelnou účinnost a maximální tlak ve válci. Dále snižuje emise CO a nespálených uhlovodíků, přičemž je zde marginální zvýšení emisí NO_x oproti naftě bez přísad.

KLIČOVÁ SLOVA: DIESELOVÝ MOTOR; METYLESTER OLEJE Z POUŽITÉ PODESTÝLKY DRŮBEŽE; BIODIESEL (BIONAFTA); NANOČÁSTICE OXIDU HLINITÉHO; TRANSESTERIFIKACE; ETANOL; VÝKON; SPALOVÁNÍ; EMISE.



1. INTRODUCTION

Conventional fossil fuels cause environmental pollution and with demand for them ever increasing, they are being depleted at a fast pace. This situation necessitates paying greater attention to alternative fuels from natural resources, such as biodiesel and ethanol-biodiesel blends. Both biodiesel and ethanol can be synthesized from feedstock, which is a renewable resource. The carbon in the biodiesel comes from the CO₂ present in the air, so the CO₂ engine emissions when running on biodiesel overall add much less to global warming compared to fossil fuels. Efforts have been made to replace petroleum-based fuels with as much biofuel as possible because biodiesel by itself cannot be entirely used as a fuel [13] (Xiaoyan Shi et al. 2006). Biodiesel can be produced using the process of transesterification of vegetable/animal oil or fat with a short-chain alcohol like methanol or ethanol. The reaction gives mono-alkyl esters which can be used as biodiesel. Neat oil cannot be used as a fuel mainly due to its high viscosity (28-40mm²/s), which leads to deposition of carbon particles in the injector in a CI engine. This causes poorer atomization of fuel particles into the combustion chamber [2] (Darunde Dhiraj S. et al. 2012). Since neat vegetable/animal oil or fat cannot be used as a fuel, transesterification is carried out to reduce the viscosity. Transesterification is the reaction between a triglyceride molecule (found in vegetable oil or animal fat) and excess alcohol in the presence of a catalyst, such as KOH, NaOH etc., to give methyl esters and glycerin as a by-product [11] (Sri Harsha Tirumala et al. 2012). The process occurs in several reversible steps where the triglyceride is converted to diglyceride, which is further converted to monoglyceride. These monoglycerides are then converted to esters and glycerol. The esters can be separated from glycerol using a separating funnel due to their density difference. In our experiment, the ester is called Poultry Litter Oil Methyl Ester [3] (Dr. Sadhik B. J. et al. 2012). At present, diesel fuel additives are used to lower the particulate emissions and enhance fuel characteristics such as oxidation rate. Additives also help to reduce emissions. One such additive are nanoparticles, which are pre-dissolved in the fuel and help increase the efficiency of the fuel and completion of the combustion process to reduce emissions of various harmful gases and particulate matter [8] (Nithin Samuel et al. 2015). With Aluminium oxide nanoparticles as an additive, an increase in brake thermal efficiency and a reduction in emissions were observed. Also, to increase the overall performance, combustion and emission characteristics of the engine, nanoparticles are the most suitable additive [9] (S.P. Venkatesan et al. 2015). To further improve the performance of the engine, the potential use of biodiesel with an ethanol blend was investigated. Ethanol improves the flow property of the fuel and helps ensure better atomization. It enhances the oxygen content of the fuel to help

reduce emissions. The potential of poultry litter biodiesel with a blend of ethanol as a renewable energy resource is presented in this paper.

2. TRANSESTERIFICATION

2.1 ESTERIFICATION SETUP

The oil used for biodiesel production was non-edible raw poultry litter oil. Production was carried out using a laboratory setup. The setup consisted of beakers, flasks, a thermometer and a magnetic stirrer with temperature control and adjustable stirring speed. The properties of diesel fuel and PLOME are listed according to ASTM standards in Table 4. The acid value of raw oil had been calculated using a standard titrimetric method as per European standard EN14104. A conical flask was used as a laboratory scale reactor to carry out the transesterification process. The magnetic stirrer consisted of a heating coil with adjustable temperature. The flask was kept on the stirrer and the mixture was heated. The temperature for the reaction was maintained at 50-60°C and the mixture was stirred at constant speed at all times. The esterification process was carried out in two steps since the oil viscosity was high.

2.2.1 ACID CATALYSED TRANSESTERIFICATION

Acid transesterification was carried out by pouring 1 litre of raw poultry oil into the conical flask and heating it to a temperature of 50°C. Once the oil reached this constant temperature, 500 ml of methanol was added and stirred for a few minutes. 10 ml of concentrated sulphuric acid was added to the mixture. This final mixture was maintained at a temperature of 50°C and stirred for 45 minutes at atmospheric pressure. The flask was removed from the stirrer and the mixture was allowed to settle. Two layers separate out and were visible to the naked eye. The layers were separated using a separating funnel. The top layer consisted of excess methanol, sulphuric acid and light impurities, which were removed. The lower layer was poured into a different flask for the next step of experimentation.

2.2.2 BASE CATALYSED TRANSESTERIFICATION

The final product from the first experimental setup of the acid catalysed process was used for alkaline esterification. The product was again heated to a temperature of 50°C in the flask. Meanwhile, 0.24 g of KOH was added to 100 ml of methanol in a beaker and thoroughly dissolved. This mixture was poured into the flask and heated at 50°C for 45 minutes. Once the heating was complete, the mixture was allowed to cool down. Again, layer separation was noticeable. This time the lower layer consisted of glycerol and impurities, which were discarded. The top layer



TABLE 1: Fuel properties
TABULKA 1: Vlastnosti paliv

Sl. No.	Property	ASTM Method	Limits (B100)	Units	Diesel	PLOME
1	Colour	-	-	-	Orange	Pale Yellow
2	Density	D941	-	kg/m ³	850	737
3	Kinematic viscosity, 40°C	D445	1.9-6	mm ² /s	2.5	5.48
4	Calorific value	D2015	-	kJ/kg	42000	29000
5	Fire point	D93	-	°C	56	178
6	Flash point	D93	130 min.	°C	50	154
7	Cetane index	D613	47 min.	-	55	61

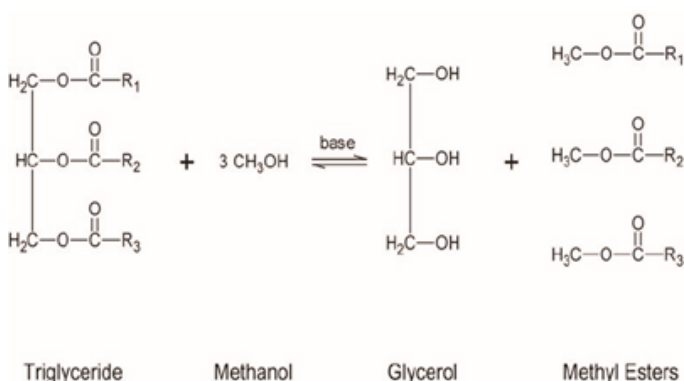


FIGURE 1: Mechanism of the transesterification process
OBRAZEK 1: Mechanismus procesu transesterifikace

was the methyl ester, which was separated using the separating funnel. This ester contained some impurities and was therefore water washed. Hot distilled water, 10% by volume, was sprayed over the surface of the ester and gently stirred. The water carried impurities and settled down at the bottom of the flask. The top layer (yellow colour) was the biodiesel which was separated and collected.

2.2.3 PREPARATION OF BLEND

B20PLOME was prepared by mixing 20% by volume biodiesel with 80% by volume diesel in a beaker and stirring it for 15 minutes at constant room temperature. B20PLOME30A was prepared by adding 30 mg of alumina nanoparticles to 1 litre of B20PLOME biodiesel blend. B20PIOME30A15E was prepared by adding 15 ml/l of pure ethanol to the B20PLOME30A blend.

2.2.4 ADDITION OF ALUMINA NANOPARTICLES

The nanoparticles were added to B20PLOME biodiesel fuel with the help of an ultrasonicator at a frequency of 24 kHz. The process was carried out for 30 minutes. The mass fraction of the nanoparticles was 30 mg/l. It was weighed using an electronic

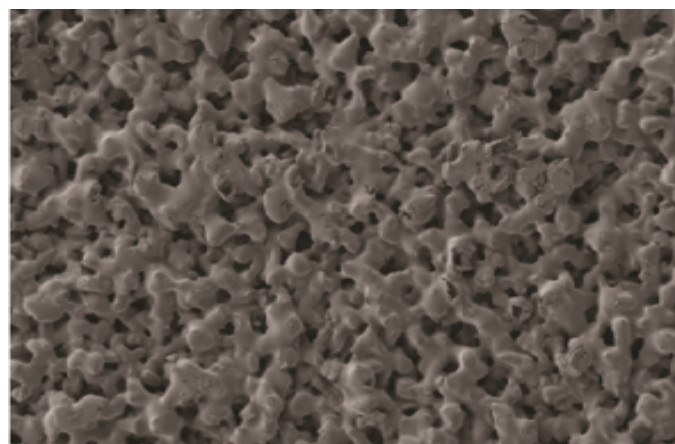
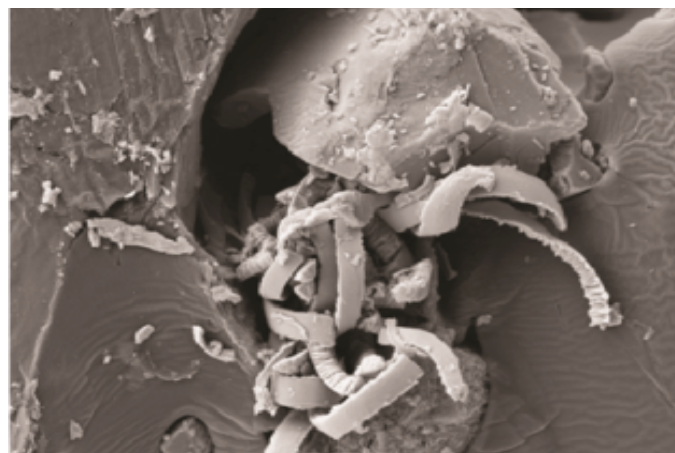


FIGURE 2: Transmission electron microscope image of alumina nanoparticle
OBRAZEK 2: Obrázek elektronového mikroskopu hliníkových nanočástic

weighing machine with readability of 1 mg. The ultrasonication technique disperses the nanoparticles in a base fluid, which in this case was the biodiesel fuel. It is the best suited technique since it prevents the aggregation of nanoparticles by agitating the particles using pulsating ultrasonic frequencies. The alumina nanoparticle specification is shown in Table 1. Figure 2 shows the morphology of alumina nanoparticles. Surfactants were added to lower the surface tension between the liquid fuel and solid nanoparticles in order to stabilize the nanoparticles.

2.2.5 ADDITION OF ETHANOL

Ethanol was added with a composition of 15 ml of ethanol per litre of B20PLOME30A biodiesel fuel. The mixing process was carried out by constant stirring on the magnetic stirrer for 30 minutes without any heating, maintaining the mixture at room temperature. This final mixture is designated B20PLOME30A15E.

3. ENGINE TEST

The engine test was conducted on a single cylinder four-stroke diesel engine with injection timing of 23 degrees BTDC, injection pressure of 180, 17.5:1 compression ratio and a speed



TABLE 2: Specification of alumina nanoparticles
TABULKA 2: Vlastnosti hliníkových nanočástic

Properties	Specification
Chemical name	Gamma Aluminium Oxide (Alumina, Al ₂ O ₃) Nanopowder, gamma phase, 99.9%
Average particle size	20–50 nm
Appearance	White
Melting point	2045 °C
Boiling point	2980 °C
Density	3.9 g/cm ³

TABLE 3: Specifications of the OROTECH exhaust gas analyser
TABULKA 3: Specifikace analyzátoru výfukových plynů OROTECH

Measurement Parameters	Range	Resolution
Carbon monoxide (CO)	0–10% vol.	0.001% vol.
Hydrocarbon (HC)	0–9999% ppm vol.	1.0 ppm vol.
Oxides of nitrogen (NO _x)	0–5000 ppm vol.	1.0 ppm vol.

TABLE 4: Specification of the AVL437C smoke meter
TABULKA 4: Specifikace kouřoměru AVL437C

Measurement Parameters	Range	Resolution
Opacity	0–99.9%	0.1%
Linearity	±0.1 m ⁻¹	
Repeatability	±0.1 m ⁻¹	
Response time- physical	< 0.4 seconds	
Response time- electrical	< 1 millisecond	
Warm up time at atm. conditions	< 7 minutes	
Engine RPM	400–9990 RPM	10 RPM
Engine oil temperature	0-150°C	1°C
Operating temperature	5°C to 50°C	
Smoke measuring cell length	215mm (430mm folded length)	

of 1500 RPM. The engine was initially hand cranked with a pure diesel supply to bring it to a steady state. The engine was coupled to an eddy current dynamometer that allowed varying of the engine load from no-load to full load. The engine test rig was computerized and both the engine and dynamometer were interfaced to a control panel in a computer. The computer had 'Engine Analysis Software' which recorded test parameters such as temperature, air flow rate, fuel flow rate, load etc. It also plotted the engine performance characteristics such as brake thermal efficiency, heat release rate etc. The load was varied in four steps from no-load to full load. The engine was run with B20PLOME, B20PLOME30A and B20PLOM30A15E whilst keeping all the above conditions constant. The performance, combustion and emissions tests were carried out. An OROTECH Exhaust Gas Analyzer, as specified in Table 2, was used for exhaust gas analysis. The AVL437C Smoke Meter, as specified in Table 3, was used for recording smoke opacity.

3.1 UNCERTAINTY ANALYSIS

The uncertainties of the parameters are calculated by sequential perturbation. The average uncertainties of measured and calculated parameters are air flow rate (1.1%), liquid fuel flow rate (0.1%), gas flow rate (2%), engine load (0.1%), engine speed (1.3%), cylinder pressure (0.8%), temperature (1.0%) and LCV of liquid fuel (1.0%). Based on these, the calculated accuracy of the performance and combustion studies of the engine is found to be within ±4.6%. However, the accuracy of the emission study is found to be ±4.6%. The maximum values of coefficient of variance (COV) of the performance parameters, viz., BTE and BSFC are 3 and 4% respectively. Whereas, the combustion emission parameters, namely Peak Cylinder Pressure, Ignition Delay, CO, HC and NO_x, are shown to have COVs of 5, 4, 2, 2 and 6% respectively.

4. RESULTS AND DISCUSSION

4.1 PERFORMANCE CHARACTERISTICS

4.1.1 BRAKE THERMAL EFFICIENCY

Figure 3 shows the variation of BTE with load. The BTE of all the blends increased as load increases. The maximum load on the engine was 30 Nm of torque and the brake mean effective pressure at maximum load was 4 bar. The B20PLOME blend showed an increase in BTE due to better combustion. This is due to the oxygen content within the methyl ester. The addition of nanoparticles (B20PLOME30A) further improved BTE because of the enhanced surface area to volume ratio, which leads to more fuel reacting with air causing rapid evaporation and combustion. B20PLOME30A15E blend showed a further increase in the combustion efficiency due to additional oxygen content from



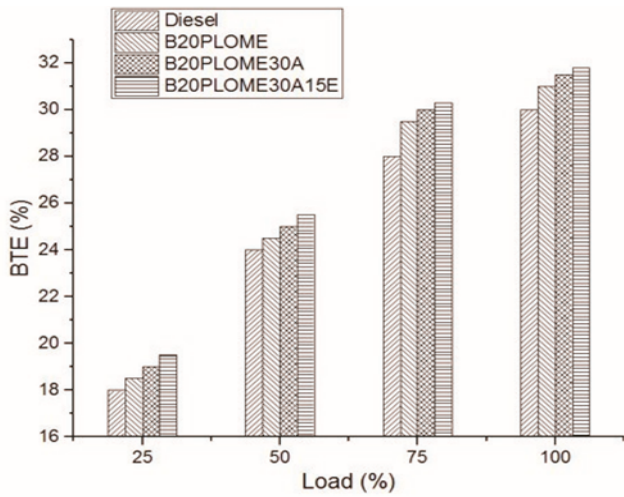


FIGURE 3: Variation of BTE with load
OBRÁZEK 3: Změna tepelné účinnosti v závislosti na zátěži

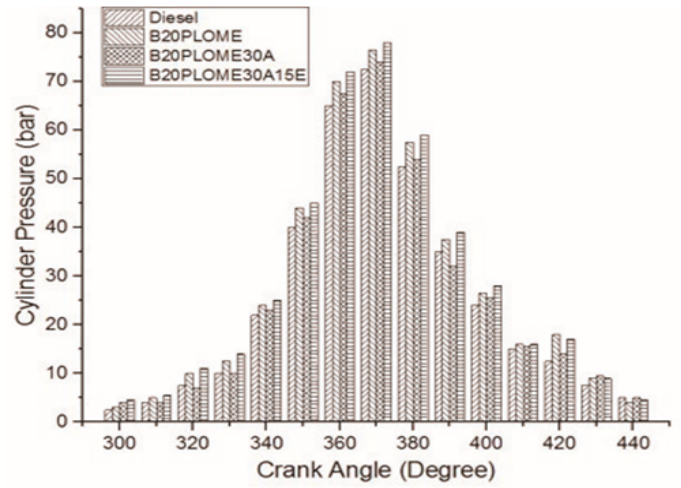


FIGURE 4: Variation of cylinder pressure with crank angle
OBRÁZEK 4: Změna tlaku ve válci v závislosti na natočení klikového hřídele

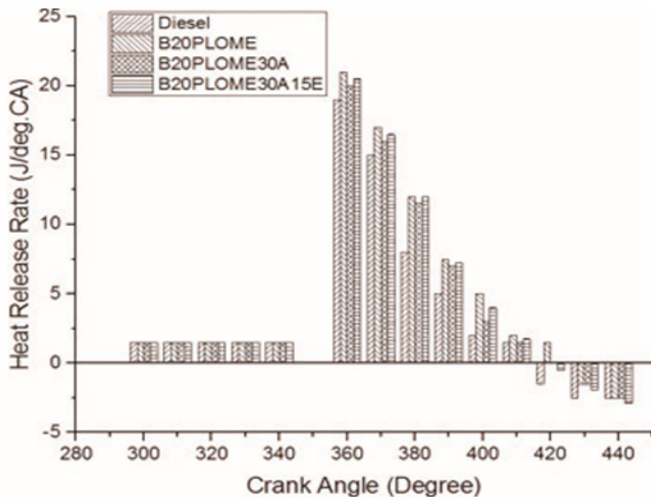


FIGURE 5: Variation of HRR with crank angle
OBRÁZEK 5: Změna HRR v závislosti na poloze klikového hřídele

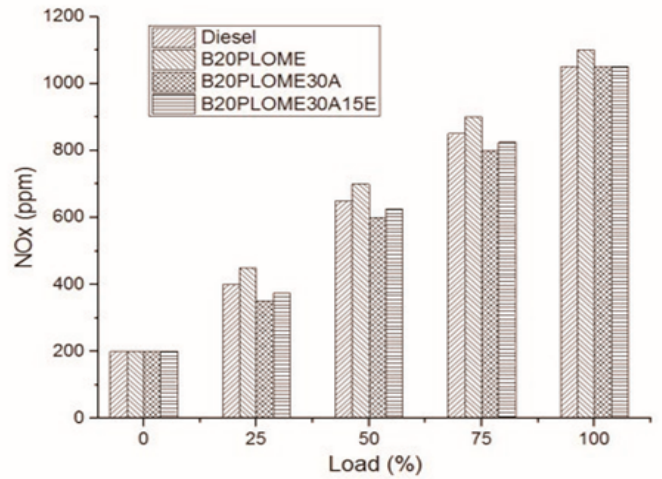


FIGURE 6: Variation of NO_x with load
OBRÁZEK 6: Změna emisí NO_x v závislosti na zátěži

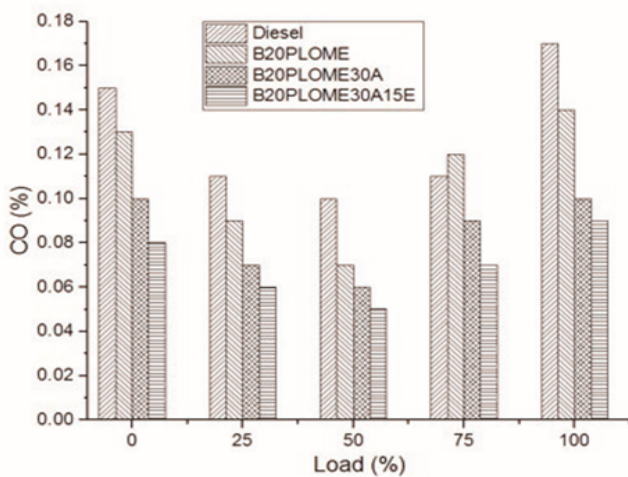


FIGURE 7: Variation of CO with load
OBRÁZEK 7: Změna emisí CO v závislosti na zátěži

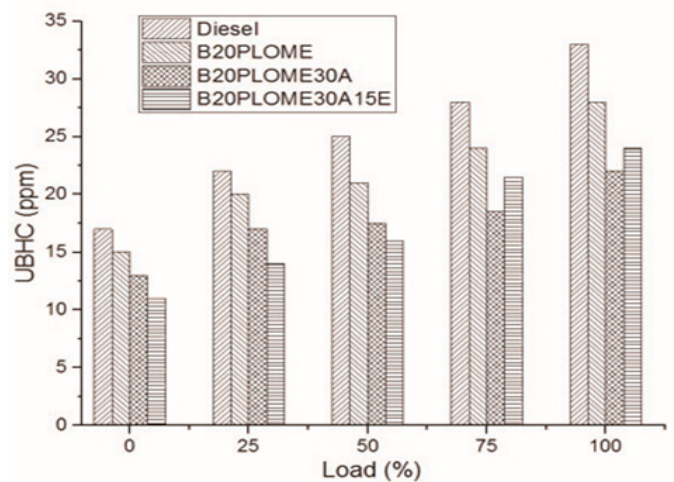


FIGURE 8: Variation of UBHC with load
OBRÁZEK 8: Změna UBHC v závislosti na zátěži



ethanol. Ethanol also decreased the density and viscosity of the fuel, which improved atomization.

4.2 COMBUSTION CHARACTERISTICS

4.2.1 PEAK CYLINDER PRESSURE

The variation of peak pressure displayed by the different fuels for various crank angles is shown in Figure 4. At full load, the peak pressure of B20PLOME was higher than that of diesel for all loads. This can be attributed to the longer ignition delay and higher oxygen content in the case of B20PLOME. At full load, B20PLOME30A showed higher peak pressure than pure diesel due to higher ignition delay and more complete combustion because of the improved surface area volume ratio. For B20PLOME30A15E, the combustion pressure increased due to better mixing of air and fuel, which resulted in better combustion, and the addition of ethanol results in a lower cetane number of the blend and hence longer ignition delay [6] (Krzysztof Gorski et al. 2011).

4.2.2 HEAT RELEASE RATE

Figure 5 shows the variation of HRR for various crank angles. B20PLOME displays a marginal increase in HRR when compared to diesel. At full load, HRR was slightly greater than diesel due to more oxygen molecules being present in B20PLOME than in diesel. B20PLOME30A shows a marginal increase in HRR compared to diesel because of better combustion, improved atomization and rapid evaporation. The HRR of B20PLOME30A was slightly lower than B20PLOME because the addition of nanoparticles causes advancement in combustion. B20PLOME30A15E showed higher HRR than B20PLOME30A because the longer ignition delay due to addition of ethanol causes rapid combustion in the premixed phase and results in an increase of HRR [12] (V. Arul MozhiSelvan et al. 2009).

4.3 EMISSION CHARACTERISTICS

4.3.1 OXIDES OF NITROGEN

Figure 6 shows the variation of NO_x for various loads. Atmospheric nitrogen is stable at normal temperature and pressure, and exists as a diatomic molecule. However, inside the engine cylinder, where it is subjected to high temperature and pressure, it reacts with oxygen to form various oxides. These are designated NO_x . NO_x formation is a strongly time and temperature dependent phenomena. NO_x emissions increased with increasing load for all fuels because as load increases, the temperature of the combustion chamber and rate at which temperature rises in the cylinder also increases. The HRR was high in the case of B20PLOME as a result of the temperature inside cylinder increasing rapidly, thereby increasing NO_x emissions when compared to diesel. The NO_x emissions of B20PLOME30A appear to decrease marginally compared to that of diesel, which was

because the catalytic behaviour of nanoparticles promotes the reaction in the forward direction and form final products with the least thermal break down of the hydrocarbon compounds. The B20PLOME30A15E blend showed a marginal increase in NO_x emissions when compared to diesel. This can be attributed to the higher heat release rate of the B20PLOME30A15E blend.

4.3.2 CARBON MONOXIDE EMISSIONS

Figure 7 shows the variation of CO emissions for various loads. CO emissions decreased at part load and again increased at full load conditions for all fuels. The B20PLOME blend showed a decrease in CO emissions when compared to diesel. This can be attributed to the higher oxygen content in the methyl esters. The catalytic behaviour of nanoparticles, improved ignition characteristics of alumina nanoparticles and the shortening of ignition delay further decreased the CO emissions of the B20PLOME30A blend when compared to the B20PLOME blend. The higher oxygen content of the B20PLOME30A15E blend further promoted the oxidation of CO to CO_2 and decreased CO emissions when compared to the B20PLOME blend [5] (K. Ramarao et al. 2015).

4.3.3 UNBURNT HYDROCARBONS (UBHC)

Figure 8 shows the variation of UBHC emissions for various loads. The UBHC emissions for all fuels increased with increasing load. UBHC emissions for all blends are lower than for diesel. At full load, B20PLOME, B20PLOME30A and B20PLOME30A15E showed respectively a 21.2%, 37.5% and 30.3% reduction in UBHC emissions when compared to diesel. The B20PLOME blend is comprised of animal fat oil methyl esters, i.e., it contains hydrocarbon chains whose one end of the chain is oxygenated. The presence of oxygen in biodiesel promotes combustion that leads to lowering the hydrocarbon emissions [10] (Senthil Kumar et al. 2001). The B20PLOME30A blend showed a further decrease in UBHC emissions, which can be attributed to the catalytic behaviour of alumina nanoparticles. The alumina nanoparticles were responsible for shortening the ignition delay and hence further reduced UBHC emissions [14] (Yetter R. et al. 2009). At lower loads the B20PLOME30A15E blend displayed a decrease in UBHC emissions when compared to B20PLOME30A. However, at loads above 50% an increase in UBHC emissions was observed when compared to B20PLOME30A. This is because of the lower combustion temperature caused by the higher latent heat of vaporisation of ethanol [4] (Hwanam Kim et al. 2010).

4.3.4 SMOKE OPACITY

Figure 9 shows the variation of smoke opacity with load. It was observed that the smoke opacity of exhaust gases increases with load for all fuels. Smoke emission is closely related to the ignition delay, volatility and fuel oxygen content. The extended ignition



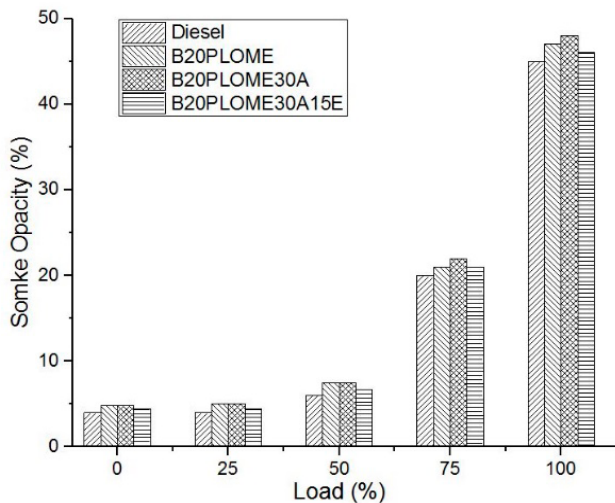


FIGURE 9: Variation of smoke opacity with load
OBRAZĚK 9: Změna kouřivosti v závislosti na zátěži

delay and high volatility can improve the fuel-air mixing process, and the oxygen in fuel can reduce the formation of soot precursors and enhance soot oxidation [15] (Zunquing Zheng et al. 2016). Due to the higher viscosity of B20PLOME and B20PLOME30A, the volatility and air-fuel mixing of these blends was poor. Also, since the molecules of B20PLOME and B20PLOME30A were heavier, they lead to an increase in smoke opacity of exhaust gases when compared to diesel [1] (Baluswamy T et al. 2007). It can be observed that the smoke opacity of B20PLOME30A15E was marginally higher than that of diesel and lower than that of B20PLOME and B20PLOME30A. This is because adding ethanol to the blend increased the oxygen content and volatility and reduced soot precursor concentration [7] (M. Mofijur et al. 2015).

5. CONCLUSION

The engine tests were conducted with B20PLOME, B20PLOME30A and B20PLOME30A15E from no load to full load conditions and the corresponding performance, combustion and emission characteristics were studied in comparison with diesel. The following results were observed – upon transesterification of poultry litter oil, it was observed that there was a reduction in kinematic viscosity and density whereas the calorific value was observed to increase. All the three blends showed increased BTE when compared to diesel. B20PLOME30A15E showed a 10.7% increase in BTE when compared to diesel. The highest cylinder pressure was recorded for B20PLOME30A15E. The addition of ethanol increases the volatility and oxygen content, which promotes combustion and as a result a further reduction in CO emissions and smoke opacity were observed when compared to B20PLOME and B20PLOME30A. The addition of ethanol increases the ignition delay period, and as a result B20PLOME30A15E shows maximum peak cylinder pressure

and hence the NO_x emissions of B20PLOME30A15E were marginally higher than that of B20PLOME30A. At 50% load, the UBHC emissions of B20PLOME30A15E were marginally higher than that of B20PLOME30A; this is due to higher latent heat of vaporisation of ethanol, which reduces the combustion temperature. This proves that poultry litter oil biodiesel with alumina nanoparticles and ethanol as an additive can be used as a renewable and environmentally friendly fuel, minimising the use of mineral diesel. Also, poultry litter oil can be utilized as a fuel through this waste management technique.

LIST OF NOTATIONS AND ABBREVIATIONS

CI	Compression Ignition
BTDC	Before Top Dead Centre
BP	Brake Power
BTE	Brake Thermal Efficiency
HRR	Heat Release Rate
CO	Carbon Monoxide
NO _x	Oxides of Nitrogen
UBHC	Unburnt Hydrocarbons
O ₂	Oxygen
ppm	Parts per million
ASTM	American Society for Testing and Materials
PLOME	Poultry Litter Oil Methyl Ester
B20	20% Biodiesel + 80% Diesel
B20PLOME	20% Poultry Litter Methyl Ester + 80% Diesel
B20PLOME30A	20% Poultry Litter Methyl Ester + 80% Diesel + 30mg/l AL ₂ O ₃
B20PLOME30A15E	20% Poultry Litter Methyl Ester + 80% Diesel + 30mg/l AL ₂ O ₃ + 15ml Ethanol/l

REFERENCES

- [1] Baluswamy T, Marappan R, Performance evaluation of direct injection diesel engine with blends of Thevetiaperuviana seed oil and diesel, *Journal for Scientific and Industrial Research*, Vol 66, December 2007, 1035-1040
- [2] Darunde Dhiraj S., Prof. Deshmukh Mangesh M., Biodiesel Production from Animal Fats and Its Impact On the Diesel Engine with Ethanol-Diesel Blends: A Review, *IJETAE*, Vol 2, Issue 10, October 2012, ISSN 2250-2459
- [3] Dr. Sadhik B. J., Anand, R. B. Effects of nanoparticle additive in the water diesel emulsion fuel on the performance, emission and combustion characteristics of a diesel engine, *Journal of Vehicle Design*, Vol 59, Issue 2/3, 164-181, 2012
- [4] Hwanam Kim, Byungchul Choi, the effect of biodiesel and bioethanol blended diesel fuel on nanoparticles and exhaust emissions from CRDI diesel engine, *Renewable Energy*, 2010, Vol 35, Issue 1, 157-163



- [5] K. Ramarao, C. J. Rao , D. Sreeramulu, The Experimental Investigation on Performance and Emission Characteristics of a Single Cylinder Diesel Engine using Nano Additives in Diesel and Biodiesel, *Indian Journal of Science and Technology*, Vol 8, Issue 29, November 2015
- [6] Krzysztof Gorski, Ruslands Smigins, Impact of ether/ ethanol and biodiesel blends on combustion process of compression ignition engine, *Engineering for Rural Development*, Jelgava, 26, 2011.
- [7] M. Mofijur, M.G. Rasul, J. Hyde, Recent developments on internal combustion engine performance and emissions fuelled with biodiesel-diesel-ethanol blends, *Procedia Engineering*, Vol 105, 2015, 658–664
- [8] Nithin Samuel, Muhammed Shefeek K, Performance and Emission Characteristics of a C.I. Engine with Cerium Oxide Nanoparticles as Additive to Diesel, *IJSR*, Vol 4, Issue 7, July 2015, ISSN (Online): 2319-7064
- [9] S.P. Venkatesan, Kadiresh PN, Influence of Aluminum Oxide Nanoparticle Additive on Performance and Exhaust Emissions of Diesel Engine, *IJAER*, Vol 10, Issue 3, Jan 2015, 5741-5749
- [10] Senthil Kumar, Ramesh A and Nagalingam B, Experimental investigation on Jatropha oil-Methanol dual fuel engine, SAE Technical Paper, Vol 0153, Issue 01, 2001
- [11] Sri Harsha Tirumala, A.V.Rohit, Siva Krishna.M, Sudipta Saha, Synthesis of neem biodiesel, *IJAET*, Vol 3, Issue 1, January-March, 2012, 316-318, E-ISSN 0976-3945
- [12] V. Arul MozhiSelvan, R. B. Anand and M. Udayakumar, Effects of cerium oxide nanoparticle addition in diesel and diesel-biodiesel-ethanol blends on the performance and emission characteristics of a CI engine, *ARPN Journal of Engineering and Applied Sciences*, Vol 4, Issue 7, September 2009, ISSN 1819-6608
- [13] Xiaoyan Shi, Xiaobing Pang, Yujing Mu, Hong He, Shijin Shuai, Jianxin Wang, Hu Chen, Rulong Li, Emission reduction potential of using ethanol–biodiesel–diesel fuel blend on a heavy-duty diesel engine, *Atmospheric Environment*, Vol 40 Issue 14, May 2006, 2567–2574
- [14] Yetter R. A., Grant A R, Steven F S, Metal particle combustion and nanotechnology, Proceedings of the Combustion Institute 2009, Vol 32, Issue 2, 1819-1838
- [15] Zunqing Zheng, Xiaofeng Wang, Xiaofan Zhong, Bin Hu, Haifeng Liu, Mingfa Yao, Experimental study on the combustion and emission fuelling biodiesel/n-butanol, biodiesel/ethanol, and biodiesel/2,5-dimethylfuran on a diesel engine, *Elsevier Energy*, Vol 115, Issue 1, November 2016, 539–549



GUIDELINES FOR AUTHORS

A. LANGUAGE

- 01) Language of paper – American English
- 02) Abstract, captions and keywords will be bilingual English and Czech, optionally English and Slovak. Authors from the Czech and Slovak Republic should prepare abstract, keywords and captions in English and native language. The abstract and captions for other authors will be translated by the publisher to Czech language.

B. LENGTH

- Title** should not exceed 10 words
Subtitle should not exceed 15 words
Abstract should not exceed 200 words
Paper without limit

C. ORDER OF CONTENTS

- 01) Title
- 02) Author(s) name: per author company/institute, address, and e-mail (on new line)
- 03) Abstract
- 04) Keywords
- 05) Body of the paper. The paper should be divided into logical numbered sections.
- 06) Preferred structure:
 - Introduction: Background – Motivation – Goals
 - Used methods
 - Results
 - Analysis of results and evaluation
 - Conclusion: Result Utilization – Prospects
- 07) Acknowledgements
- 08) List of notations and abbreviations (in alphabetical order)
- 09) References
- 10) Appendices: Long derivation of equations, description and parameters of experimental equipment or methods, etc.

To facilitate the blind reviewing process, the authors are asked provide on a separate first page the items 1) and 2) and to start the main part of the article with 1) Title; and then 3) Abstract, and so on.

D. GRAPHICAL ARRANGEMENT

Title: Times New Roman 17b, Bold

Body of paper, abstract, equation numbering: Times New Roman 11b.

Titles of sections Times New Roman 12b Bold. Symbols of physical quantities used in text: italic. SI units, wherever possible. Combined units should be written with dot (example: N.m, m.s⁻², ...).

Authors should avoid the usage of footnotes.

Captions: Times New Roman 10b, in bold – number and caption, normal – text of legend. See examples:

Figure 1: This is a figure.

Table 1: This is a table.

All illustrations should be numbered sequentially with arabic numbers.

Equations: Times New Roman italic. Variable 12b, Index 7b, Small index 5b, Symbol 18b, Small symbol 12b. Mathematical operators and constants (Ex.: sin, e, π , ...) Times New Roman 12b normal.

All equations should be numbered sequentially with arabic numbers. List of notations either under every equation, or at the end of paper – see paragraph D (according to number and content of equations). Long derivation as appendix on the end of paper.

References: References referred in text in square brackets in format of text (Ex: [1])

Format of references, examples:

- [1] Author A., Author B. and Author C. (2002). This is journal article, In: *Journal for Interesting Papers*, Vol. 10, No. 3, p. 130–145. ISSN
- [2] Author A., Author B. and Author C. (eds.). *Our Book on Car Technology*, MIT Press, Massachusetts, 2002, p. 23-145. ISBN
- [3] Author A., Author B. and Author C. (2002). My paper in a conference, In: Editor A., Editor B. and Editor C. (eds.). *Proceedings Of Our Meeting in a Far Away Exotic Place*, MIT Press, Massachusetts, p. 78-89. ISBN

E. ILLUSTRATIONS

The Journal is **full-color**.

The authors are responsible for delivering high-quality graphic material. In the case of illustrations sent via mail, the orientation of illustrations should be indicated, as well as their number in the article. The illustrations sent electronically, should be sent in the correct orientation and in a resolution at least 300 dpi, in common graphical formats.

F. SUBMISSION OF MANUSCRIPTS

Text should be in all cases prepared in electronical form. Paper can be sent via mail (the contents of mail should be illustrations and diskette 3,5" or CD with text), or via e-mail on the address mentioned below.

Text should be sent in format MS Word 2000 or older (format doc, or rtf). Do not merge illustrations in the text to avoid excessive file size. All illustrations should be sent in separate files. No illustrations will be returned unless specifically requested.

Contact address for submission of paper:

ČVUT, FS, MECCA

Gabriela Achtenová

Technická 4, 166 07 Praha 6, Czech Republic

Tel.: +420 2 24 35 24 99, Fax: +420 2 24 35 25 00

E-mail: gabriela.achtenova@fs.cvut.cz

G. COPYRIGHT

The papers submitted to journal MECCA have not been previously published or submitted elsewhere. The copyright of accepted papers becomes the property of Czech Technical University, and usage of any part of papers without permission of Czech Technical University will be not allowed. Authors who wish to reproduce already published illustrations should asked the permission by the copyright holder. Authors are asked to sign copyright agreement.

H. PUBLICATION

All articles will be blind reviewed. The first author, if no other contact person is marked, will be informed about the decision as soon as possible.

Authors will get 3 copies of the journal in which the article is published.



MASTER OF AUTOMOTIVE ENGINEERING

ENTRANCE LEVEL: Technical bachelor (mechanical, transport, or electro engineering)

CTU
Prague
Czech republic

(E)

ITB
Bandung
Indonesia

(E), (I)

ENSTA
Brest
France

(F)

TUCH
Chemnitz
Germany

(G)

3rd SEMESTER

Entrance exam IFP

ENSTA
- Design of Vehicles
- Modelisation and Computation

(F)

HAN
Vehicle Dynamics and Intelligent Transport Systems

(E)

CTU
Advanced Powertrains

(E)

TUCH
Alternative Powertrains

(G)

IFP
Paris
France

(F)+(E)

4th SEMESTER devoted to final thesis and 5 months internship in an industrial or academic environment anywhere in the world

MASTER DEGREE IN AUTOMOTIVE ENGINEERING

Master degree from 2 countries with respect to chosen specialisation in 3rd semester

(F) – in French, (E) – in English, (I) – in Indonesian, (G) – in German

CTU

Czech Technical University in Prague
Czech Republic
Gabriela Achtenová
gabriela.achtenova@fs.cvut.cz
Tel.: +420 224 352 499

ITB

Institut Teknologi Bandung
Indonesia
Andi Isra Mahyuddin
aim@ftmd.itb.ac.id

ENSTA

ENSTA Bretagne
France
Yann Marco
yann.marco@ensta-bretagne.fr
Tel.: +33 298 348 844

TUCH

Technische Universität Chemnitz
Germany
Diana Lohse
diana.lohse@mb.tu-chemnitz.de
Tel.: +49 371 531 337 94

HAN

Hogeschool van Arnhem en Nijmegen
The Netherlands
Kea Bouwman
kea.bouwman@han.nl
Tel.: + 31 26 384 93 14

DEADLINE FOR: NON EU STUDENTS 1ST MAY 2018, EU STUDENTS 30TH JUNE 2018

For application form, detailed programme, studying conditions, tuition fees and all other informations, please see: www.emae.eu

